UNIVERSITÀ DEGLI STUDI DI PADOVA

Università degli Studi di Padova

Dipartimento di Scienze Chimiche

Corso di Dottorato in Scienza e Ingegneria dei Materiali e delle Nanostrutture

SMART CONCRETE FOR URBAN AREAS: IMPROVED PERFORMANCE AND SUSTAINABILITY OF FUNCTIONALIZED GRAPHENE RELATED MATERIALS IN CEMENTITIOUS PRODUCTS

Thesis written with the contribution of Italcementi S.p.A

Coordinatore: Prof. Leonardo Prins

Supervisore: Prof. Michele Maggini

Co-Supervisore: Dr. Claudia Capone

Dottorando: Andrea Cacciatore

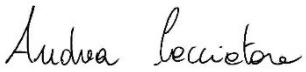

Abstract

This work resumes the most interesting experimental results achieved during the industrial PhD signed between Italcementi S.p.A and the Department of Chemical Sciences of the Università degli Studi di Padova.

Cement composite materials (CCMs), that include paste, mortar, and concrete, are the most widely used and highly performing construction materials. Nevertheless, extensive efforts are still necessary to improve their tensile strength and strain capacity, and to reduce their brittle nature. Several studies have been focused to address these problems, concerning the addition of specific admixtures, nanomaterials, or their combined use. Among them, Graphene Based Materials GBMs (graphene, graphene oxide, graphene nanoplatelets, etc.), thanks to their high surface areas, tensile strength, and aspect ratio, represent the ideal candidates to enhance the properties of cementitious materials. If well dispersed into cementitious matrix, GBMs can promote sustainable building, consuming less cement (preserving mechanical properties), emitting less CO_2, showing excellent durability, and reducing construction cycle time thanks their high early strength.

Despite their excellent intrinsic properties, the incorporation of GBMs in cementitious matrix is particularly challenging due to their poor dispersion in aqueous media.

A possible solution to improve the dispersibility of GBMs in water environment is their covalent functionalization with hydrophilic groups, that requires the addition of specific moieties that form covalent bonds on the basal plane of the carbon lattice.

This doctoral research was focused on the covalent functionalization of commercial GBMs, increasing their hydrophilicity and preparing new compounds able to be homogeneously dispersed in cementitious matrix.

Firstly, we functionalized single layer graphene (SLG) attaching different para-substituted anilines. More in detail, we modified SLG by the Tour reaction, introducing sulfonate group, polyethylene glycol chain, or a quaternary ammonium group. We also replicated this reaction using different GBMs: few layers graphene, high-quality graphene nanoplatelets, and low-quality graphene nanoplatelets, finding the most suitable GBMs and functional groups to obtain high functionalization yields.

Subsequently, we investigated the role of functionalized GBMs to improve mechanical performance of CCMs by preparing mortar samples with different percentage of graphenic

products. Moreover, we evaluated two different mixing procedures, combining mechanical and chemical approaches to further enhance the dispersibility of GBMs in the cementitious matrix.

The fruitful research carried out in the PhD path provides new perspectives for a more effective and aware use of GBMs in performing as well as sustainable cementitious building materials.

Riassunto

Questo lavoro riassume i più interessanti risultati sperimentali raggiunti durante il dottorato industriale promosso in collaborazione tra Italcementi S.p.A. ed il Dipartimento di Scienze Chimiche dell'Università degli Studi di Padova.

I compositi cementizi (pasta cementizia, malta e calcestruzzo) sono i materiali da costruzione più performanti e largamente impiegati in campo edilizio. D'altro canto, in un'ottica di miglioramento continuo, rientra la progettazione di mix design sempre più innovativi, con ambizione almeno duplice. Da un lato, lo sforzo resta orientato sull'incremento della resistenza a trazione e della capacità di deformazione, per ridurne la fragilità. Dall'altro, diventa prioritario affiancare, alla proposta di applicazioni tecnicamente avanzate, soluzioni che soddisfino gli attuali requisiti di sostenibilità ambientale e sociale (oltre che economica) del loro impatto.

L'utilizzo di nanomateriali sembrerebbe essere tra le migliori risposte ad ambo le urgenze; in particolare, se impiegati in combinazione con agenti superfluidificanti atti a favorirne una più omogenea dispersione in matrice cementizia.

Grazie alle loro elevate aree superficiali e resistenza alla trazione, i graphene based materials (GBMs) sono considerati i nanomateriali più promettenti per migliorare le proprietà meccaniche dei materiali compositi cementizi (CCMs). Se ben dispersi, i GBMs possono promuovere l'edilizia sostenibile, permettendo di realizzare malte e calcestruzzi con ridotti contenuti di cemento e minore impronta carbonica, preservandone le consolidate proprietà meccaniche e di durabilità. A causa della loro scarsa dispersione in mezzi acquosi, un'efficace distribuzione di GBMs in matrice cementizia è particolarmente impegnativa.

Tra le più sfidanti soluzioni per migliorare la dispersione dei GBMs in ambiente acquoso la funzionalizzazione covalente con gruppi idrofili riveste un ruolo di particolare rilievo.

Questa ricerca di dottorato si è concentrata sulla funzionalizzazione covalente di GBMs commerciali, per ottenere nanomateriali idrofili in grado di essere omogeneamente dispersi in matrice cementizia.

In primo luogo, abbiamo funzionalizzato il grafene a strato singolo (SLG) legandolo chimicamente con diverse aniline para-sostituite. Più in dettaglio, abbiamo modificato i SLG tramite la reazione di Tour, introducendo gruppi solfonati, catene polietilenglicole o gruppi ammonio quaternari. Abbiamo altresì replicato questa reazione utilizzando diversi GBMs: pregiati grafene few layers, grafene nanoplatelest di alta e bassa qualità, individuando i GBM e i gruppi funzionali più adatti per ottenere rese di funzionalizzazione elevate.

Successivamente, abbiamo studiato il ruolo dei GBMs funzionalizzati per migliorare le prestazioni meccaniche dei CCMs, preparando campioni di malta con diverse percentuali di prodotti a base di grafene. Inoltre, abbiamo valutato due diverse procedure di miscelazione, combinando approcci meccanici e chimici per potenziare ulteriormente la dispersione dei GBM nella matrice cementizia.

I risultati della ricerca condotta in questo percorso di dottorato delineano nuove prospettive per un uso più efficace e consapevole dei GBMs nella progettazione ed applicazione di materiali cementizi non solo tecnologicamente avanzati ma anche ambientalmente sostenibili.

Summary

Abbreviations

G ..... Graphene

SLG ..... Single Layer Graphene

GO ..... Graphene Oxide

rGO ..... Reduced Graphite Oxide

CNTs ..... Carbon Nanotubes

MWCNTs ..... Multi-Walled Carbon Nanotubes

GNPs ..... Graphene Nanoplatelets

GBMs ..... Graphene Based Materials

CCMs ..... Cementitious Composite Materials

SEM ..... Scanning Tunneling Microscopy

UV-vis ..... Ultra Violet-visible spectroscopy

TGA ..... Thermo-Gravimetric Analysis

FT-IR ..... Fourier Transform Infrared

TEM ..... Transmission Electron Microscopy

XPS ..... X-ray Photoelectron Spectroscopy

XRD ..... X-ray Diffraction

ESI-MS ..... Electrospray ionization Mass Spectroscopy

NMR ..... Nuclear Magnetic Resonance

NMP N-Methyl-2–Pyrrolidone

EtOH ..... Ethanol

MeOH ..... Methanol

1. Introduction

Currently, the global annual production of concrete is estimated at around 4.4 billion tons, but it is projected to exceed 5.5 billion tons by 2050 as developing countries increasingly urbanize [1]. Cement is the main concrete constituent; its production requires a very energy/carbon-intensive process and releases approximately 1 ton of CO_2 for each ton of cement. Despite the efforts already undertook to gradually transition towards more efficient and sustainable production models, cement industry remains the third largest consumer of industrial energy in the world, accounting for 7% of industrial energy consumption, and the second largest industrial emitter of CO_2, with approximately 7% of global emissions [2].

It is no wonder that, taking into account the aforesaid information, the sustainability of the concrete and cement industries has to be improved.

In order to limit the CO_2 emissions, a more and more aware and efficient use of cement is necessary. This requires the development of innovative materials, able to replicate the required mechanical properties with a lesser amount of energetically demanding cement. In this context Graphene Based Materials (GBMs) represents an interesting solution, because of their intrinsic properties, allowing the production of concrete with improved mechanical performance, using less cement.

The successful action of GBMs in enhancing cement composites properties or, alternatively, allowing same performance using less cement, mainly depend on their challenging homogenous dispersion in cementitious matrix, due to the graphene intrinsic hydrophobicity. In the present thesis, we study how the choice of the starting pristine GBM, and a proper structural modification, influence its dispersion in a cementitious matrix. The mechanical properties of the newly obtained cement composite materials (CCMs) were investigated with the aim to develop a more effective and durable cement composite materials, able to play a vital role in the more sustainable world of tomorrow.

1.1 Cement overview

Cement represents the fundamental ingredient of the modern building materials, it can be described as a hydraulic binder, with adhesive and cohesive properties, that chemically reacts with water by converting a shapeable mixture into a rigid matrix able to agglomerate other solid materials. Actually, the most used cement is “Portland cement”, a fine powder produced by heating, at ~ 1400 °C, limestone and clay minerals in a kiln to produce clinker, which is

subsequently ground and mixed with gypsum ($CaSO_4.2H_20$) or anhydrite ($CaSO_4$) to obtain the final product.

Gypsum is added to slow down the hydration rate of cement; in practice, clinker cannot be used simply by mixing with water, because its reaction led to a quick setting, making useless the transport and the application on job sites. On the other hand, when clinker is ground with a proper amount of calcium sulphate (3-4% in terms of SO_3), Portland cement reacts more slowly, allowing its practical uses. For this reason, gypsum and anhydrite are called set regulators.

In addition to Portland cement, many other cement types are commercially available, and can contain other natural or artificial materials, including natural volcanic pozzolan, artificial pozzolan, granulated blast furnace slag, fly ash, silica fume, limestone, and calcined shale. The European standard EN 197-1 defines the composition, specifications, and conformity criteria for common cements.

Cement is the main constituent of concrete [3]. More in detail, concrete contains two fundamental components: natural/artificial aggregates, which consist of sand and natural gravel or crushed stone, and the cement matrix, which consist of cement and water. The cement matrix (commonly known as cement paste) coats and links the individual aggregate elements, keeping them together over time. The mixture of the above ingredients without coarse aggregate (i.e. diameter greater than 5 mm) is referred to as mortar, which, in contrast to concrete, is used in applications requiring reduced mechanical performances/thickness (rendering, adhesive joint between stones or bricks, grouting).

During the chemical reactions between water and cement, there is a progressive decrease of the workability until the cement paste ceases to be shapeable (setting). Subsequently, there is a progressive increase of the strength, to form a hardened material. For these reasons the technical attention is necessarily put on two states of cementitious materials: the fresh state and the final hard state.

1.1.1 Cement constituents

Four compounds are usually regarded as the major constituents of cement: they are listed in Table 1, together with their abbreviated symbols. This shortened notation, used by cement chemists, describes each oxide by one letter: CaO = C; SiO_2 = S; Al_2O_3 = A; and Fe_2O_3 = F.

Table 1: main compounds of Portland cement.

Name of compound	***Oxide composition***	***Abbreviation***
Tricalcium silicate	$3CaO.SiO_2$	C_3S
Dicalcium silicate	$2CaO.SiO_2$	C_2S
Tricalcium aluminate	$3CaO.Al_2O_3$	C_3A
Tetracalcium aluminoferrite	$4CaO.Al_2O_3.Fe2O_3$	C_4AF

In reality, silicates in cement are not pure compounds, but contain minor oxides. In addition to the main compounds listed in Table 1, minor compounds (in terms of quantity and not to their importance) exist, such as MgO, TiO_2, Mn_2O_3, K_2O and Na_2O; they usually amount to not more than a few per cent of the mass of cement (0-0.5%).

Calcium silicates represent about the 80% of the cement, while calcium aluminates the remainder 20%. The two aluminates, C_3A and C_4AF play an important role in the setting process through the early reaction of cement with water, whilst the two silicates, C_2S and C_3S, play a more important role during the hardening.

1.1.2 The hydration of Portland cement

Cement hydration is a heterogeneous process where a collection of coupled transformations, that occurs at different rates, are involved. These processes fall into the following categories: dissolution/dissociation, diffusion, growth, nucleation, complexation, adsorption which may operate in series, in parallel, or in some more complex combination. Unfortunately, the rigorous application of these concepts to cement hydration continues to be elusive because of the difficulty of isolating the individual chemical processes for detailed study [4].

The progress of hydration and its kinetics are influenced by a variety of factors, especially:

- by the phase composition of the cement and the presence of foreign minor oxides within the crystalline lattices of the individual clinker phases;
- by the fineness of the cement (< 100 µm), in particular by its particle size distribution and specific surface;
- by the water-cement ratio used (w/c);
- by the curing temperature;
- by the presence of additives, i.e materials interground with cement in larger amounts, such as granulated blast furnace slag or pulverised fly ash.

Due to the complexity of the hydration reactions in Portland cement, it makes good sense to discuss separately the hydration of the individual minerals that constitute the Portland cement clinker.

Tricalcium silicate C_3S, is the main and most important constituent of Portland cement, which to a great extent controls its setting and hardening. In cement, C_3S exists as an impure material which is doped with other ions present in the original raw mix (typically Mg) and is called "alite". The products of its hydration at ambient temperature are formed as an amorphous calcium silicate hydrate phase with a CaO/SiO_2 molar ratio of less than 3.0, defined as "C-S-H phase" (or "C-S-H gel"), and calcium hydroxide ($Ca(OH)_2$ abbreviated CH).

$C_3S + H_2O \rightarrow C\text{-}S\text{-}H + Ca(OH)_2$ *Eq. 1*

Due to its amorphous character, the hydration of tricalcium silicate is rather complex and is still not fully understood [4].

Several stages may be distinguished in the hydration of C_3S:

- *Pre-induction period*. Immediately after contact with water, an intense, but short-lived hydration of C_3S gets under way (few minutes), in which an intense liberation of heat may be observed.
- *Induction (dormant) period*. The pre-induction period is followed by a period in which the rate of reaction slows down and the hydration heat is also significantly reduced (few hours).
- *Acceleration (post-induction) period*. After several hours the rate of hydration accelerates and the $Ca(OH)_2$ concentration in the liquid phase attains a maximum value. In this period the second main heat peak is observed.
- *Deceleration period*. After reaching a maximum the rate of hydration starts to slow down gradually; however, a measurable reaction may persist even after months of curing.

Dicalcium silicate C_2S is the second constituent of the Portland cement, in which exists as an impure material called "belite". Also in this case, the products of hydration are an amorphous calcium silicate hydrate phase, "C-S-H phase", and calcium hydroxide CH.

$C_2S + H_2O \rightarrow C\text{-}S\text{-}H + Ca(OH)_2$ *Eq. 2*

The hydration mechanisms of C_2S are like the ones of C_3S, even though the whole process progress more slowly. With respect to C_2S, C_3S is faster both in reacting with water and in developing the corresponding strength (see Figure 1).

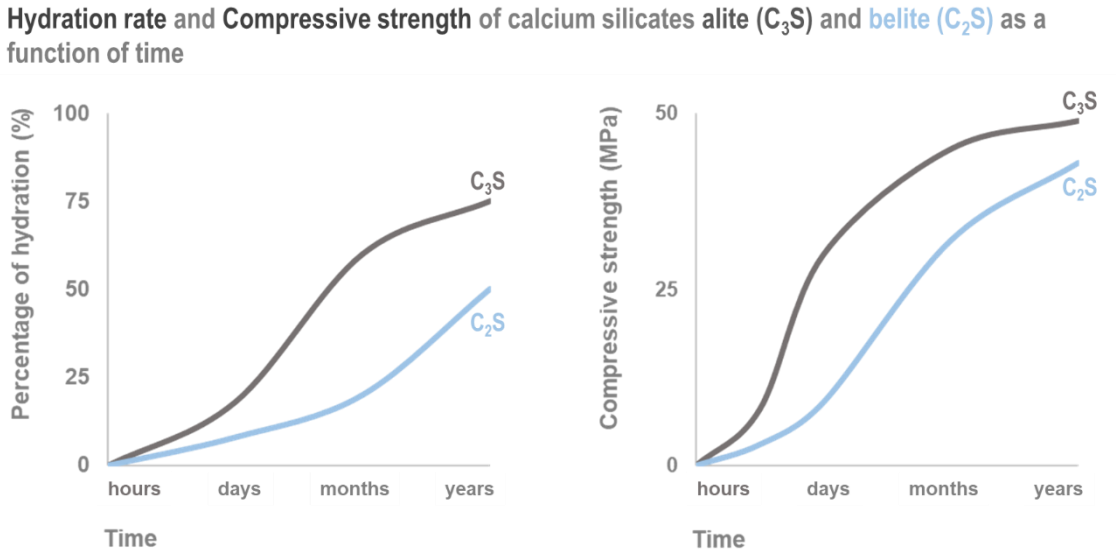

Figure 1: Schematic trend of hydration degree and compressive strength of calcium silicates as a function of time.

However, for both silicates the hydration degree and the strength are negligible during the first hours, whilst the strength is almost identical at long aging (years). The different behaviour in terms of performance is observed after 1 day, 1 week, and 1 month (this behaviour is extremely relevant from a practical point of view, as an example, the strength after few days can affect the time of removing the formworks, while the 28-day compressive strength is very important for structural applications).

Both silicates require approximately the same amount of water for their hydration, but C_3S produces more than twice as much $Ca(OH)_2$ as is formed by the hydration of C_2S (the hydration rate for Eq. 2 is lower than that Eq.1).

The percentage of C_3S in Portland cement is usually much higher than that of C_2S (about 3:1) except in the case of belitic cements.

The C-S-H morphology is prevalently fibre-like even though it may be found in other particle forms (flakes, honeycombs, tightly packed grains or of a seemingly featureless dense material). C-S-H fibres develop on the granules of adjacent C_3S or C_2S, firstly touching each other, and then interlacing. Figure 2 shows SEM image of C-S-H.

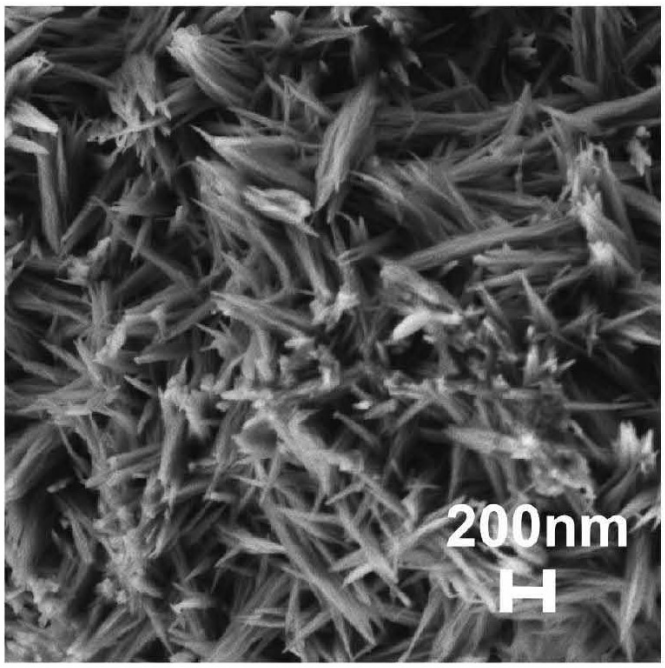

Figure 2: SEM images of C-S-H (Reproduced with the permission from reference [5], copyright Elsevier Ltd., 2017).

Portlandite CH, which always results from hydration of silicates, precipitates in the form of crystals and become evenly distributed within the hardened paste. CH does not contribute to the development of strength due to its not fibre-like morphology, but it plays an important role for the protection of metallic bars of reinforced concrete from corrosion. Indeed, in alkaline environment (pH > 11.5), steel is coated by a very thin and compact ferric oxide film (passivation) which protects it from corrosion (i.e. rusting resulting from humidity and oxygen).

Tricalcium aluminate C_3A and *Tetracalcium aluminoferrite C_4AF* provide similar products during their hydration reactions; however, their reactivity is different and depends on the type and quantity of other elements (e.g. Al, Fe). At ordinary temperature, and in the absence of gypsum, the hydration product of C_3A and C_4AF is a crystalline calcium aluminate hydrate phase, defined as C-A-H (that is not a chemical formula but the generic acronym of Calcium-Aluminate-Hydrated).

C_3A (or C_4AF) + $H_2O \rightarrow$ C-A-H *Eq. 3*

Despite their rapid reaction with water, C_4AF and C_3A do not contribute much to the development of the mechanical properties, except for the quick but very small strength increase occurring in the first hours of the hydration. Basically, the rapid reaction of the aluminates with water is accompanied by an immediate loss of plasticity (quick setting). This phenomenon results from the morphology of the C-A-H, which is based prevalently on sheet-like products. Therefore,

and in contrast to what happens with fibre-like C-S-H products, the development of strength is negligible.

The fast hydration of the aluminates, that leading to rapid set (quick setting), is limited by the use of sulphates, that always are added to Portland cement clinkers. The reaction is slowed down directly by absorption of sulphate ions on reactive sites [6], resulting in the regained of the essential period of workability.

C_3A (or C_4AF) + H_2O + $CaSO_4.2H_2O \rightarrow C_3A(F).3CaSO_4.H_{32}$ (ettringite) *Eq. 4*

In this process, gypsum or anhydrite acts as set regulator and modifies the hydration rate of the aluminates producing ettringite instead of C-A-H. As ettringite is gradually consumed, calcium aluminate hydrates also re-start to form.

In few words, the hydration of Portland cement is a complex reaction between clinker phases, calcium sulphate and water, resulting in the formation of hydrates and leading to setting and hardening. It is an exothermic process and can be followed by isothermal calorimetry; Figure 3 shows a typical calorimetry curve for the hydration of Portland Cement.

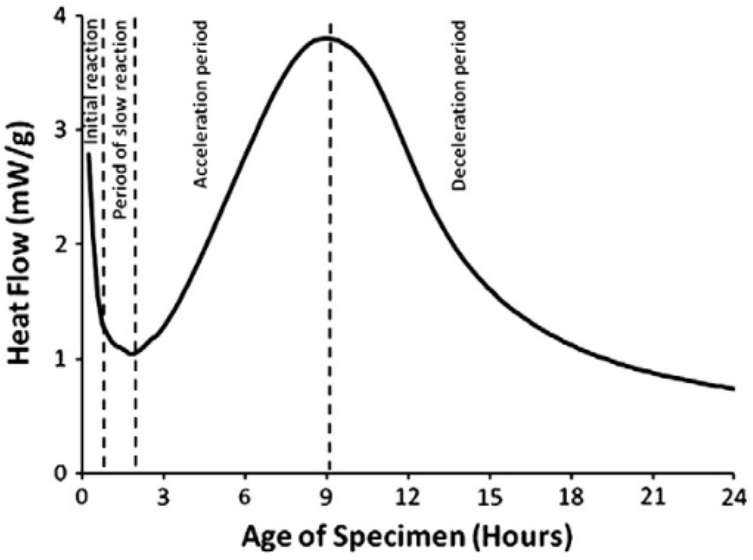

Figure 3: schematic representation of Portland cement calorimetry curve (Reproduced with the permission from reference [4], copyright Elsevier Ltd., 2011).

The initial period is characterized by rapid reactions between C_3S and water that begin immediately upon wetting, characterized by an intense exothermic signal. Second, the addition of water lead to a thin layer of hydrate forms on the surface of the grains, which inhibits their

further reaction, consequently, there is a sudden slowdown in the reaction, followed by a period of low chemical activity. This, so called slow reaction period, is of great practical importance as it provides a time in which concrete can be transported and placed before setting. Thirdly, there is the main hydration peak, resulting from the hydration of C_3S and C_2S that lead to the massive precipitation of C-S-H and CH. After the main hydration peak there is a deceleration period, with low activity, that is important in concrete technology because of the slower strength development [7].

Figure 4 shows the different stages of hydration process of cement particles during the reaction with water. After adding water (Figure 4a), an ettringite film is formed on the surfaces of cement particles (Figure 4b). Subsequently, this film is saturated with water and forms C-S-H, and Portlandite as shown in (Figure 4c). The hydration still continues but at lower speed, because C-S-H hinders the diffusion of water toward the nucleus of the cement powder, which can remain unhydrated for years (Figure 4d).

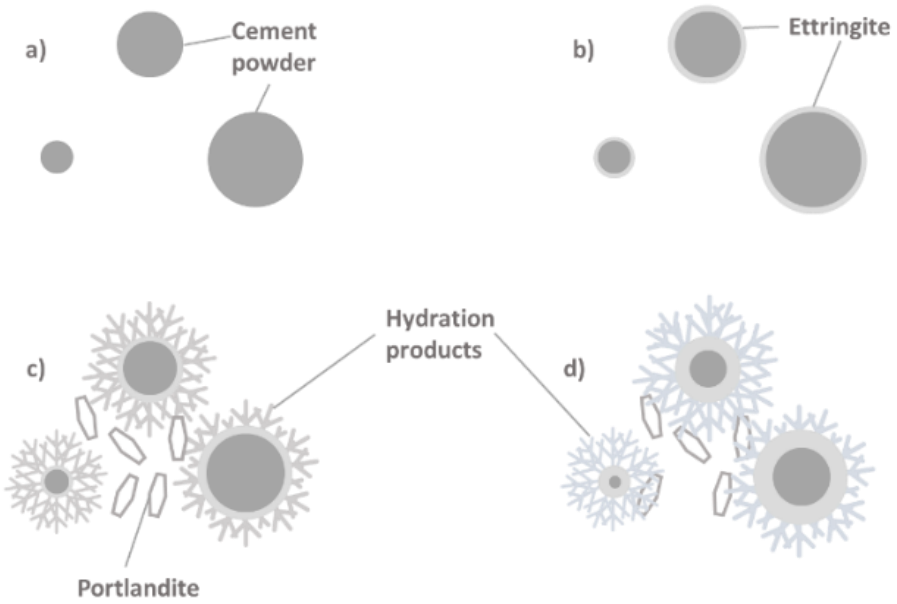

Figure 4: schematic progress of Portland cement hydration.

1.1.3 Strength of cement

The “strength of cement” is defined as the strength of mortar test specimens prepared, cured, and tested according to a national or international standards, to eliminate the effect of factors other than cement quality on the obtained value.

The main factors determining the strength of hardened cement pastes are:

- the nature of the binder which determines the 'intrinsic bonding properties' of the hydrated material;
- the fineness of the binder, which is one of the factors that determines the kinetics of the hydration process and thus the rate of strength development;
- the water/cement ratio, which determines the porosity of the hydrated cement paste;
- the hydration time, as the amount of hydrated material and thus the strength increases with progressing hydration;
- the hydration temperature, which affects both the rate of hydration and the structure and thus the intrinsic bond properties of the hydrated material which is formed.

In the case of mortar or concrete, the strength depends also on the cohesion of the cement paste, the adhesion to the aggregate particles, and the strength of the aggregate itself.

Strength tests are not made on a neat cement paste because of difficulties of moulding and testing with a consequent large variability of test results. Cement-sand mortar and, in some cases, concrete of prescribed proportions and made with specified materials under strictly controlled conditions, are used for the purpose of determining the strength of cement.

There are several forms of strength tests: flexure, direct tension, and direct compression; but the latter is crucial for real application. The appropriate test to determine the strength of cement is the European Standard EN 196-1, that prescribes a compressive and flexural strength test on mortar specimens. The test is performed on mortar of fixed composition, made with a 'CEN standard sand' (CEN is the acronym of the French name of the European Committee for Standardization.). The sand/cement ratio is 3 and the water/cement ratio is 0.50.

1.2 Carbon nanostructures – Graphene Based Materials

Two dimensional graphene is the basic structural unit of GBMs; it is composed of a single-layer sheet of carbon atoms (2D) that can be wrapped up into 0D fullerenes, rolled into 1D nanotubes or stacked into 3D graphite (see Figure 5) [8].

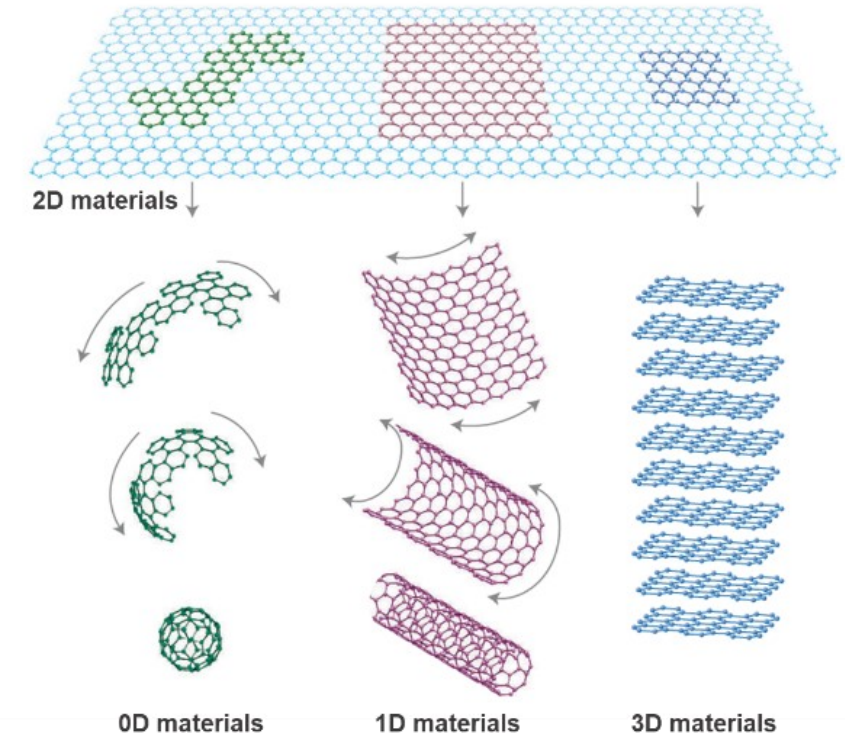

Figure 5: Graphene is a 2D building material for carbon materials of all other dimensions. It can be wrapped up into 0D buckyballs, rolled into 1D nanotubes or stacked into 3D graphite (Reproduced with the permission from reference [8], copyright Springer Nature limited, 2007).

Although all of them were largely studied for the application in CCMs (in particular Carbon Nanotubes, CNTs, due to their former discovery), the use of 2D materials in cementitious applications has some advantages compared to the rest. For example, graphene, and graphene oxide, presenting larger specific surface area (SSA) than CNTs (see Table 2). Their production is easier, more reproducible, and less hazardous for health and environment [9]; in addition, they are more dispersible in water media [10]. These characteristics, make them more attractive for various applications in construction materials.

Table 2: material properties of GBMs (GNPs' characteristics depends on the number of layers) [11].

Material	***Elastic modulus (GPa)***	***Tensile strength (GPa)***	***Elongation at break (%)***	***Density (kg/m^3)***	***Diameter/thickness (nm)***	***Surface area (m2/g)***	***Aspect ratio***
Graphene	1000	130	0.8	2200	0.08	2600	up to 600,000
GO	23-42	0.13	0.6	1800	0.67	500-1500	up to 45,000
CNTs	950	11-63	12	1330	15-40	70-400	up to 10,000

It is important to note that most of the excellent properties that have been reported are in regard to single layer defect-free graphene.

1.2.1 GBMs classification

The term graphene is used in a generic manner by scientists to describe many graphene-based materials (GBMs). The inconsistency in naming arises with the use of the term “graphene” for isolated single atom-thick sheets two-dimensional sheetlike and flake carbon forms [12]. The number of graphene layers, the average lateral size, and the carbon to oxygen (C/O) atomic ratio can be considered the three fundamental properties that cover the largest set of current graphene materials. The two morphological characteristics are included because GBMs consist of not only single-layer graphene but also few-layers graphene (i.e., 2–10 layers), graphene oxide (GO, normally a single layer), reduced graphene oxide (rGO; normally a single layer), graphene nanosheets, ultrafine graphite (i.e., more than 10 graphene sheets but below 100 nm in thickness), graphene ribbons, and graphene dots [12].

The addition of the C/O ratio as a functional attribute can be justified by the fact that GBMs are both structurally and chemically heterogeneous. The family of GBMs includes materials with widely variable surface oxygen content, for example, GO and rGO are emerging as popular materials in nanocarbon research, not only as carbon building blocks for biomedical applications but also as starting materials to produce graphene-based materials [13].

Figure 6 shows the classification grid for the categorization of different graphene types according to three fundamental GBM properties: number of graphene layers, average lateral dimension, and atomic carbon/oxygen ratio. The different materials drawn at the six corners of the box represent the ideal cases according to the lateral dimensions and the number of layers reported in the literature. The values of the three axes are related to the GBMs at the nanoscale, but it is feasible to expand the values to the microscale [13].

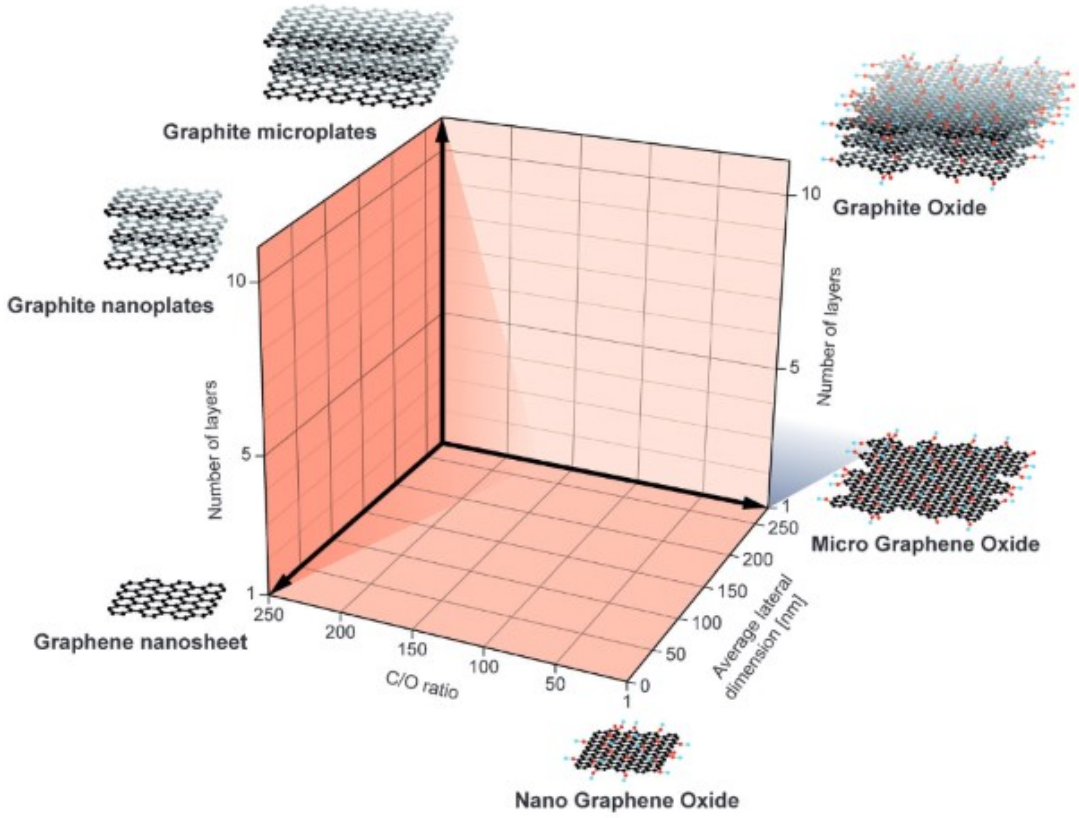

Figure 6: classification of GBMs (Reproduced with the permission from reference [13], copyright Wiley-VCH Verlag, 2014).

Graphene G is a two dimensional-carbon atom single-layer nano material. Each carbon atom is linked to other carbon atoms through three C–C bonds to form a planar 2D structure. The strength of the carbon–carbon bond gives GNP excellent mechanical strength, chemical and structural stability. The sp^2 hybridization allows the electron hosted in the remaining p orbital to be extensively delocalized within the adjacent carbons. The resulting free movement of these electrons in the carbon atom network awards GNP with excellent thermal and electrical conductivity [14]–[16]. This chemical characteristics gives GNP a variety of unique physical and chemical properties which are much different from other carbon materials [17], and hence have awarded GNP's widespread potential applications in many fields. Interestingly, the structure of carbon element in GNP makes it both, hydrophobic and oleophobic.

Graphene nanoplatelets GNPs refer to a graphene stacked body with more than 2 layers with thickness ranging from 3 to 100 nm [18]. Due great similarity in composition and structure, G and GNPs possess highly similar properties. However, the increase in thickness leads to a decrease in specific surface area of GNPs as compared to that of G which greatly hinders its applications in potential fields for instance, for adsorption purposes. On the other hand, its

multi-layer characteristics endorse it with a special spatial and spring like structures. Compared with the consistent efforts related to G production, GNPs with more layers requires lower accuracy in their preparation, and hence gives great advantages in terms of production costs.

Graphene oxide GO is a compound containing carbon, oxygen, and hydrogen in variable ratios, obtained by treating graphite with strong oxidizers and acids. By sufficiently sonicating GO, sufficient peeling of the intermediate product (GO) sheet layer can result in the formation of a single layer GO. This GO upon reduction leads to the formation of graphene as the final product. These findings demonstrate that GO and G are identical in the composition of sheet layer, and hence possess greatly similar thermal, electrical, light and mechanical properties. However, after oxidative treatment, the surface of GO becomes rich in functional groups like hydroxyl (–OH) and carboxyl (–COOH), etc., which award GO diverse chemical properties. In particular, the addition of hydroxyl, and carboxyl groups, guarantee high hydrophilicity.

1.2.2 Fabrication of graphene

One of the major challenges of graphene since it was discovered has been finding a fabrication method that can not only produce high quality graphene but also at large scale. Utilization of graphene by various industries depends mostly on finding fabrication methods for large scale production, especially for the use in construction field. There are generally two production approaches; a top-down approach where graphene is exfoliated from graphite (which is widely available and low cost) and a bottom-up approach where graphene is “grown” on silicon carbide (SiC). There are many methods to produce graphene with either approach and Figure 7 shows some common production methods along with their scalability potential in terms of graphene quality (G), cost (C), scalability (S), purity (P) and yield of the overall production process (Y).

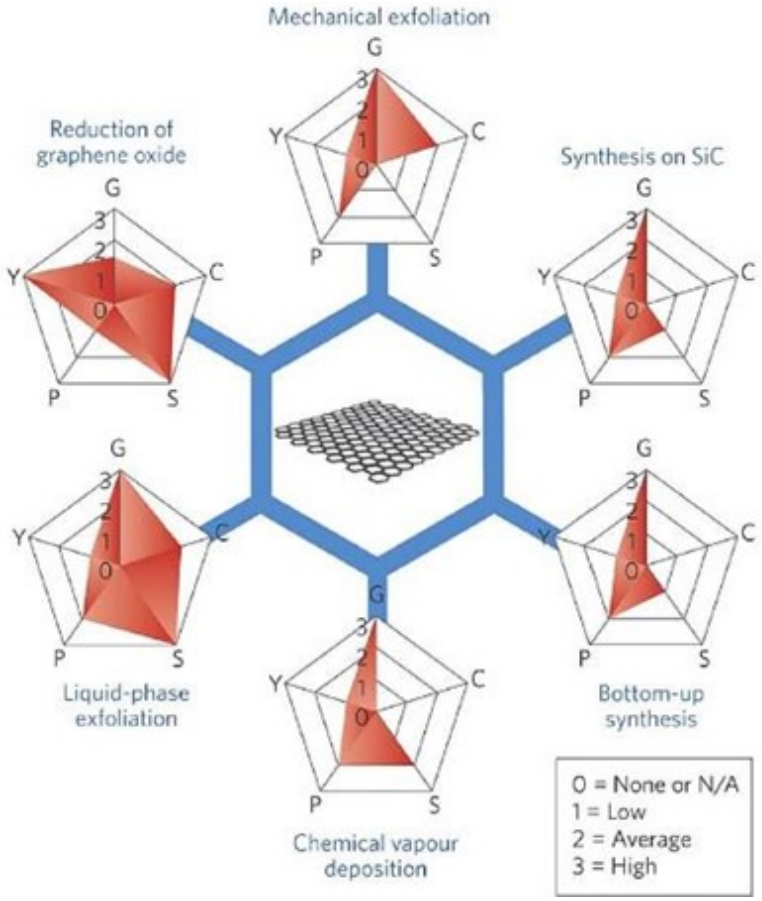

Figure 7: Common graphene production methods and scalability potential (Reproduced with the permission from reference [19], copyright Elsevier Ltd., 2017).

The key challenge with these methods is that each would produce a different quality graphene with varying fundamental properties (number of graphene layers, average lateral size and carbon-to oxygen (C/O) atomic ratio). This is a contributor to the discrepancies in the literature which makes difficult the evaluation of GBMs and their influence to enhance the mechanical performances of CCMs.

1.2.3 Characterization of GBMs

Various methods can be used either in isolation or in combination to investigate graphene status and dispersion in the liquid media, including infrared spectroscopy (FT-IR), transmission electron microscopy (TEM), Raman spectroscopy, X-ray photoelectron spectroscopy (XPS), X-ray diffraction (XRD), Ultraviolet-Visible spectroscopy (UV-Vis), thermo-gravimetric analysis (TGA), and scanning electron microscopy (SEM).

- Fourier-transform infrared spectroscopy (FT-IR) is used for chemical characterization, i.e. to establish the chemical bonds and functionalities of the available material.

- Transmission electron microscopy (TEM) is used to characterize the morphology and the structure of graphene materials.
- Raman spectroscopy assess the level of defects in the graphene nanomaterial and identify the number of layers.
- X-ray photoelectron spectroscopy (XPS) establishes the nature of the carbon-oxygen bonds at various states.
- X-ray diffraction (XRD) studies the structure and composition of the material.

Among all these techniques, for this study, only scanning electron microscopy (SEM), Ultraviolet-Visible spectroscopy (UV-Vis), and thermo-gravimetric analysis (TGA) resulted necessary to evaluate the morphology (before and after the functionalization), the water dispersion capability, and the functionalization degree of the functionalized GBMs. Since all the GBMs used in this work are commercially available, most of the information was provided by the technical data sheets and further characterization was not necessary.

Scanning Electron Microscopy (SEM)

SEM images allow fast scanning of large surface areas of a specimen that includes tens and even hundreds of different GBM flakes on the same image. SEM provides complete information about the flake size distribution, lateral size, and flake morphology. For its simplicity and robustness, in principle, SEM can even be used as a routine quality control method when GBMs production comes to industrial scale.

Ultraviolet-Visible spectroscopy (UV-Vis)

Ultraviolet-visible (UV-Vis) spectroscopy uses a light source to illuminate a sample with light across the UV to the visible wavelength range (typically 190 to 900 nm). The instruments then measure the light absorbed, transmitted, or reflected by the sample at each wavelength. UV-vis spectroscopy is a convenient technique to confirm a sample graphitic structure, with an absorption peak at ~260 nm, which is attributed to the π–π^* transitions of aromatic C–C bonds. Functionalized graphene samples, such as for instance graphene oxide, show a significant shift of the main absorption band of pristine graphene. For example, Zhou and coworkers [20] used UV-vis spectroscopy to distinguish graphene from graphene oxide samples (Figure 8) through the shift of the 254 nm graphene absorption to 227 nm.

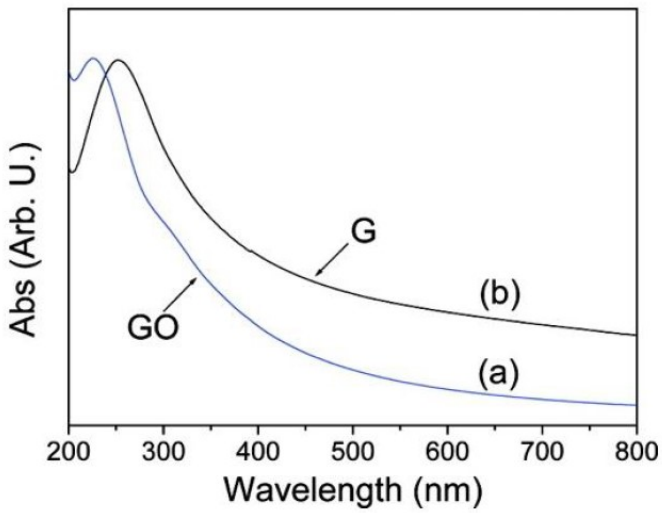

Figure 8: UV-vis spectra of the (a) graphene oxide (GO) and (b) graphene (Reproduced with the permission from reference [20], copyright American Chemical Society, 2009).

UV-Vis spectroscopy can be used also to investigate the dispersion degree of graphene materials in water, with the underlying principle being that a higher absorbance value means higher dispersion in water. Evaluating the absorbance spectra of aqueous suspension at different concentrations of GNPs, H. Du et al. [21] confirmed that the optical absorbance of suspension exhibits a linear relationship with the concentration of particles in the solution (see Figure 9).

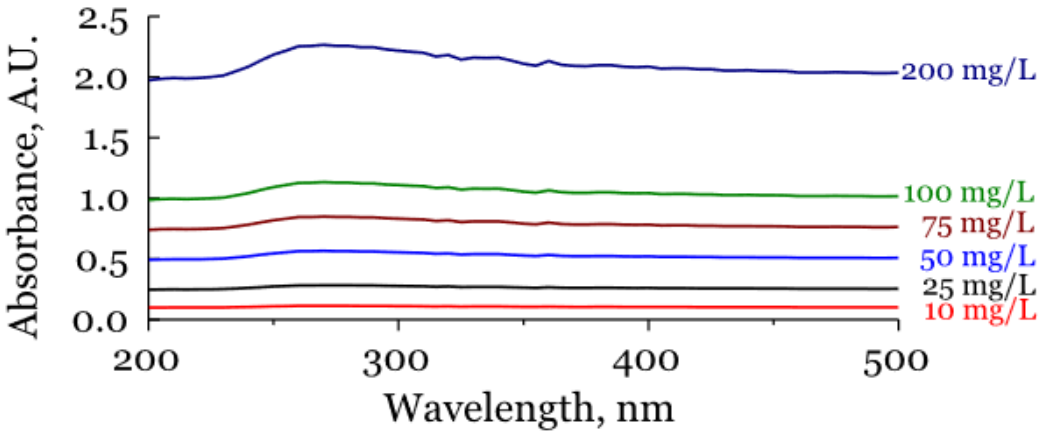

Figure 9: absorbance spectra of aqueous suspension at different GNPs' concentrations (Reproduced with the permission from reference [21], copyright Elsevier Ltd., 2018).

I. Papanikolaou et al. [22] successfully investigated the dispersion of multi-layer graphene nanoplatelets in water using polycarboxylate-based superplasticizer (PCE). In their study, the addition of commercial PCE increases the absorbance of different percentage of GNP suspension, indicating enhanced dispersion of the GNPs (see Figure 10).

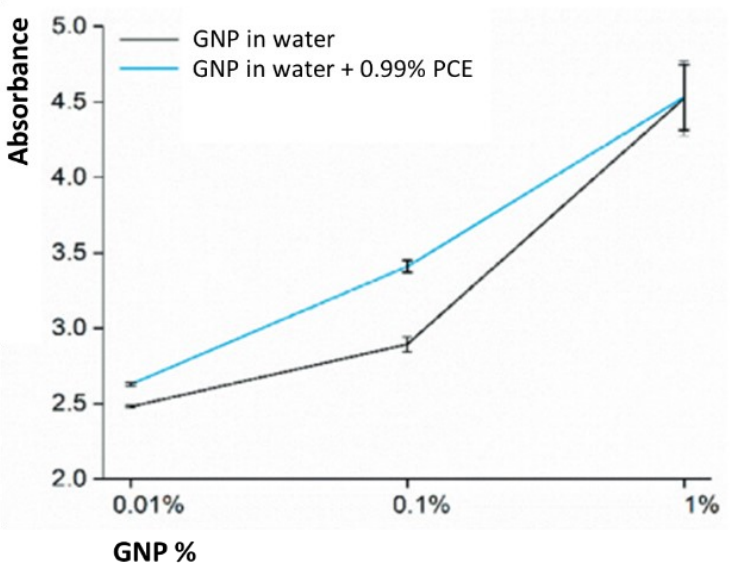

Figure 10: effect of increasing GNP dosage on the absorbance with 0.99 wt% of PCE (Reproduced with the permission from reference [22], copyright Elsevier Ltd., 2009).

Thermo-Gravimetric Analysis (TGA)

TGA is a method of thermal analysis in which the mass of a sample is measured over time as the temperature changes. This measurement provides information about physical phenomena, such as phase transitions, absorption, adsorption and desorption. It is another important technique to characterize GBMs, particularly in terms of thermal stability or degree of functionalization. Ben L. Feringa [23] and coworkers prepared two kinds of functionalized graphene (1 and 2 functionalized graphene) through a zwitterion cycloaddition onto exfoliated graphene flakes. Figure 11 shows the TGA curves of graphene, 1 and 2 functionalized graphene. The weight loss of graphene is about 5% between 200 °C and 450 °C, which is due to the defects caused by sonication, and also residual solvents. In the same temperature range, 1 and 2 functionalized graphene show about 54% and 36% weight loss, respectively. This weight loss is attributed to the decomposition of organic functional groups attached onto graphene. The degree of functionalization was estimated to be one functional group per 10 carbon atoms for 1 functionalized graphene, and per 50 carbon atoms for 2 functionalized graphene. In summary, mass variation compared to the pristine sample, underlines the presence of defects, absorbed molecules or chemical bonded functional groups.

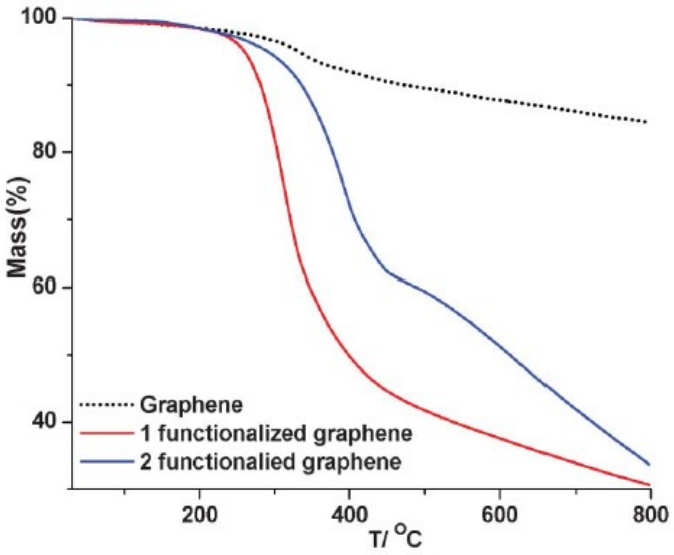

Figure 11: TGA analyses of graphene, 1 and 2 functionalized graphene (Reproduced with the permission from reference [23], copyright Royal Society of Chemistry, 2012).

1.3 Influence of nanomaterials on hydration of cement

As we already discussed in the previous section (1.1.2), the hydration of cement is an exothermic process, in which the temperature generated depends on the total heat evolved, the rate of reaction, and the thermal efficiency of the system [24].

The elevated specific surface area and the high aspect ratio (the ratio between length an thickness) of nanomaterial promotes and accelerates the chemical reaction rate of CCMs [25], by improving nucleation sites and filling the pores between hydration products, leading to a stronger matrix. As a consequence, they improve the early mechanical strengths, and the interfacial connectivity among aggregates and cement hydration products [26]. In addition, due to their reduced dimension, nanomaterials act as super-filler, reducing the porosities and improving the packing densities of CCMs, with positive effects for their service-life [27]. For example, it was demonstrated that significant mechanical strengths improvements can be obtained using nano-Al_2O_3 [28], [29], nano-TiO_2 [30], [31], or GBMs [32]–[35].

The positive influence of nanomaterials to improve the hydration rate can be evaluated by isothermal calorimetry. For example, R. Palla et al. [36] studied the evolution of the hydration heat as a function of the silica nanoparticles percentage in cementitious pastes. The positive effect attributed to the addition of nanoparticles is reported in Figure 12, in which, as the amount of nanoparticles increases, the heat of hydration increases, indicating the acceleration in early hydration rate of the cementitious system.

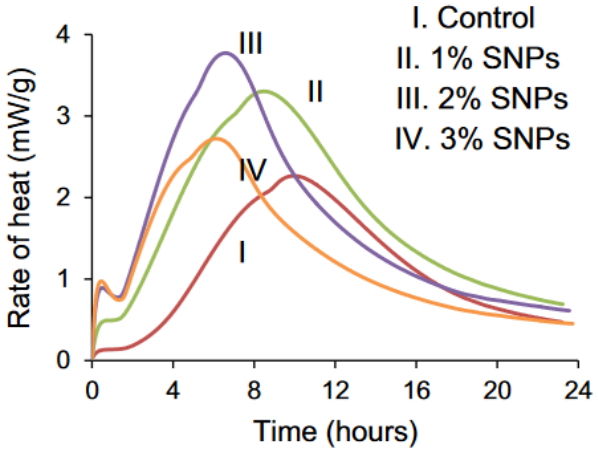

Figure 12: rate of heat of hydration varying nanoparticles content (Reproduced with the permission from reference [36], copyright Elsevier Ltd., 2017).

Other studies showed similar results [37], [38]; for all of them, the availability of a large number of nucleation centres, offered by the nanomaterials addition, accelerate the hydration reaction rate, leading to a more compact matrix with higher mechanical strength and better durability. Absorbing water on their surfaces, nanomaterials can behave as nano carriers of water, improving its dispersion and promoting the nucleation speed of cement.

Graphene based materials (GBMs), such as graphene, graphene oxide (GO), graphene nanoplatelet (GNP), and carbon nano tube (CNT), with their exceptional mechanical properties and elevated specific surfaces, are considered the most promising additives for the enhancement of CCMs performances. In addition, GBMs can be incorporated into CCMs to promote construction sustainability consuming less cement but greatly improve mechanical properties [39], promoting innovative architectural and structural designs with less self-weight, showing excellent permeability resistance due to low porosity, demonstrating high early strength that can reduce construction cycle times, providing ultra-strong electromagnetic interference (EMI) shielding property, electrical conductivity, thermal conductivity and so on [40]–[42]. More information about the chemical and physical characteristics of GBMs used in this study are reported in section 1.4.

Graphene oxide (GO), due to the hydroxyl, epoxide, carboxyl and carbonyl functional groups on its surface, exhibits superior dispersion in the cementitious matrix, making it one of the most researched GBMs in CCMs [43], [44]. In the complex system of hydrated cement, the GO nanosheets can promote the nucleation of calcium-silica-hydrates through a seeding effect, reducing the energy barrier of the hydration process, and leading to an accelerating effect [45],

[46]. Li et al. monitored the heat development of samples containing 0.04% bwc of GO, and revealed an earlier and higher heat peak, indicating the accelerated cement hydration process [47].

The positive contribution of GO for the performance of CCMs can be maximized if homogeneously distributed in cementitious matrix. The hydrophilicity of GO favours its dispersion in aqueous media, nevertheless its use in cementitious matrix can be limited due to the alkaline cement pore solution that contain high ions concentration (Ca^{2+}, Mg^{2+}, Na^{+}, etc.). Divalent cations crosslink GO nanosheets, causing their aggregation and limiting their homogeneous dispersion in cement [48]–[50]. More in detail, due to the alkaline pH environment, the carboxyl group of GO nanosheets are de-protonated and coordinates calcium cations released from the dissolution of alite in water [51]. With the removal of functional groups, the electrostatic repulsion between GO sheets decreases (and the hydrophobicity increases), leading to the aggregation of GO. Therefore, the positive apport to the strength improvement and the realization of more compacted structure in CCMs is negatively affected.

Graphene (G) has theoretical specific surface area (SSA) up to 2630 m^2/g, which is much larger than that reported to date for GO (1800 m^2/g) or CNTs (1330 m^2/g). Similarly, all the other characteristics, such as tensile strength, Young's modulus, aspect ratio, are extremely superior compared to the rest of GBMs. Due to its remarkable mechanical performances, its use as nano reinforcing material in cement generated great attention. Unfortunately, due to its hydrophobic behaviour and strong intermolecular van der Waals interactions, tends to form aggregates in aqueous media. Thus, the key factor to increase the interfacial interaction between graphene and the cement matrix is improving the graphene dispersity in water. It would represent the first key step for scalable production of graphene sheets modified concrete [9].

Graphene nanoplatelets (GNPs) are comprised of layers of graphene sheets (typically $10 < n < 100$, with n being number of layers) with thickness <100 nm and diameter of several micrometres, presenting intermediate properties compared to graphene. Due to its increased thickness, GNPs are a cheaper alternative to graphene and therefore the preferred form of GNS for cementitious composites [52]. Similarly to graphene, the use of GNPs for application in CCMs is limited by the difficulties to obtain homogeneous distribution in the cementitious matrix. In summary, dispersion methods appear as the most practical approaches to encourage the application of GBMs reinforced cement materials in the construction practice.

1.3.1 Mechanical properties of CCMs containing GBMs

GBMs act as pores' fillers in the cementitious matrix and make it more compact. Thanks to their high specific surfaces, these nanomaterials provide extra nucleation sites and promote the hydration of the cement, leading to extra C-S-H clusters formation. In addition, the bridging effect offered by the graphene in the cement composites can effectively prevent the formation and constrain the propagation of microcracks [53]–[55]. As a result of refining micro-cracks and filling pores, GBMs increase the homogeneity of cementitious matrix and enable the network stronger than the traditional cementitious materials [56], with positive effects on the mechanical strength. Several other studies have observed considerable mechanical enhancements using nano additives and nano-filler such as nano-silica, nano-iron oxide, nano-alumina, nano-titania, and nano-carbon additives [57]–[60]. In addition, the incorporation of nanomaterials also providing completely new functionalities and capabilities.

It was demonstrated that the addition of GO allows to improve the mechanical performance of cementitious materials [34], [61], [62], also where no special treatment for ensuring appropriate GO dispersion within cement matrix was applied [63]. The introduction of a little amount of GO, (less than 0.1% bwc), can increase the compressive strength of CCMs by 15–47% [34], [64]–[66] and can provide other smart properties, such as electrical conductivity, self-sensing capacity, and so on [67].

In addition, thanks to its high surface area (up to 1550 m^2/g), GO provides high contact area with cementitious materials. In this way GO creates a strong network within the cementitious matrix and provides high bond capacity of the matrix composites and dense structure.

Over the past years, cement composites infilled with graphene or GNPs have been continuously reported to exhibit remarkable enhancement on the mechanical properties [68]–[72]. The enhancement of graphene to the compressive strength, flexural strength and energy absorption capacity are different and vary from 3% to 80%.

The reasons leading to different enhancement on mechanical properties can be attributed to different dosage of graphene used in the cement composites, different degree of dispersion of graphene in water (and subsequently in the cement matrix), and different specific surface area of graphene used in the cement composites. These three aspects are crucial in determining the wide variability of GBMS effects, sometimes contrasting, on the performance of GBMs debated in the literature. They need more in-depth studies, to distinguish their single or coupled potential contribution.

In addition, although previous studies have demonstrated the positive correlation between the dosage of graphene and the mechanical performance improvement the cement composites, no specific indication has yet been indicated. As a results, if well integrated with GBMs, CCMs can improve their sustainability, reducing the cement requirements and counteract strength reduction.

1.4 GBMs dispersion

The dispersion of GBMs in the cement matrix is a key challenge, upon which the mechanical and durability properties depend. Well dispersed graphene materials, can fill in the larger pores, bridge the cracks in the cement matrix and promote hydration [73]. On the contrary, agglomerated graphene materials will not contribute as much to the performance improvement. Consequently, an effective dispersion is essential, and represent the focus of this research.

In this regard, mechanical and chemical methods (or their combination), such as sonication, high-shear mixing, electromagnetic stirring, the use of surfactants, and chemical surface functionalization, can be used for the homogenous dispersion of GBMs in aqueous media [22], [74].

Among mechanical method, sonication is often preferred for dispersing graphene in an aqueous solution because it avoids damage to the material that could be induced through other mechanical methods [75].

The chemical methods include covalent functionalization and noncovalent interaction; the first involves the chemical modification of the graphenic material, while the latter is based on weak bonds (in particular with superplasticizers) that preserve the GBMs structure. The dispersion capability of surfactants is achieved by wetting, electrostatic repulsion and/or steric hindrance effects [75].

1.4.1 Mechanical method: Sonication

Sonication of GBMs in an aqueous solution is one of the most commonly employed dispersion methods in the literature. Sonication works by mechanical vibrations that are transferred in the liquid and create pressure waves, which cause the formation and collapse of microscopic bubbles (cavitation). Cavitation is responsible for the increase in temperature in the liquid as it causes the release of high energy levels which in turns aids the dispersion of materials [76]. The

effect of sonication duration has been investigated when the process was performed using a power output of 300 W and a probe frequency of 20 kHz. It was shown that a sonication period of at least 60 minutes is required to ensure the deflocculating of graphene nanoplatelets agglomerates and stabilisation in an aqueous solution after 24 hours (see Figure 13) [77].

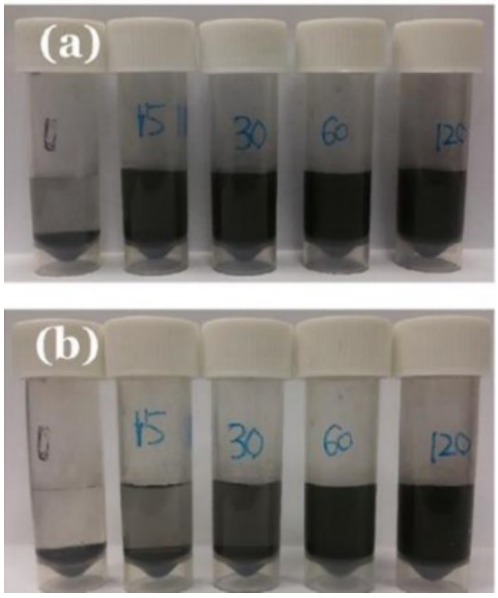

Figure 13: GNP aqueous suspensions after (a) 1 hour and (b) 24 hours. The sonication time varies from 0 minutes (left) to 120 minutes (right) (Reproduced with the permission from reference [77], copyright Elsevier Ltd., 2018).

One of the limitations of sonication treatments is the scalability; most of the industry is using ready-mixed concrete and large volumes of water are consumed per batch, meaning that sonication of large volumes of a solution could be problematic [78]. To alleviate this challenge, a possible solution could be the use of a dry mixing techniques, where the graphene nanomaterial is firstly mixed with the dry contents, followed by water and admixtures. In addition, mechanical method guarantees only the homogenous dispersion of GBMs in water, but they become ineffective when nanosheets are dispersed in alkaline solution containing divalent cations, especially for graphene oxide [79].

1.4.2 Noncovalent interactions: Superplasticizers

Superplasticizers are water soluble organic polymers that act either as high range water reducers (for reducing the water/cement ratio) or as plasticizers (for improving workability). For both the application, the average dosages range between 0.1-3 kg per 100 kg of cement. Superplasticizers, including lignosulphonates, sulphonated naphthalene-based and

polycarboxylates achieve their dispersion capability by wetting, electrostatic repulsion and/or molecule intercalation [22]. In particular, polycarboxylate-based product work primarily by steric hindrance and are effective in uniformly dispersing carbon nanomaterials.

Polycarboxylate-based superplasticizers adsorb on to the cement particles and create a physical barrier between them, so they prevent agglomeration (Figure 14). They can be engineered to meet the specific concrete requirements around workability and strength.

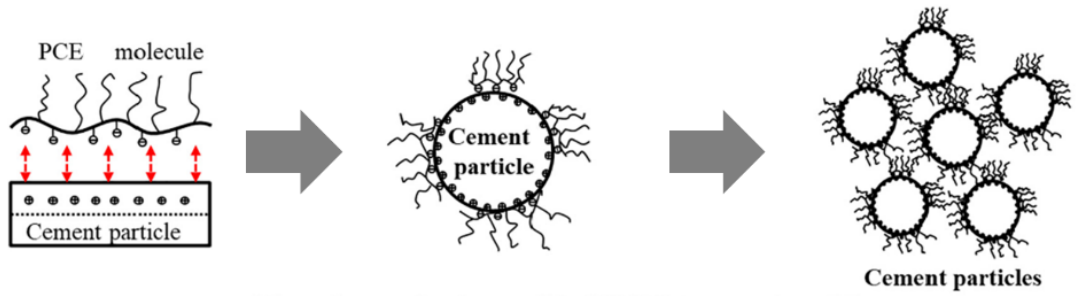

Figure 14: polycarboxylate superplasticizer working by steric hindrance effect to prevent agglomeration (Reproduced with the permission from reference [80], copyright Elsevier Ltd., 2019).

Since surfactants, such as polycarboxylate-based superplasticizer (PCE), are already routinely used in concrete mixes, they can facilitate the application of GBMs without complex modifications in the concrete fabrication processes. Recent researches have demonstrated that PCE can disperse GBMs, in particular GO, in saturated $Ca(OH)_2$ solution or in simulated chemical environment one [22], [81]–[83]. These results have been demonstrated also with calorimetry experiments (see Figure 15), in which cementitious samples containing GO and PCE showed a significantly increased heat peak flow respect to the samples without PCE, demonstrating the accelerating role of dispersed GO sheets when PCE was used [84].

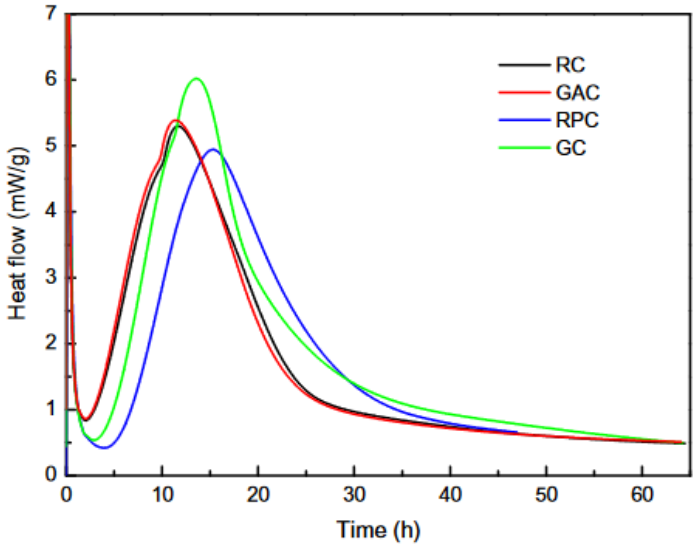

Figure 15: Hydration heat development curves of RC: reference; GAC: cement with GO; RPC: cement with PCE; GC: cement with PCE modified GO (Reproduced with the permission from reference [84], copyright Elsevier Ltd., 2009).

However, in other study [85], PCE was found to be ineffective in preventing GO from aggregating in the Portland cement paste. This inconsistency may be correlated with the specific molecular architecture of PCE (e.g. content of anchor groups, charge density, length of side/main chains, and polymer molecular weight) together with the characteristics of GO (e.g. sheet size, concentration, and oxygen content) [86]. For these reasons, the use of PCE, alone, seems to be not sufficient to disperse GO in cement pore solution, and is preferable to prevent the re-aggregation of GBMs using surfactants in combination with ultrasonication or other techniques [87], [88].

1.4.3 Covalent functionalization – Tour's reaction

Covalent functionalization of graphene represents a very challenging and important research field within the science and technology of the so-called ''synthetic carbon allotropes''. This process can be formally considered as an introduction of defects and leads to the modification of the electronic (band structure), optical, and mechanical properties of the 2-D carbon allotrope. Moreover, the covalent functionalization offers the opportunity to improve the solubility and processability of graphene, which would be otherwise difficult to master in terms of practical applications. Several strategies have been used for the covalent functionalization of GBMs, most of them employing synthetic protocols previously applied to the functionalization of fullerenes or carbon nanotubes. Synthetic strategies involving the addition to graphene of

phenyl radicals [89], diazonium compounds [90], azomethyne ylids [91], fluorinated phenyl nitrenes [92], carbenes [93], or Diels-Alder cycloaddition reactions [94], allowing the incorporation of a wide variety of chemical units onto the GBMs' surface.

A general problem of all these reactions is the rather low degree of functionalization, due to the fact that graphene is a rather inert system. Because of its planar structure and the lack of any carbon atom pyramidalization it is much less reactive with respect to fullerenes or carbon nanotubes [95]. In addition, if the graphene sheets are homogeneously dispersed in a suitable medium, it can be attacked from both sides of the plane, improving the efficiency of the functionalization process [95].

Tour reaction

The Tour reaction is one of the most used synthetic approach for the functionalization of GBMs [96] and was firstly proposed for the functionalization of carbon nanotubes in 2001 [97]. In this reaction, an aniline derivative is transformed into a diazonium salt that, upon reductive decomposition, affords aryl radical species, responsible for the functionalization of the GBMs. When the aryl radical reacts with a graphitic surface leaves a radical on the adjacent carbon that may further react or be quenched by solvent. The propensity of the initial aryl radical to dimerize or abstract a hydrogen atom from the solvent is minimized by the fact that the radical is generated at the surface of the nanotube. Indeed, herein lies the principal advantage of this method, as opposed to a solution-phase method in which the diazonium salt reduction is catalyzed by copper or other metals [98].

A schematic representation of the reaction is shown in Figure 16, where the nitrogen extrusion by reductive dissociation of the diazonium salt is evidenced.

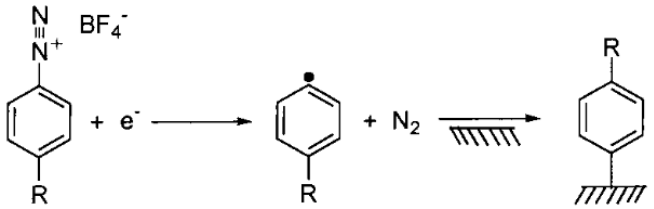

Figure 16: Electrochemical reduction of an aryl diazonium salt, giving a reactive radical that covalently attaches to a carbon surface (Reproduced with the permission from reference [98], copyright American Chemical Society, 2001).

In the case of CNTs, this process yields functionalized products with degree of functionalisation, density of defects and solubility amongst the highest reported in the literature due to the high reactivity of the radical species involved. For example, C. A. Dyke et al. [99] functionalized up to one ninth of their carbon atoms with aryl groups.

J. M. Tour extended this functionalization method also to graphene nano sheets. In particular, surfactant-wrapped graphene sheets, obtained from reduction of graphene oxide with hydrazine, were functionalized by treatment with aryl diazonium salts. The reaction most likely involves an electron transfer from graphene to the diazonium ion, as in the case of SWCNT, followed by extrusion of N_2 and a subsequent addition of the aryl radical to the graphene layer [100]. The efficacy of the functionalization was confirmed by thermogravimetric analysis (TGA). Indeed, the degree of functionalization was estimated to be ~1 functional group in 55 carbons from the weight losses.

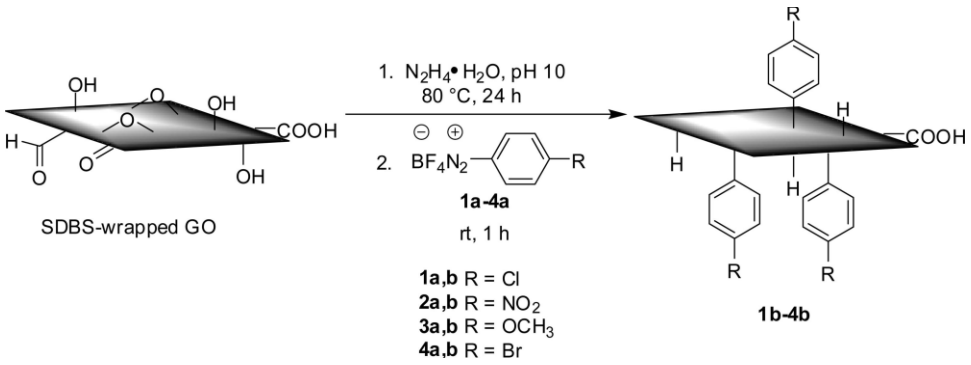

Figure 17: schematic reaction of wrapped GO reduction, and functionalization with diazonium salts (Reproduced with the permission from reference [100], copyright American Chemical Society, 2008).

Despite graphene resulted less reactive than CNTs, because of its planar structure, single graphene sheets are found to be almost 10 times more reactive than bi- or multilayers graphene. In addition, the reactivity of edges is at least two times higher than reactivity of the bulk single graphene sheets [101]. Nevertheless, the functionalization with aryl diazonium salts was successfully used also to modify graphene nanoplatelets, both in organic solvent [102], [103], and in aqueous media [96], [104]–[107]. If a reaction proceeds in water then replacement of environmentally unfriendly, potentially dangerous, and/or expensive organic solvents with water would be beneficial, [108]. Even reactions with water-insoluble solids have generated successful results, proving water solubility is not always necessary [109].

Also the substituent groups on the phenyl ring influence the functionalization' yield. Z. Tavakkoli et al. [110] demonstrated that the diazonium salts showed different activity varying functional groups, such as Cl, OH, NO_2, OCH_3 or SO_3^-. Finally, they found that methyl group led to higher functional degree.

Finally, the use of aryl diazonium salts, generated in situ, allows the preparation of self-tailored functional GBMs with improved dispersion capability in aqueous solvent, providing the

possibility to reduced re-agglomeration effects that occur in cementitious matrix. For all these aspects, the functionalization processes by diazonium chemistry resulted fundamental for this thesis work, in particular for the application of low quality cheap GBMs, essential for the use in construction field.

1.5 Scope of the thesis

This thesis aims to functionalized commercial Graphene Based Materials (GBMs), through covalent reaction, to improve their homogeneous dispersion in water, and consequently, in cementitious matrix.

The functionalization reaction was performed by adding the reagents responsible for the diazonium salts formation to four different commercial GBMs, providing a negative, positive, or neutral groups to their surfaces. The functionalization yield and its positive effect to increase the hydrophilicity of GBMs were evaluated through thermogravimetric analysis (TGA), and UV-visible spectroscopy.

Preparing cementitious mortars, and using two different pre-mixing techniques, we also evaluated the positive contribution of these materials to improve the mechanical strengths of Cement Composite Materials (CCMs).

Structure of the thesis

- *Chapter one* begins by outlining the state of the art of cement with particular emphasis on the use of nanomaterials as strengthening agents. It also provides an introduction to the chemical and physical characteristics of GBMs.
- *Chapter two* deals with the fast functionalization of GBMs with different functional groups. It reports a step by step description of the reaction used for the production of functionalized GBMs.
- *Chapter three* presents the mechanical performance of mortar samples prepared using GBMs, evaluating the influence of the different functional groups used for the functionalization and their percentages.
- *Chapter four* compares the results obtained in the chapters 3 and 4, evaluating the influence of GBMs and providing the final findings.
- *Chapter five* describes the mechanical performance of mortar samples prepared with functionalized CNTs, provided by research group of prof. Enzo Menna.

2. Covalent functionalization of Graphene Based Materials

Graphene based materials (GBMs), due to their hydrophobic nature, tend to irreversibly form agglomerates or even restack to form graphite when dispersed in an aqueous media [21]. The addition of hydrophilic groups, through chemical functionalization, can prevent this phenomenon thanks to an increased water solubility. Tailoring of graphene sheets become necessary for their final applications, enabling this material to be processed by solvent, improving its dispersion in aqueous media, and preventing the agglomeration of single layer graphene (SLG). In this regard, the chemical modification of carbon nanostructures by the Tour reaction is a versatile strategy to obtain soluble nanomaterials with high degrees of functionalization. In this way, the functionalization of GBMs is performed by adding the reagents responsible for the diazonium salts formation, an aniline derivative and an alkyl nitrite, to a graphenic suspension obtained dispersing GBMs in the solvent (N-methyl pyrrolidone (NMP) or water).

Starting from these premises, we have functionalized four different commercial GBMs through their covalent modification and preparing new compounds able to give homogeneous dispersions in a cementitious matrix. The aim was to increase solubility and dispersion by inter-layer electrostatic repulsion and promote intercalation of hydrophilic functional moieties, providing positive, neutral, or negative charge to the GBMs surfaces.

It is important to note that not all the hydrophilic groups can be considered suitable for the functionalization process. For example, the use of carboxylic moieties, due to their notable coordinating ability, would represent a limit for the dispersion of GBMs in cementitious environment. Indeed, the divalent cations present in the cementitious matrix (Ca^{2+} and Mg^{2+}) would cross-link with carboxylate groups from GBMs, resulting in the agglomeration of their nanosheets [50], [111].

For these reasons, we selected:

- arylsulfonate as a negatively-charged functional group, introducing non-coordinating anion to limit the possible Ca^{2+} and Mg^{2+} cross-linking phenomena with graphene sheets;
- polyethylene glycol chain as a neutral group, exploiting its water solubility to solvate divalent cations and stabilize the graphene layers in polar solvents;
- quaternary ammonium salt as a positively-charged group, introducing positive charges that avoid the GBMs' aggregation by repulsive forces.

The functionalization reaction with different para-substituted anilines is pictured in Figure 18. The molar ratio between carbon and the aniline derivate was fixed at 5:1.

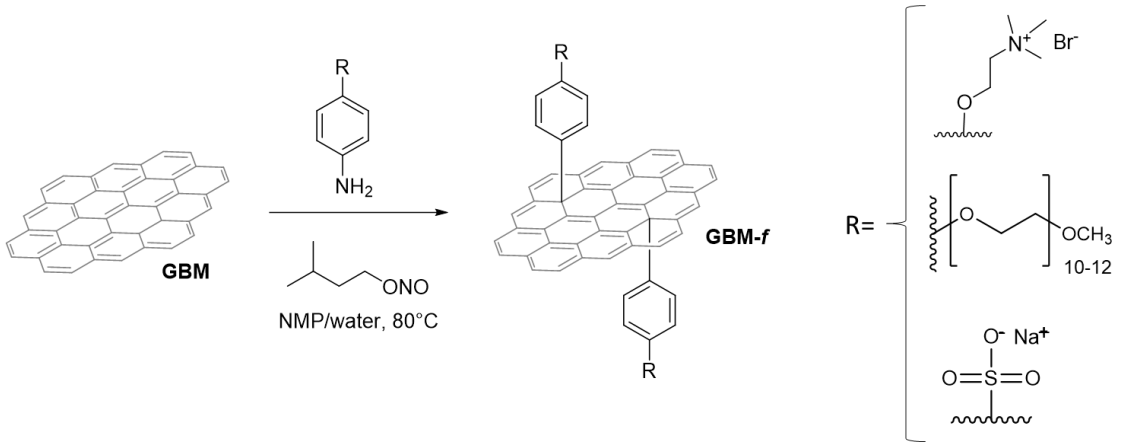

Figure 18: functionalization of GBMs by Tour reaction.

The number of layers and the quality of starting GBMs are relevant features to obtain materials with high degree of functionalization [95]. These aspects encouraged us to start this work functionalizing single layer graphene, as the high superficial area guarantees the maximum functionalization yield. Subsequently, the same methodology was extended to few layers GMBs and nanoplatelets.

The functionalization yield and its capability to increase the hydrophilicity of GBMs were evaluated through thermogravimetric analysis (TGA), and UV-visible spectroscopy. In addition, SEM images were collected to check the aspect ratio of individual graphene-based sheets, and their morphology after the functionalization process.

2.1 Functionalization with a quaternary ammonium group

In this section, we report an approach to synthesize a positively charged SLG by Tour reaction. Firstly, we have synthesized *Compound 1d* (see experimental section 2.6) [112], an aniline suitable for this covalent functionalization (see Figure 19).

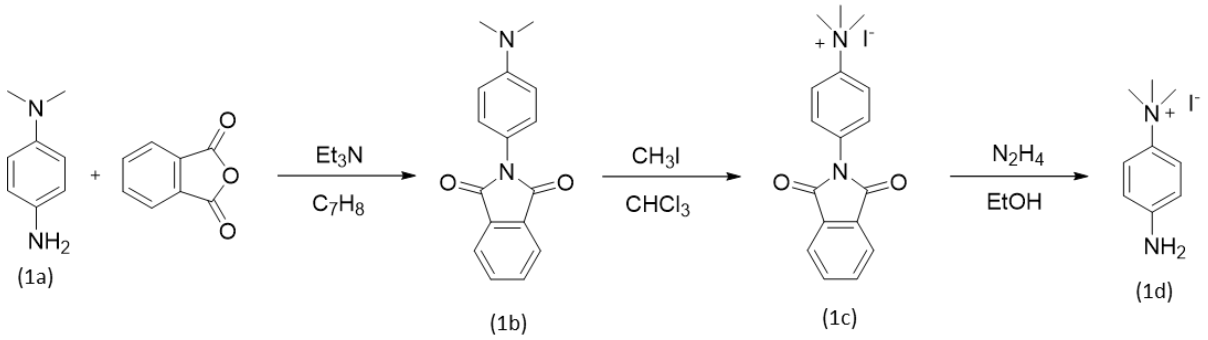

Figure 19: synthesis of Compound 1d [112].

The quaternary ammonium group shown in Figure 19 was obtained after 3 steps reaction, starting from commercial N,N-Dimethyl-p-phenylenediamine. Despite we efficiently have synthesized the desired molecule, as confirmed by NMR and ESI-MS analyses (see experimental section), the functionalization carried out on SLG with this group (sample *CE-1d*) resulted in a negligible functionalization yield, and no relevant weight variation was measured in TGA. In addition, also UV-vis spectroscopy confirmed this aspect, indeed no absorbance signal was measured.

After the first attempt, we efficiently synthesized another aniline bearing a quaternary ammonium group, *Compound 2d* (see experimental section 2.6), that was used for the covalent functionalization of SLG (see Figure 20).

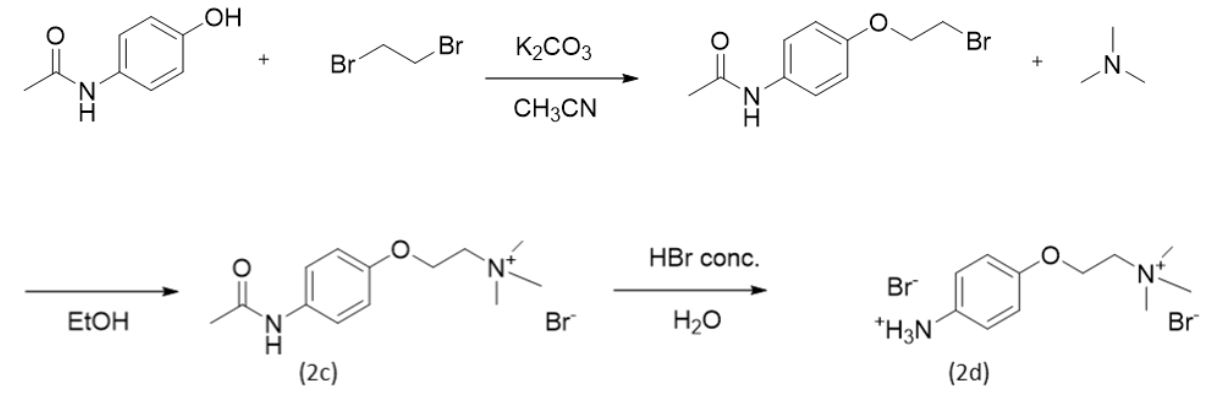

Figure 20: synthesis of Compound 2d.

Compound 2d yielding a platform with positive charges able to disrupt the hydrophobic surface of pristine graphene. Table 3 reports the functionalized product obtained.

Table 3: functionalized single layer graphene with quaternary ammonium group.

Starting GBMs	Fatures	Functionalized product
Carlo Erba **CE**	Single layer graphene	***CE-f(+)***

Results and discussion

The successful covalent functionalization of CE graphene was verified by thermogravimetric analysis (TGA). The temperature modulated curves for *CE* and *CE-f(+)*, reported in Figure 21, indicate that pristine graphene CE remain stable until 650 °C, whereas the functionalized material presents two weight losses of ~ 10% at 150 and 300 °C, respectively [113]. The first weight loss is probably related to the degradation the quaternary ammonium group, then, the degradation of the resting part of the arene fragment is observed at 300 °C. In Figure 21 we also indicated the functional degree of *CE-f(+)* measured by the weight loss between 100 °C and 650 °C, defined as the ratio between the moles of attached aryl moieties and the moles of carbon, FD=1/68.

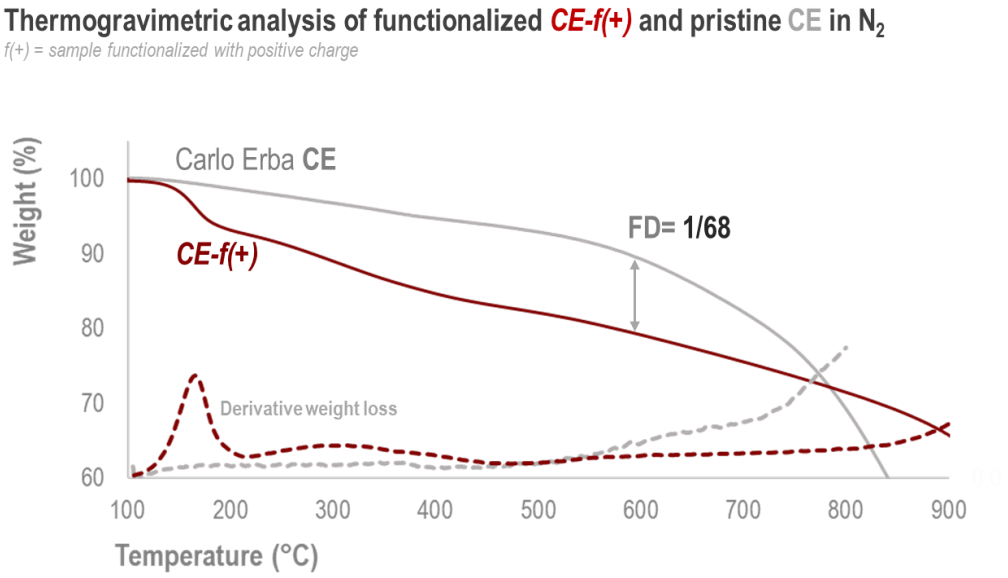

Figure 21: TGA for positive functionalized single layer graphene CE-f(+).

The dispersion behaviour of GBMs in water deserves attention because it can give an indication of their distribution in the cementitious matrix. Figure 22 shows the UV-vis spectra of the supernatant obtained sonicating *CE-f(+)* with water (see experimental section). The highest absorbance value was measured around 270 nm, this value is similar to the specific absorption peak of graphene [114]. The curve trend indicates enhanced dispersion capability in water (the supernatant was diluted 29 times to reach the evaluable concentration).

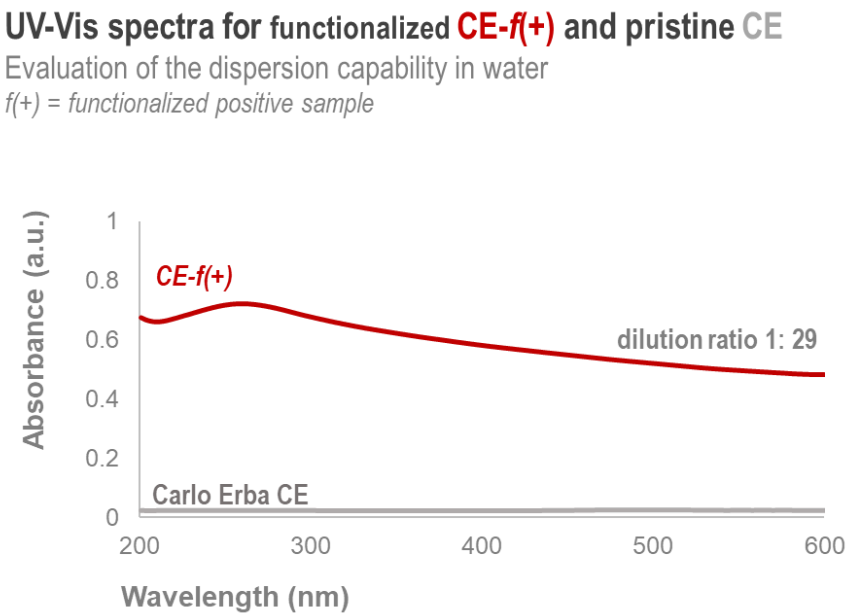

Figure 22: UV-vis analysis of functionalized GBMs with positive moiety CE-f(+).

Figure 23 shows representative SEM micrographs of pristine and functionalized single layer graphene *CE-f(+)*. The layers size varies between 0.5 and 6 µm, with most of the flakes being ~3 µm. Both, functionalized and not functionalized graphene products, display a network of intense wrinkles and ripples on their surface, and no relevant difference between their morphology was noticed.

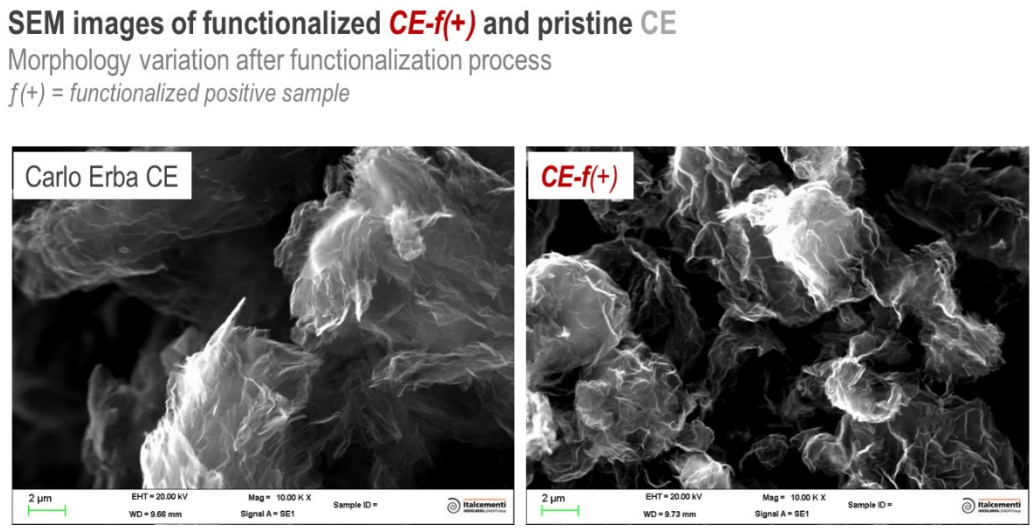

Figure 23: SEM images of the pristine (on the left) and functionalized (on the right) graphene CE.

Figure 24 shows the TGA of functional sample *CE-1d*, for which no relevant weight variation was measured in TGA.

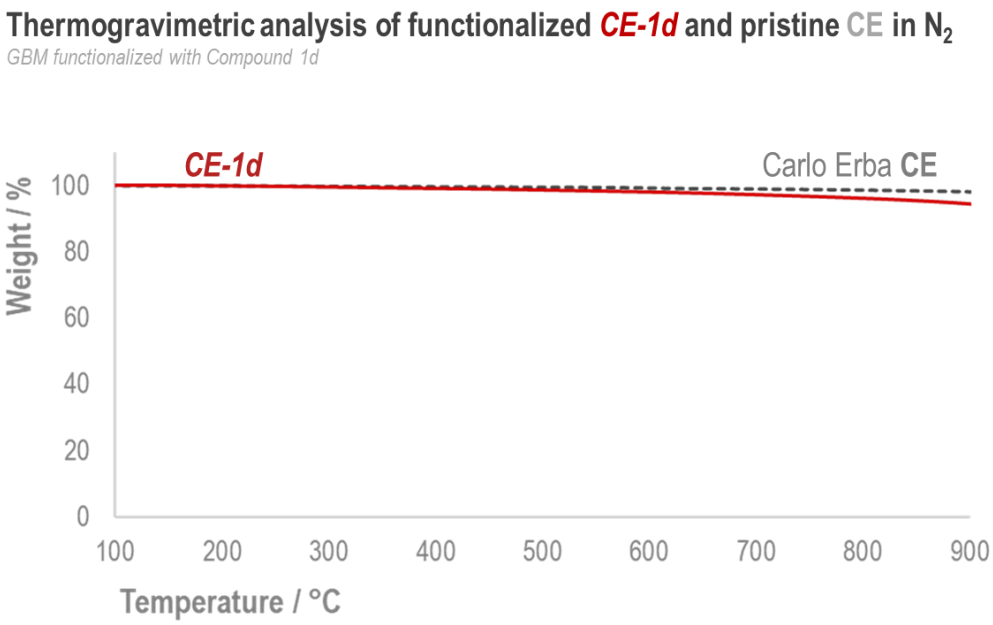

Figure 24: TGA for positive functionalized single layer graphene CE-1d.

Figure 25 shows the UV-vis spectra of the supernatant obtained sonicating *CE-1d* with water (see experimental section).

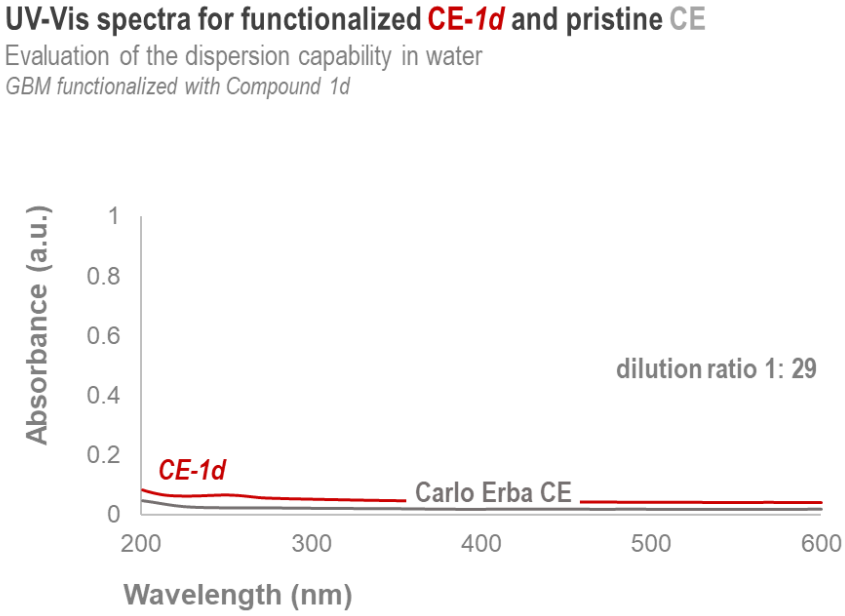

Figure 25: UV-vis analysis of functionalized GBMs with positive moiety CE-1d.

2.2 Functionalization with Polyethylene glycol chain

In this section report the synthesis of *Compound 3c* (see experimental section 2.6) an aniline functionalized with a long polyethylene glycol chain to covalently functionalize pristine high-quality graphene by Tour reaction.

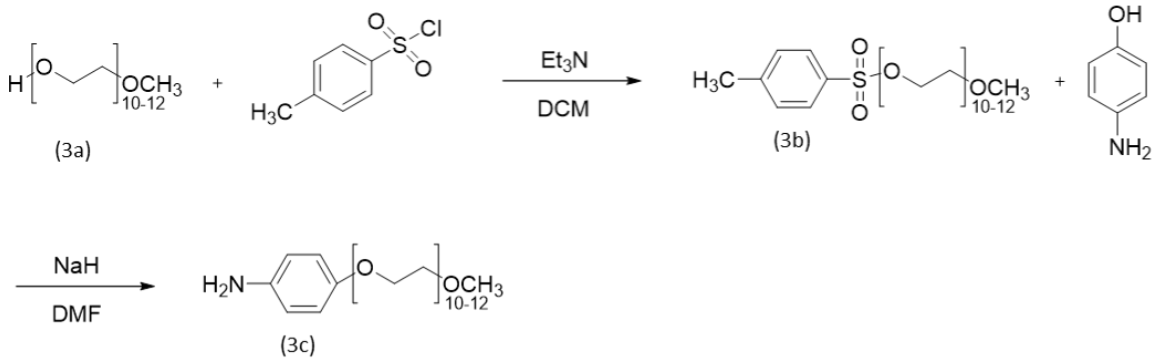

Figure 26: synthesis of Compound 3c [115].

The *Compound 3c* (see experimental section 2.6) was obtained after 2 steps reaction [115], starting from commercial Poly(ethylene glycol) methyl ether, with average molecular weight of 550 (Mn), where the terminal hydroxyl groups was tosylated and then reacted with 4-aminophenol in order to obtain the suitable aniline for the introduction of the functional groups to graphene lattice. The functionalized GBM is reported in Table 4.

Table 4: functionalized single layer graphene with Polyethylene glycol chain.

Starting GBMs	Fatures	Functionalized product
Carlo Erba **CE**	Single layer graphene	***CE-f(N)***

Results and discussion

Thermal properties of GBMs are dependent on many parameters such as particle size, number of layers, defects, and presence of functional groups. Figure 27 shows the key mass loss event of *CE-f(N)* at ~ 360°C, reaching ~ 30% of weight variation, which can be explained by the removal of functional groups from the carbon lattice. The subsequent degradation is related to the oxidative pyrolysis of carbon framework [116]. Pristine graphene *CE*, reported as grey curve in Figure 27, remain stable until 650 °C. The functional degree of *CE-f(N)*, measured on the weight loss between 100 and 650 °C was FD=1/128.

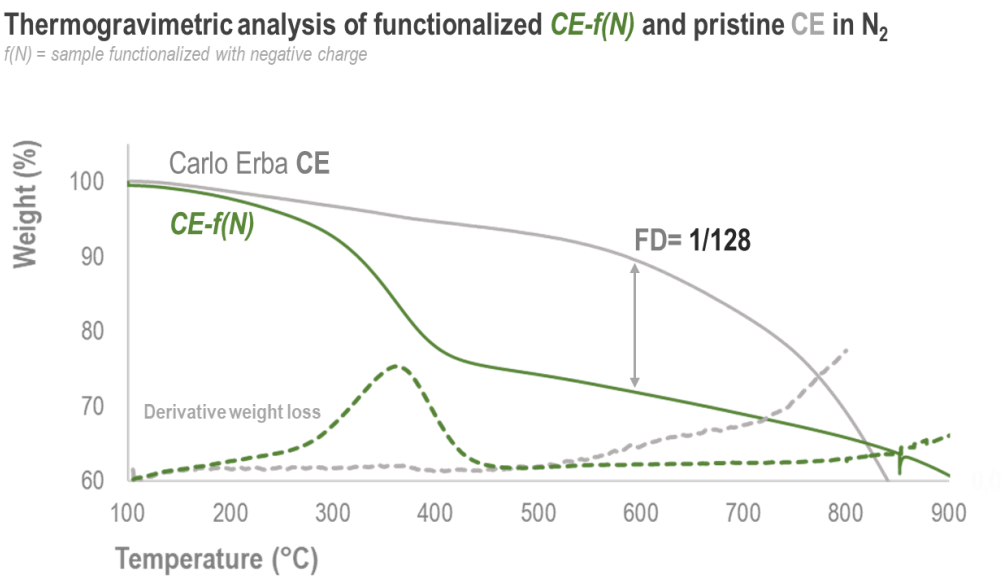

Figure 27: TGA for neutral charged functionalized graphene (CE).

The effects of functionalization on the dispersion of graphene in water were evaluated by ultraviolet–visible (UV–vis) absorption spectroscopy. Figure 28 shows the spectra of aqueous *CE-f(N)* dispersion, that exhibits the characteristic feature peak of graphene at ~ 270 nm [114]. The water dispersion remained stable for several hours (see experimental section for the preparation of *CE-f(+)* water dispersion).

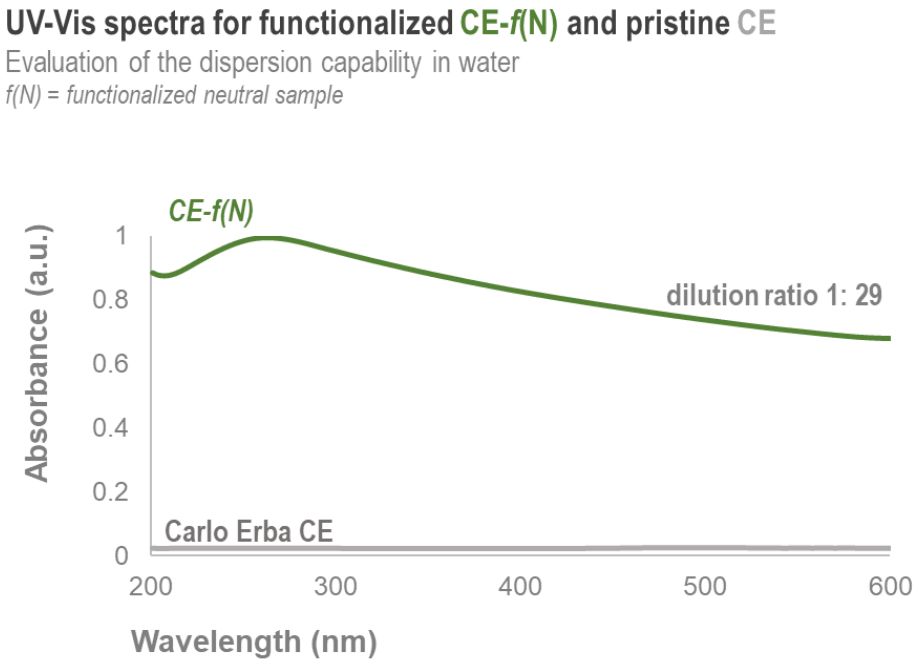

Figure 28: UV-vis analysis of functionalized GBMs with neutral moiety CE-f(N).

The morphology of the *CE-f(N)* graphene sheets was characterized using SEM analysis. In Figure 29, the products exhibit surface corrugations (wrinkles and ripples) and crumples, and there are no relevant differences between pristine and functionalized graphene. The layers size varies between 0.5 and 6 µm, with most of the flakes being ~3 µm.

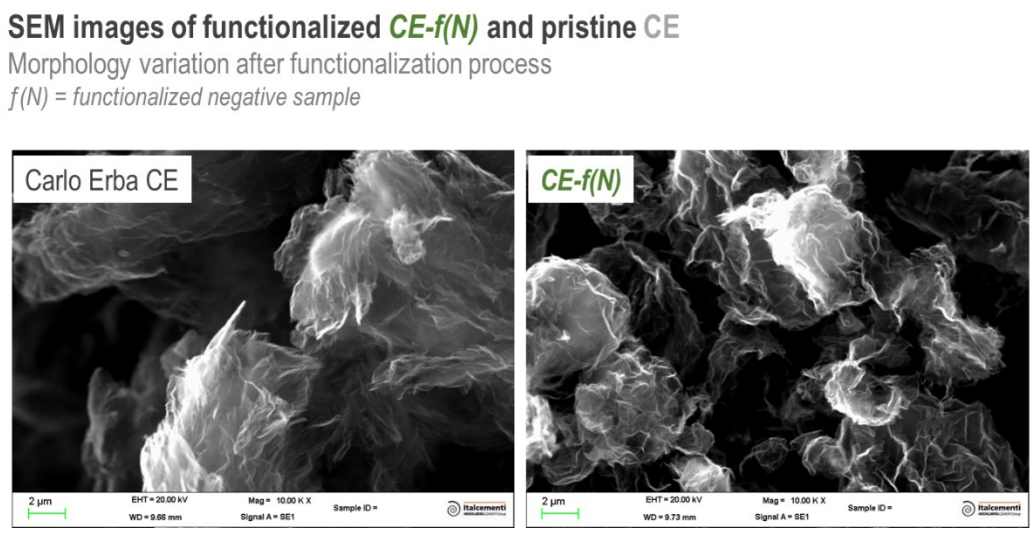

Figure 29: SEM images of the pristine (on the left) and functionalized (on the right) graphene CE.

2.3 Functionalization with Sulfonate group

For this study we have developed a chemical route to functionalize aqueous solutions of GBMs sheets by introducing sulfonate groups (see experimental section 2.6). The charged -SO^-_3 units prevent the sheets from aggregating, producing sulfonated graphene with improved water solubility [106]. The synthesis of functionalized SLG by Tour reaction was reported in Table 5.

Starting GBMs	Features	Sulfonate group
Carlo Erba **CE**	Single layer	***CE-f(-)***

Table 5: functionalized single layer graphene with Sulfonate group.

After the promises results obtained by the functionalized single layer graphene *CE-f(-)*, we selected other three commercial GBMs, from few layers to graphene nanoplatelets, with different quality e costs. Table 7 reports all the products synthesized.

Starting GBMs	Features	Sulfonate group
Proton Power **PP**	Few layer	***PP-f(-)***
NanoXplore **0X**	Nanoplatelets	***0X-f(-)***
NanoXplore **3X**	Nanoplatelets	***3X-f(-)***

Table 6: functionalized GBMs with Sulfonate group.

Results and discussion

Representative TGA graph for samples *CE-f(-)* is presented in Figure 30, showing TGA curve on the top and the corresponding first derivative thermogravimetry DTG curve on the bottom. The functional degree of *CE-f(N)*, measured between 100 and 650 °C, was FD=1/65.

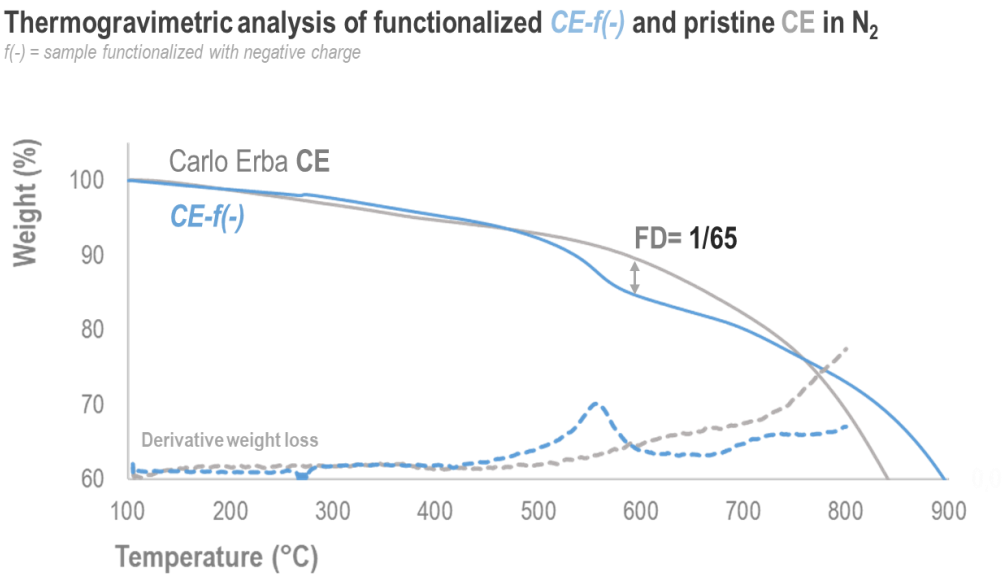

Figure 30: negative charged graphene single layer.

Sample *CE-f(-)* showed a weight reduction up to 10 %, compared to the starting material (CE). This is observed by the derivate weight loss peak measured at about 550 °C, that is consistent with the functional group covalently linked to the carbon lattice [102]. The presence of a single sharp peak confirmed the uniform functionalization of the GBMs with the sulfonate moieties.

The characterization of the other functionalized GBMs through thermo-gravimetric analysis is reported in Figure 31. No relevant weight variation was revealed for samples *PP-f(-)*, *0X-f(-)*, and *3X-f(-)* when TGA was conducted in N_2.

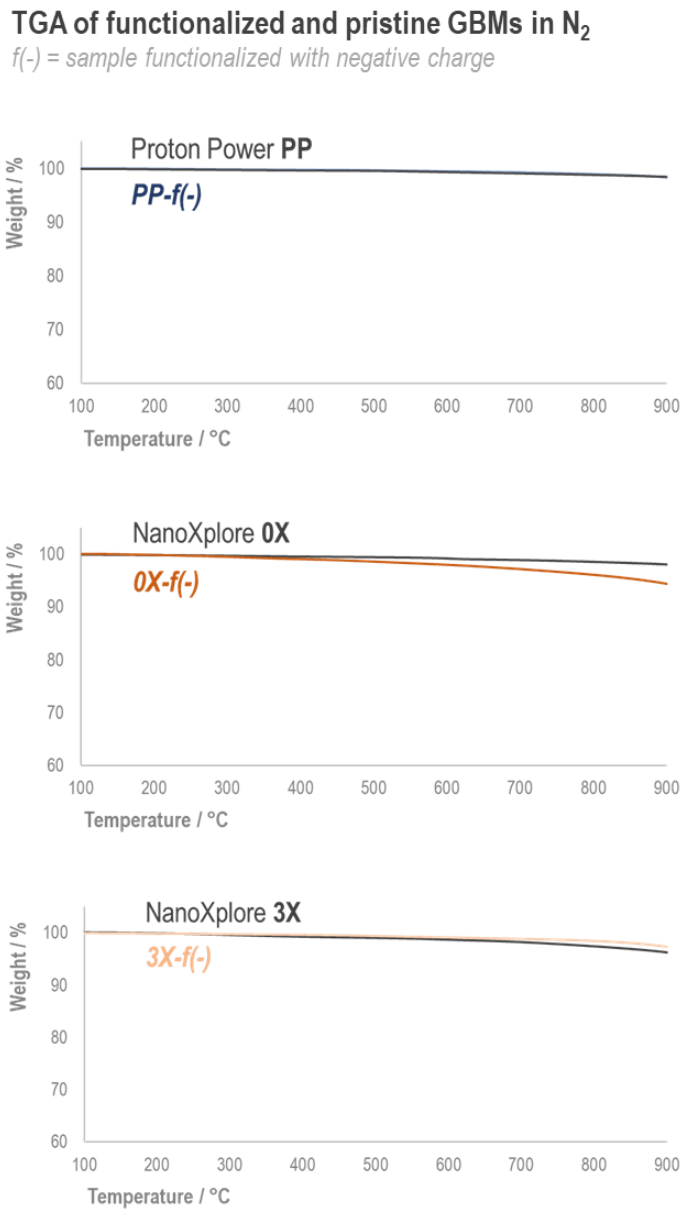

Figure 31: thermogravimetric analysis of pristine and functionalized GBMs in N_2/air. All the sample were functionalized with negative charged molecule.

The degradation temperature of GBMs exhibit a direct and linear relationship with their particle size and their nature (GO, graphene and graphite). In particular, carbon materials, with larger particle size and higher number of layers, tend to shift their degradation temperature to higher values because of slower combustion kinetics [117]. Excluding single layer graphene *CE*, all the other pristine products remained stable until approximately 800 °C in N_2, demanding more heat energy due to their stronger carbon network. Despite the technical data sheets declare that all the GBMs have less own 10 layers (see experimental section), the elevated degradation temperature measured in TGA would suggest that *PP*, *0X* and *3X* products behave more like high-layer products (i.e. graphite) than few-layer ones.

Figure 32 shows the UV-vis spectra of single layer graphene CE functionalized with negative charge (*CE-f(-)*).

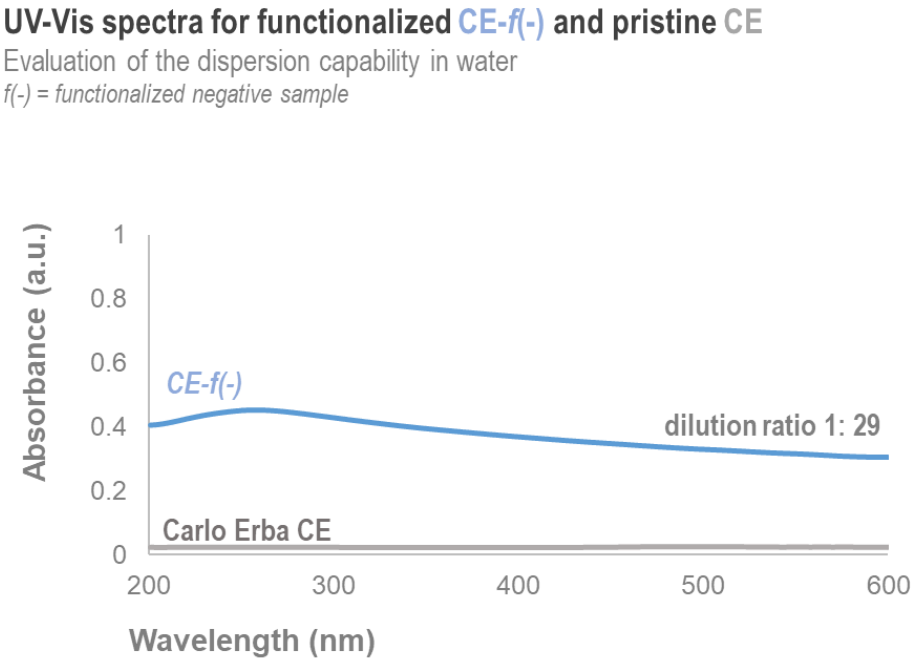

Figure 32: UV-vis analysis of functionalized GBMs with neutral moiety CE-f(-).

The absorption band measured around 270 nm for sample *CE-f(-)*, indicates the enhanced dispersion capability in water (dilution ratio 1:29) with respect to the pristine sample. A similar peak was observed also for the other functionalized GBMs, however, in order to get a noticeable difference with the corresponding pristine samples we had to prepare more concentrated solutions (dilution ratio 1:2). Figure 33 reports the water dispersion capability of the *PP-f(-)*, *3X-f(-)*, and *0X-f(-).*

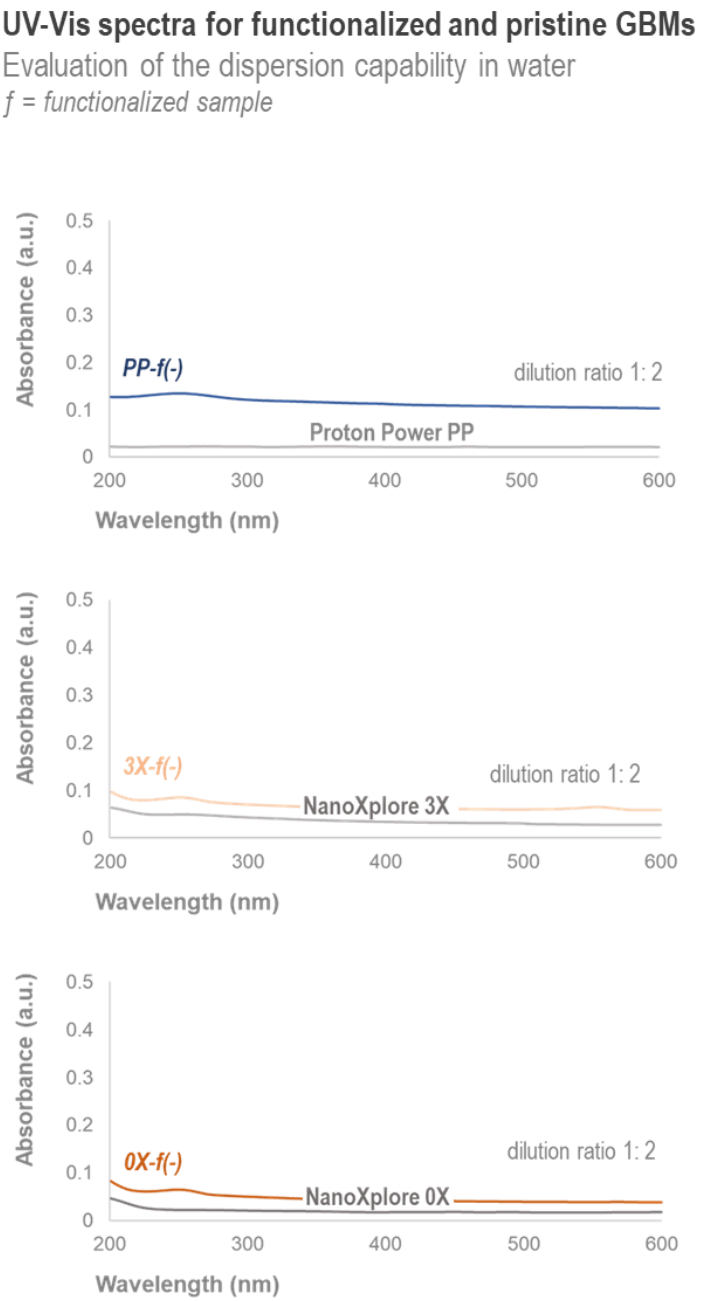

Figure 33: UV-vis analysis of functionalized GBMs with negative moieties.

The morphology of the negative charged SLG was studied by SEM, and the representative microphotographs is reported in Figure 34. For a better evaluation both *CE* and *CE-f(-)* images were reported.

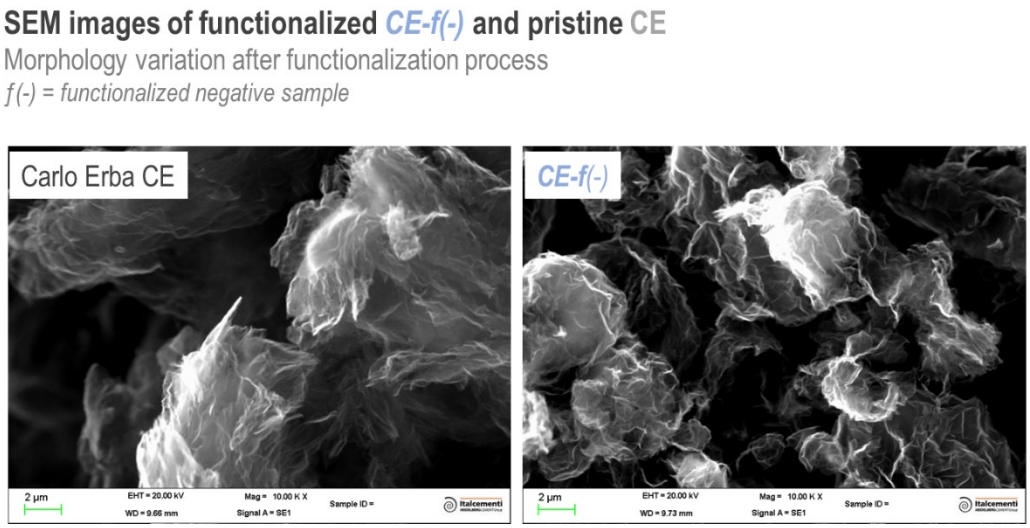

Figure 34: SEM images of the pristine (on the left) and functionalized (on the right) graphene CE.

Figure 35 reports SEM images of negative charged GBMs *PP-f(-)*, *3X-f(-)*, and *0X-f(-).*

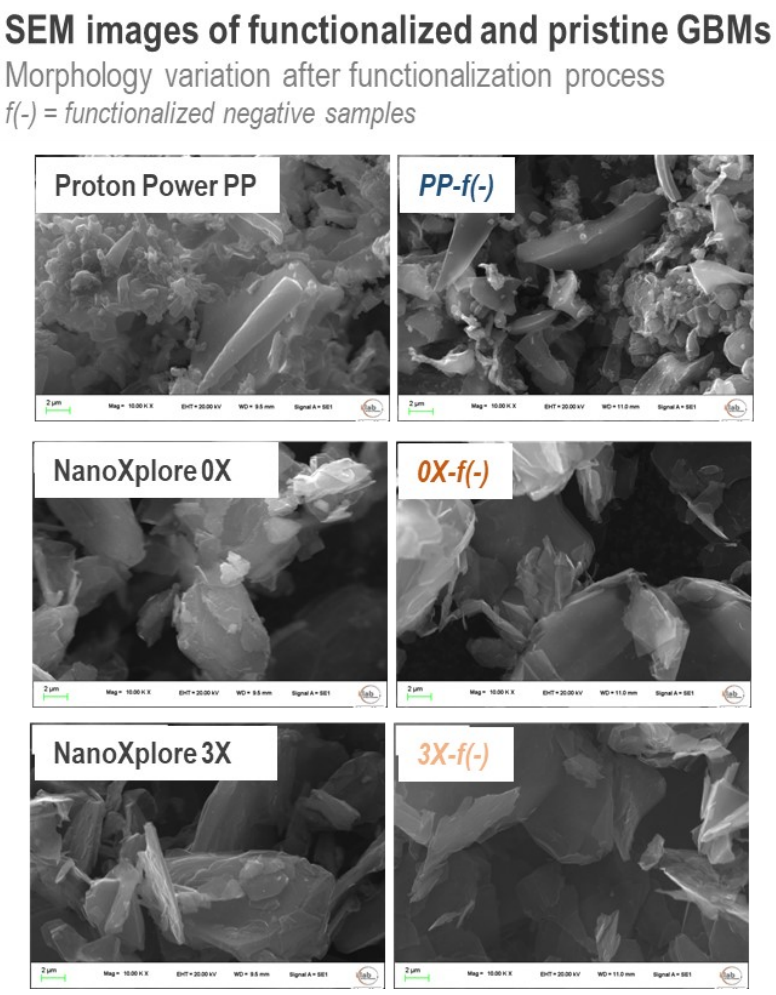

Figure 35: SEM images of the pristine (on the left) and functionalized (on the right) GBMs.

Comparing all the products, single layer graphene, both pristine and functionalized (sample CE and sample *CE-f(-)*), shows the highest lateral dimension (~ 6 µm) and the lowest thickness. In addition, CE graphene has a wrinkled and folded morphology that can guarantee high specific surfaces. In general, the pristine (on the left), and the functionalized GBMs (on the right) does not reveal any visible evidence of the functionalization process, nor significant change in their morphology. The size of folded platelets is ranging from several hundred nanometres to micrometres, according to the technical data sheets.

2.4 Dispersion capability of functionalized GBMs over time

The dispersion stability of the functionalized SLG was monitored for 60 minutes without seeing any absorbance variations (see Figure 36). This confirms the presence of negatively charged units ($-SO^{-}_{3}$) which in turn, impart sufficient electrostatic repulsion to keep carbon sheets separated during reduction.

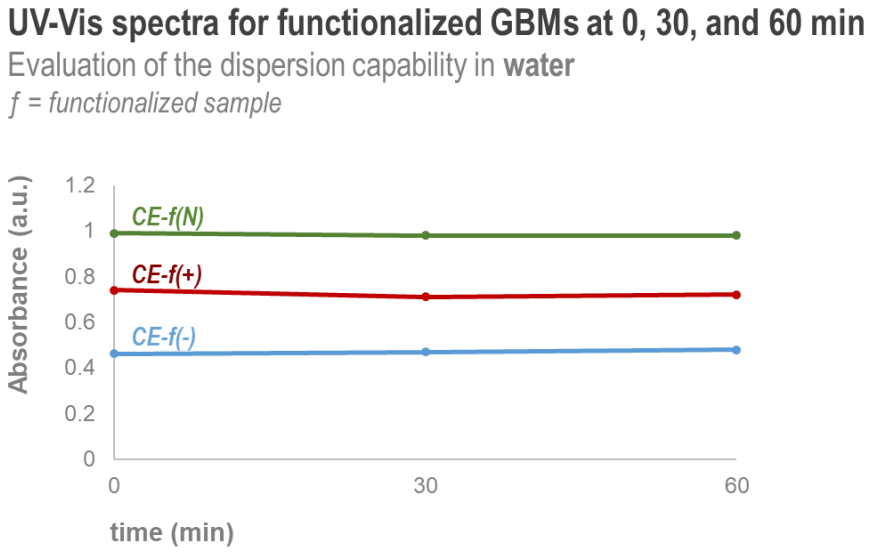

Figure 36: stability over time of functionalized GBMs in water – pristine graphene CE absorbance was zero.

Figure 37 reports the visually observation of pristine and functionalized *CE* before the supernatant sampling (see experimental section). All the functionalized products remain stable and homogenously dispersed for several hour, on the contrary pristine CE sample settled at the bottom of the tube and no dispersion was achieved.

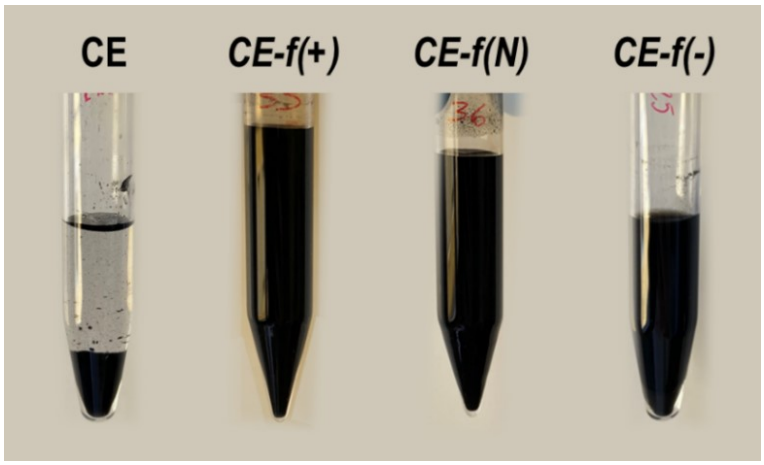

Figure 37: water dispersion of pristine and functionalized CE samples.

Contrary to *CE-f(-)*, in the visual observation of *PP-f(-)*, *0X-f(-)*, and *3X-f(-)* all the samples settled at the bottom of the tube and no dispersion was achieved (see Figure 38). It seems that the functionalization of GBMs took place only using single layer graphene.

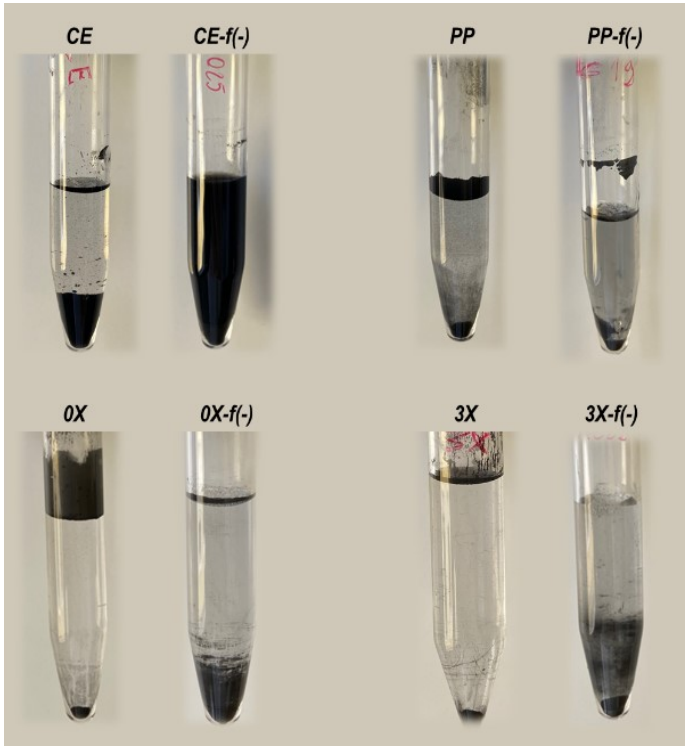

Figure 38: water dispersion of pristine and GBMs functionalized with arylsulfonate groups.

To study the dispersion of the GBMs in an alkaline cement environment, CE samples were dispersed both in saturated $Ca(OH)_2$ (pH= 12.5) and in a simulated cement pore solution (pH= 12.6). The results, reported in Figure 39, demonstrate that the absorbance remains constant at

least 60 min for all the functionalized products, and confirmed the stability of the samples also in severe environment conditions. Different from graphene oxide, functionalized GBMs are found to not agglomerate in the simulated cement alkaline environment [118].

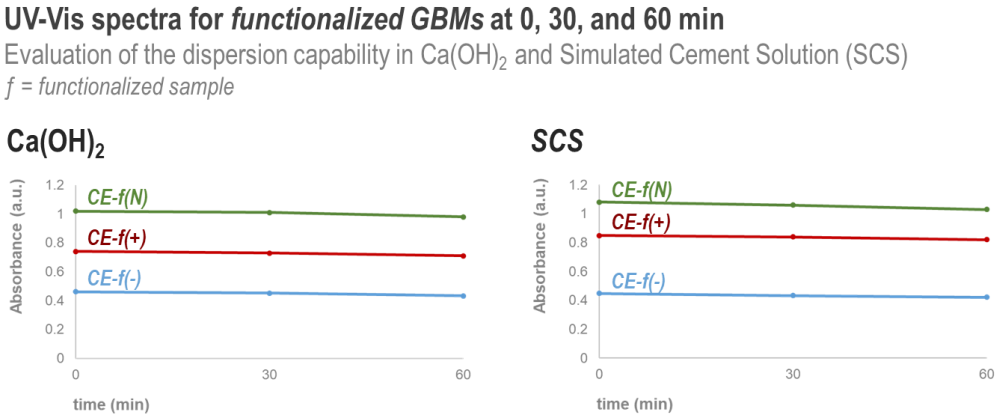

Figure 39: stability over time of functionalized GBMs – pristine graphene CE absorbance was zero.

2.5 Final findings

The quality of starting materials, as well as the functional groups characteristics, are key factors to obtain high functionalization degree. Literature data [95], [119] assert that high quality graphene provides an ideal substrate for the functional groups' attachment, for this reason, we firstly tested the feasibility of the functionalization on single layer graphene (high quality) before extending the methodology to few layers and nanoplatelets GBMs (lower quality). However, the possibility to use low grade, and low cost GBMs become necessary for their extended use in construction field, where versatile and economic water soluble graphenic materials are necessary. Hence, we studied the functionalization of GBMs using single layer graphene (CE) and attaching different para-substituted anilines that increased its hydrophilicity and water dispersions capability. In more detail, we modified CE graphene by the Tour functionalization, in order to introduce a sulfonate as negatively charge group, a polyethylene glycol chain as neutral group, or a quaternary ammonium as positively charged group.

The experimental results demonstrated that all functionalities attached to the CE surfaces guaranteed a significant weight variation in TGA (***CE-f(-)***= 10%, ***CE-f(+)***= 20%, and ***CE-f(N)***= 30%), but the higher functionalization degree (FD) was measured for sulfonate moieties. Table 7 shows that one in sixty five carbon atoms of ***CE-f(-)*** are functionalized with $-SO_3^-$, while the FD value was only 125 using polyethylene glycol chain.

Table 7: functionalization degree of functionalized CE graphene.

	Functionalization Degree (FD)		
starting GBMs	**negative charge *CE-f(-)***	**neutral charge *CE-f(N)***	**positive charge *CE-f(+)***
Carlo Erba **CE**	**1/65**	**1/128**	**1/68**

The UV-vis spectroscopy showed that all the functionalized CE samples absorbed around 270 nm, with similarly intense peaks and, consequently, similar dispersion capability in water (dilution ratio used = 1:29).

SEM analysis does not reveal any visible evidence of the functionalization process, nor significant change in the morphology of pristine and functionalized CE graphene. In all the cases the size of folded platelets is ranging from few nanometres to several hundred nanometres, according to the technical data sheets.

Since the functionalization with sulfonate moieties guaranteed the best results in the case of CE single layer graphene, we replicated this reaction using different GBMs: few layers graphene (PP), high quality graphene nanoplatelets (0X), and low-quality graphene nanoplatelets (3X). In addition, the Tour reaction with sulfonate groups is easy, economic and guarantee several advantages compared to the other functionalities: low-cost raw materials (without preliminary preparation), water as solvent, and easy washing process.

Also in these cases, SEM analysis does not reveal any visible evidence of the functionalization process, nor significant variation in the morphologies of pristine and functionalized GBMs. Single layer graphene CE confirmed to be the only product with high specific surface and, for this characteristic, it appears like the most promising product for the cementitious reinforcement [120]. The characterization of the functionalized GBMs through thermo-gravimetric analysis confirmed that pristine products remain stable until ~ 800 °C in N_2. As we already discussed previously, samples *CE-f(-)* showed a weight reduction up to 10 %, while no weight variation for samples *PP-f(-)*, *0X-f(-)*, and *3X-f(-)* was measure when TGA was performed in N_2. The functional degrees of these products, measured in N_2, are shown in Table 8 and CE single layer graphene confirmed the best result.

Table 8: functionalization degree of synthesized GBMs.

		Functionalization Degree (FD)
starting GBMs		**negative charge *f*(-)**
Proton Power	***PP-(f-)***	1/2105
NanoXplore 0X	***0X-f(-)***	1/532
NanoXplore 3X	***3X-f(-)***	1/1356
CarloErba	***CE-f(-)***	1/65

TGA, SEM, and UV-vis analyses confirmed the necessity to use high quality graphene to obtain measurable functionalization yield and consequently good dispersion in water. Despite functionalized single layer graphene represents the best candidate in terms of specific surface, aspect ratio, functionalization degree, and dispersion capability, the possibility to use lower grade products could guarantee their extended uses in construction applications and for this reason we believe that the use of these products have to be explored in cementitious matrix. Due to their different characteristics and behaviour in aqueous media, the functionalized GBMs should differently influence the final properties of cementitious materials.

2.6 Experimental Section

Material and Reagents

The GBMs used in this study have different features in terms of number of layers, lateral size, and carbon percentage (as declared in their technical data sheets):

0. **Graphene CE**: single layer graphene powder, with average lateral size up to 5 µm, and 99.9% C; purchased from Carlo Erba *(cost ~ 250,000.00 €/kg)*.
1. **Graphene PP**: few layers graphene powder (1-5 layers), with average lateral size up to 9 µm, and 99.9% C; supplied by Proton Power (*cost ~ 2.000,00 €/kg*).
2. **Graphene nanoplatelets 0X**: few layers graphene powder (6-10 layers), with average lateral size up to 1 µm, and more than 95% C; supplied by NanoXplore *(cost ~ 15.00 €/kg)*.
3. **Graphene nanoplatelets 3X**: few layers graphene powder (6-10 layers), with average lateral size up to 2 µm, and more than 91% C; supplied by NanoXplore *(cost ~ 12.00 €/kg)*.

All the other reagents used for this study were purchased from Sigma Aldrich and were used as received.

Anilines derivative preparation

- *Quaternary Ammonium group: Compound 1d*

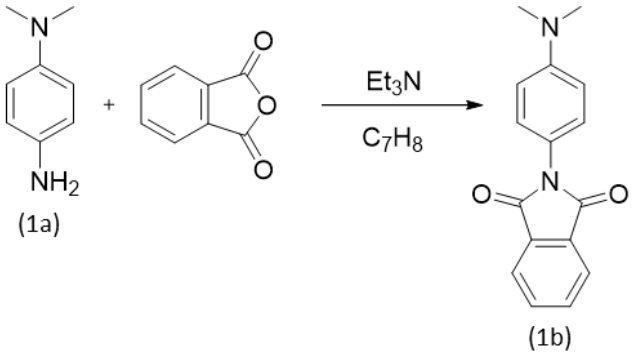

The reaction was performed following a reported procedure with minor modifications [112]. *Compound 1a* (4.0 g, 29 mmol), phthalic anhydride (8.7 g, 59 mmol) and triethylamine (2.0 mL, 2.7×10^2 mmol) were added in toluene (100 mL). The suspension was stirred in a Dean-Stark apparatus and was heated at 130 °C overnight. The mixture was cooled down and solvents evaporated under reduced pressure to 20 mL. The resulting solid was filtered and washed several times with cold toluene, MeOH and Et_2O to give *Compound 1b* as a yellow solid (7.1 g, 91%). ^{1}H NMR (300 MHz, $CDCl_3$) δ 7.93 (2H, m, CH_{Ar}), 7.76 (2H, m, CH_{Ar}), 7.25 (2H, d, *J* = 8.9 Hz, CH_{Ar}), 6.80 (2H, d, *J* = 9.0 Hz, CH_{Ar}), 3.00 (6H, s, CH_3). The characterization results matched those reported in the literature [112].

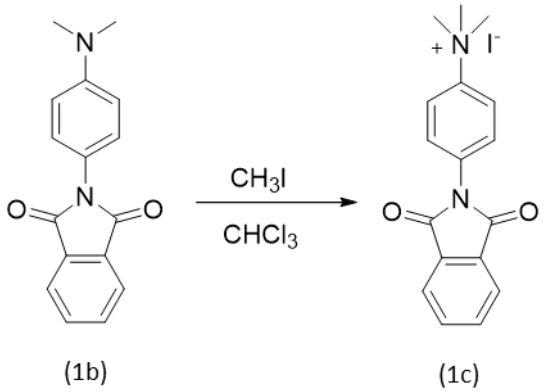

The reaction was performed following a reported procedure with minor modifications [112]. *Compound 1b* (6.0 g, 23 mmol) was diluted in $CHCl_3$ (100 mL) and was added to CH_3I (6.0 mL, 96 mmol) in a pyrex tube. The mixture was heated at 50°C for 24 hours and during the reaction, compound 1c precipitated. The solid is filtered and washed with cold $CHCl_3$ and Et_2O to give *Compound 1c* as a white solid (5.9 g, 64 %). ^{1}H NMR (300 MHz, DMSO-d_6) δ 8.15 (2H, d, *J* = 9.1 Hz, CH_{Ar}), 7.96 (4H, m, CH_{Ar}), 7.73 (2H, d, *J* = 9.1 Hz, CH_{Ar}), 3.67 (9H, s, CH_3). The characterization results matched those reported in the literature [112].

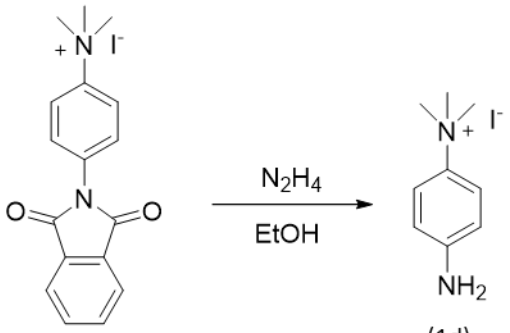

(1c) (1d)

The reaction was performed following a reported procedure with minor modifications [112]. *Compound 1c* (5.50 g, 14 mmol) was suspended in in EtOH (20 mL) and hydrazine monohydrate (3.0 mL, 59 mmol) was added. The mixture was stirred for 24 hours at room temperature and filtered. The filtrate, containing the final product, was then evaporated under reduced pressure. The resulting solid was recrystallized with EtOH to give 1d as a beige solid (2.50 g, 69 %). ^{1}H NMR (200 MHz, DMSO-d_6) δ 7.56 (2H, d, *J* = 8.0 Hz, CH_{Ar}), 6.66 (2H, d, *J* = 7.7 Hz, CH_{Ar}), 5.64 (2H, s, NH_2), 3.51 (9H, s, CH_3). The characterization results matched those reported in the literature [112].

- *Quaternary Ammonium group: Compound 2d*

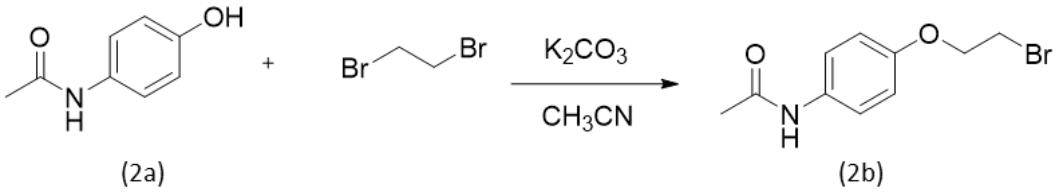

(2a) (2b)

The reaction was performed following a reported procedure with minor modifications [121]. *Compound 2a* (3.60 g, 23 mmol) and K_2CO_3 (8.1 g, 59.0 mmol) were suspended in CH_3CN (65 mL). 1,2 dibromoethane (10.0 mL, 1.2 × 10^2 mmol) was added and the mixture was refluxed for 3 days with a condenser equipped with a tube filled with $CaCl_2$. The resulting mixture was poured in an ice/water bath and filtrated. The solid was washed with water (3 × 20 mL) and extracted with hot ethanol (100 mL). The solution was evaporated to dryness yielding *Compound 2b* as a white solid (3.6 g, 60%). ^{1}H NMR (300 MHz, $CDCl_3$) δ 7.40 (CH_{Ar}, d, J = 9.0 Hz, 2H), 7.11 (NH, s, 1H), 6.87 (CH_{Ar}, d, J = 9.0 Hz, 2H), 4.27 (CH_2, t, J = 6.3 Hz, 2H), 3.62 (CH_2, t, J = 6.3 Hz, 1H), 2.16 (CH3, s, 3H). The characterization results matched those reported in the literature [121].

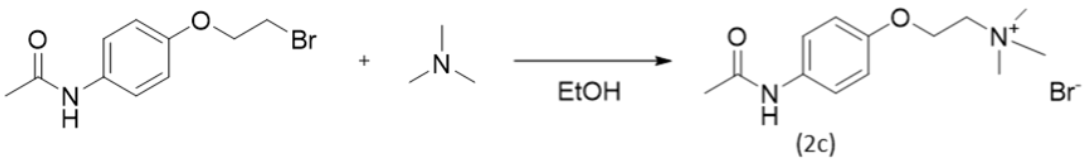

The reaction was performed following a reported procedure with minor modifications [121]. *Compound 2b* (3.6 g, 14 mmol) was suspended in a 4.2 M solution of trimethylamine in EtOH (35 mL) and stirred at room temperature for one week. The resulting suspension was filtrated and the solid was washed with acetone (3 × 5 mL). *Product 2c* was obtained as a white solid (4.0 g, 89%). ^{1}H NMR (200 MHz, D_2O) δ 7.37 (CH_{Ar}, d, J = 9.0 Hz, 2H), 7.06 (CH_{Ar}, d, J = 8.9 Hz, 2H), 4.53 (CH_2, m, 2H), 3.84 (CH_2, m, 2H), 3.27 (CH_3, s, 9H), 2.16 (CH_3, s, 3H). The characterization results matched those reported in the literature [121].

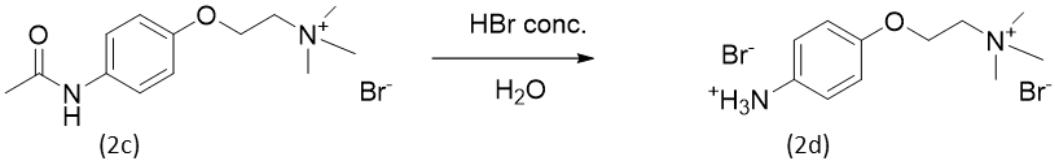

The reaction was performed following a reported procedure with minor modifications [121]. HBr 48% (14 mL) was carefully added to water (10 mL). *Compound 2c* (4.0 g, 13.0 mmol) was added, and the resulting mixture was refluxed for 30 minutes. The final solution was concentrated to approximately 10 mL, then ethanol (3 mL) and ethyl ether (5 mL) were added in sequence to induce the product precipitation. The solid was filtrated and washed with ethanol (3 mL) then with diethyl ether (3 ml) obtaining *Compound 2d* as a yellowish solid (3.5 g, 79%). ^{1}H NMR (200 MHz, D_2O) δ 7.39 (CH_{Ar}, d, J = 9.0 Hz, 2H), 7.15 (CH_{Ar}, d, J = 9.0 Hz, 2H), 4.56 (CH_2, m, 2H), 3.86 (CH_2, m, 2H), 3.27 (CH_3, s, 9H). The characterization results matched those reported in the literature [121].

- *Amino Polyethylene glycol chain*

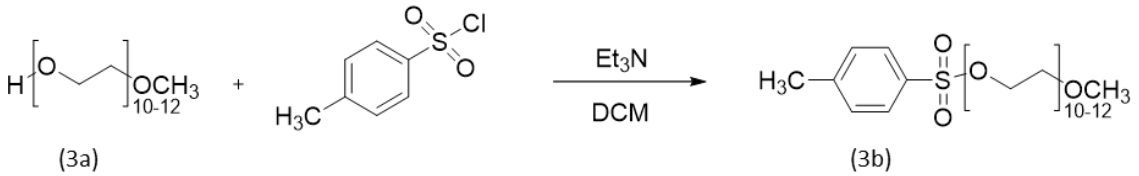

The reaction was performed following a reported procedure with minor modifications [115]. *Compound 3a* (10.0 g, 18. mmol) and an excess of triethylamine (3.0 ml, 21 mmol), were

dissolved in DCM (50 mL), and added dropwise to a suspension of tosyl chloride (4,1 g, 21 mmol) in DCM (50 mL) in an ice bath. The suspension was stirred overnight at room temperature. The mixture was washed with 1M hydrochloric acid (50 mL × 2) and water (50 mL). The solution was dried over anhydrous sodium sulfate and the solvent was removed by rotary evaporation. The sample obtained was purified by column chromatography on silica gel, using methanol/ethyl acetate (10:90) as eluent. *Compound 3b* was obtained as a colourless oil (6.7 g, 52%). ^{1}H NMR (200 MHz, $CDCl_3$) δ 7.83 (2H, d, *J* = 8.2 Hz, CH_{Ar}), 7.37 (2H, d, *J* = 8.1 Hz, CH_{Ar}), 4.18 (2H, m, CH_2), 3.68 (42H, m, CH_2), 3.41 (3H, s, OCH_3), 2.48 (3H, s, CH_3).

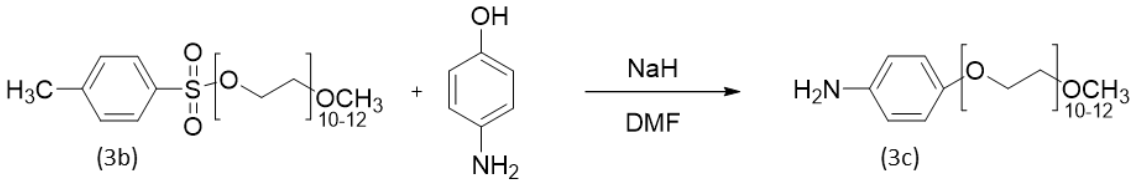

The reaction was performed following a reported procedure with minor modifications [122]. Under nitrogen atmosphere, *Compound 3b* (6.7 g, 9.5 mmol) was added dropwise to a suspension of 4-aminophenol (1.7 g, 10 mmol) and sodium hydride dispersion (60% in mineral oil, 0.41 g, 10. mmol), in anhydrous N,N-Dimethylformamide (20 mL) in an ice bath. The reaction mixture was stirred overnight at room temperature. The product obtained was diluted with water (80 ml), extracted with DCM (50 mL × 3), and the solvent was evaporated to dryness to obtain *Compound 3c* as a dark oil (5.6 g, 90%). ^{1}H NMR (300 MHz, $CDCl_3$) δ 6.76 (2H, d, *J* = 8.8 Hz, CH_{Ar}), 6.64 (2H, d, *J* = 8.8 Hz, CH_{Ar}), 4.05 (2H, m, CH_2), 3.81 (2H, m, CH_2), 3.64 (40H, m, CH_2), 3.37 (3H, s, OCH_3). The characterization results matched those reported in the literature [123].

- *Sulfonate group*

The aniline derivate used to synthesize sulfonated GBMs was purchased from Sigma Aldrich and was used as received. Before to mix with GBMs water suspension, Sulfanilic acid was dissolved in water and was neutralized with NaOH. The reaction was performed following a reported procedure with minor modifications [106].

GBMs functionalization procedure

In a typical functionalization procedure GBMs (5.0×10^2 mg, 42 mmol) and water or NMP solvent (150 ml) were mixed in a test tube and were sonicated for 20 min using a bath sonicator (Misonix 3000) to obtain a homogeneous dispersion. The selected aniline derivate (8.0 mmol) was added to GBMs solution, degassed by bubbling N_2, and mixed for 15 min under magnetic stirring at 550 rpm. After the addition of the alkyl nitrite (8.0 mmol), the mixture was stirred at 80 °C overnight in N_2 atmosphere. The resulting suspension was recovered by filtration on a Polytetrafluoroethylene (for NMP) or Polycarbonate (for water) membranes, washed with methanol and/or water (until a colourless solution was obtained), and the solid obtained was dried at 40°C for 2 hours. The Tour reaction steps are shown in Figure 40.

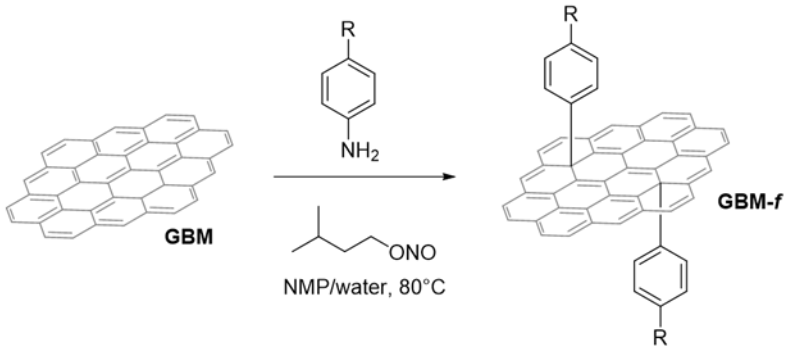

Figure 40: Tour reaction steps for GBMs' functionalization.

Table 1 reports the syntheses designed for this study.

		Aniline derivate		
starting GBMs		**arylsulfonate** *negative charge ƒ(-)*	**Polyethylene glycol** *neutral charge ƒ(N)*	**Ammonium quaternary** *positive charge ƒ(+)*
Carlo Erba	**CE**	CE-*ƒ*(-)	CE-*ƒ*(N)	CE-*ƒ*(+)
Proton Power	**PP**	PP-*ƒ*(-)	-	-
NanoXplore 0X	**0X**	0X-*ƒ*(-)	-	-
NanoXplore 3X	**3X**	3X-*ƒ*(-)	-	-

Figure 41 shows the set up used for the functionalization process of GBMs.

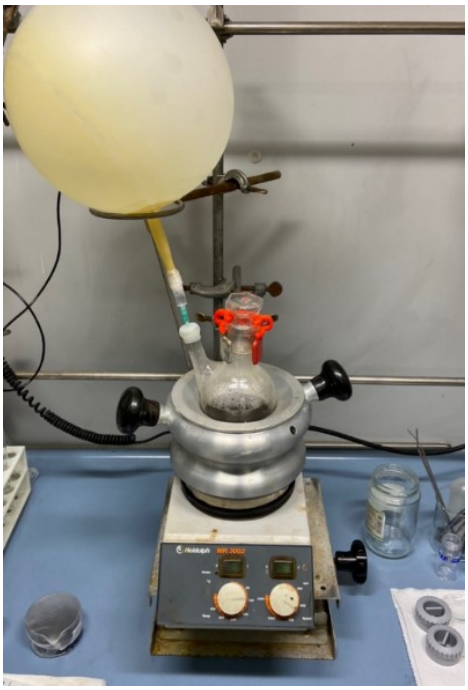

Figure 41: set up used for the functionalization reaction.

Instruments

The functionalized GBMs were characterized by Scanning Electron Microscopy, UV-vis spectroscopy, and Thermo-Gravimetric Analysis.

Scanning Electron Microscopy images were obtained on a field emission scanning electron microscope (Zeiss EVO MA15).

Thermogravimetric analyses of the samples were carried out within platinum pans with a Q5000IR TGA (TA Instruments). The analysis was performed keeping the sample at 100 °C for 10 min and subsequently heating it up to 900 °C with a 10 °C/min ramp in air or N_2.

UV-Vis spectra were recorded on an Agilent Cary 50 instrument in the 200 – 800 nm range when 1 cm quartz cuvettes were used.

The anilines derivate synthesized for this study were characterized by ESI-MS and NMR analysis. The NMR experiments were performed on a Varian Gemini (200 MHz) NMR spectrometer (proton frequency: 200 MHz; carbon frequency: 50 MHz). ESI-MS spectra were recorded on MeOH solutions with an LCQ Advantage Thermofluxional instrument.

Functionalization degree

By analysing the weight losses due to the main thermal decompositions, it is possible to calculate the functional degree (FD) of functionalized-GBMs as the ratio between the moles of attached aryl moieties n_{FG} and those of carbon in the substrate n_C:

$$FD = \frac{n_{FG}}{n_C}$$

In particular, the moles of functional group (n_{FG}) are obtained by the ratio between the weight loss due to the functional group, in this case assumed to decompose in the range 100-650 °C, divided by the molecular weight of the functional group (MW_{FG}). Instead, the moles of carbon (n_C) are given by the residual weight at the decomposition temperature of GBMs, divided by the atomic weight of carbon (MW_C):

$$n_{FG} = \frac{W_{100°C} - W_{650\,°C}}{MW_{FG}}$$

$$n_C = \frac{W_{650\,°C}}{MW_C}$$

GBMs stability in water and alkaline solution

The stability of the graphenic products in aqueous media was performed mixing the selected GBM (10 mg) in distilled water (7 mL). The suspension obtained was sonicated for 2 minutes using a probe sonicator (Misonix 3000) and was centrifuged at 3500 rpm for 5 minutes. The supernatant (100 µL for 1:29 dilution ratio or 1000 µL for 1:2 dilution ratio) was fill up to 3 ml with water, or saturated $Ca(OH)_2$ solution, or simulated cement pore solution (prepared with components as listed in Table 9).

Table 9: composition of the simulated cement pore solution [124].

SCS Component	Concentration (g/L)
$Ca(OH)_2$	saturated
$CaSO_4$	27.6
NaOH	8.2
KOH	22.4

3. Mechanical performance of cementitious mortars

As already demonstrated in previous studies [125]–[128], the reinforcing mechanism of GBMs is attributed to the chemical interaction between graphenic nanosheets and cement hydration products. Due to their high specific surface area, and the presence of functional groups (in the case of graphene oxide or functionalized products), GBMs promote the growth of cement hydration crystals by creating a great number of nucleation sites. Therefore, a key challenge to use GBMs in cementitious composites is their homogenous dispersion, because their large surface area can lead to high van der Waals forces and because of their hydrophobic nature which leads to their aggregation in aqueous systems

In this chapter we combined functionalized GBMs with Ordinary Portland Cement (OPC) preparing mortar specimens and evaluating possible improvements of their mechanical properties. In particular, for this study, we selected a white Portland limestone cement type II featuring high normalized strength and high early strength.

Mechanical performance of mortar samples was evaluated according to the standard method UNI EN 196-1:2016, measuring flexural and compressive strength after 7 and 28 curing time days. The test material was made with cementitious binder, sand, and water weighed in specific proportion (see experimental section).

The synthesized GBMs were combined with CCMs following two different preliminary procedures:

- **Method A - Dry premixed binder**: the GBMs were mixed with cement, using a powder blender mixer, to form a dry cementitious binder. Subsequently it was added to water, and sand for the mortar sample preparation.
- **Method B - Wet sonicated solution**: the GBMs were sonicated with water and superplasticizer (SP), using a tip sonicator, to form an aqueous suspension. The suspension was used as “water” for the mortar preparation, adding cement and sand.

Finally, we selected two of the functionalized products to study the mechanical behaviour of mortar samples containing 0.05, 0.1 and 0.5% of GBMs (by weight of cement).

3.1 Method A: dry premixed binder

The possible improvement of GBMs dispersion in cement composites, promoted by the use of specific admixtures (usually water dispersion in the presence of a surfactant) has been extensively studied in recent years. However, it is worth considering that the availability of a GBM in a powder form opens the possibility to the preparation of dry binder for more versatile applications. In other words, literature data assert that the application of polycarboxylate, methylcellulose, or naphthalene-sulfonate based liquid admixtures are able to ensure the appropriate dispersion of nanomaterial within cementitious matrix [74], [129]. Nevertheless, the possibility to use dry cementitious binders, with strengthening nanomaterials as additives, can guarantee several advantages for the industrial applications, and deserve more attention. For example, premixed binders, in which the ingredients are properly dosed, guarantee quality improvement, cost reduction, and production flexibility.

In this section, we describe the results obtained by the preparation of dry premixed cementitious binder, containing 0.05% of GBM by weight of cement, that was necessary for the mortar samples preparation. The water-to-cement ratio was kept at 0.5 and the quantity of sand at a proportion of 3 times the weight of cement. It is important to notice that no additives, such as superplasticizer, were employed for the modification of the workability.

Eleven different mortar samples were prepared using a mortar mixer and were investigated at the ages of 7 and 28 days by compressive and flexural strength tests. In order to verify the reproducibility of the results, we have cast at least three samples for each evaluation. The mortar samples and the control mix (coded *Standard* and realized without GBMs) were prepared following the mix proportions reported in Table 10.

Table 10: mix proportion of mortar samples prepared following method A.

	Mortar code	GBMs	Functionalization	GBM [g]	Cement [g]	Sand [g]	Water [g]	SP [g]
Method A Dry premixed mortars	**m-CE**	Carlo Erba	-	0.225	449.8	1350	225	-
	m-CE-f(+)	Carlo Erba	Positive	0.225	449.8	1350	225	-
	m-CE-f(N)	Carlo Erba	Neutral	0.225	449.8	1350	225	-
	m-CE-f(-)	Carlo Erba	Negative	0.225	449.8	1350	225	-
	m-PP	Procene	-	0.225	449.8	1350	225	-
	m-PP-f(-)	Procene	Negative	0.225	449.8	1350	225	-
	m-0X	Xplore 0X	-	0.225	449.8	1350	225	-
	m-0X-f(-)	Xplore 0X	Negative	0.225	449.8	1350	225	-
	m-3X	Xplore 3X	-	0.225	449.8	1350	225	-
	m-3X-f(-)	Xplore 3X	Negative	0.225	449.8	1350	225	-
	Standard	-	-	-	500.0	1350	225	-

Results and discussion

Figure 42 plots the mechanical strengths of mortar samples realized with method A, containing 0.05 % of CE single layer graphene functionalized with positive, neutral, or negative groups (the light and the dark bars refer to the mechanical performance at the age of 7 and 28 curing days, respectively).

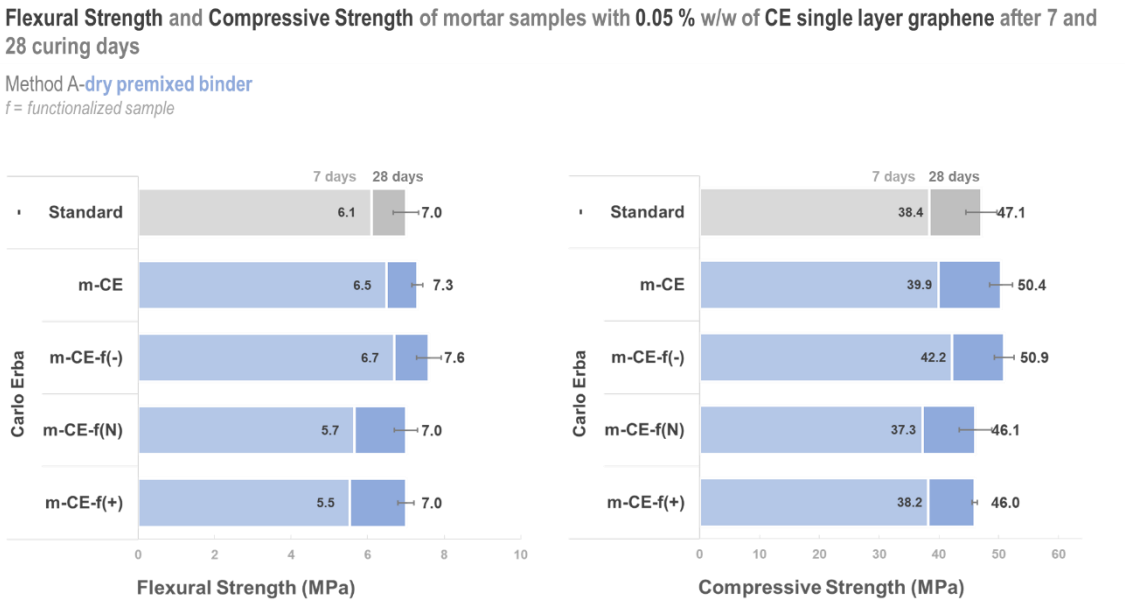

Figure 42: mechanical strengths of mortars with 0.05% of functionalized single layer graphene CE – method A.

The results demonstrated that mortars containing 0.05 % of *pristine* single layer graphene, *m-CE*, exhibit a slight increase of flexural strength up to 5% compared to the *Standard* sample. Simultaneously, the compressive strength shows the same trend with an increase of 7% (increment from 47.1 MPa to 50.4 MPa).

Using functionalized products, the mechanical performance varied differently; we noticed a flexural and compressive strength reduction when GBMs was functionalized with *neutral* (polyethylene glycol chain), and *positive* (quaternary ammonium) groups, *m-CE-f(+)* and *m-CE-f(N)*, reaching values lower than the *Standard* sample. It seems that positive and neutral functional groups have a bad impact on the cement hydration process. This trend remained valid both for 7 and 28 days of curing.

On the other hand, the introduction of negatively charged GBMs, by arylsulfonate groups, improved the flexural and the compressive strengths by 9% and 8 %, respectively.

Figure 43 reports the flexural and the compressive strengths of mortars samples prepared with 0.05% of GBMs charged with negative groups (arylsulfonate). The results refer to samples cast

using different graphenic support: single layer graphene (Carlo Erba), few layers graphene (Procene), and graphene nanoplatelets (Xplore 0X, and 3X). In addition to the preparation of the control (*Standard*), for each test, we prepared mortar samples with pristine graphenic materials.

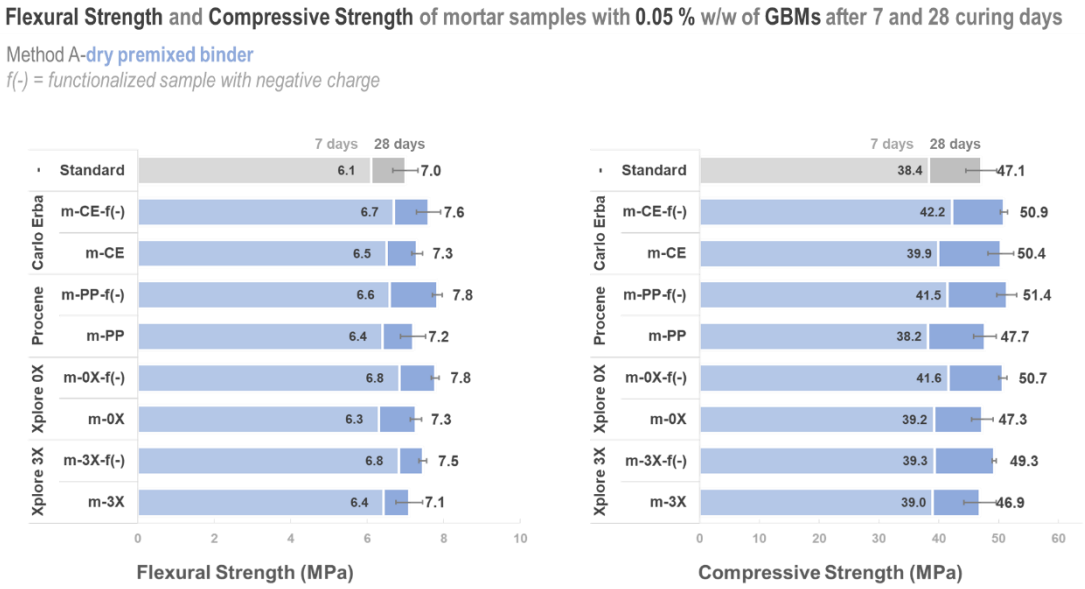

Figure 43: mechanical strengths of mortar samples with different GBMs – method A.

All the samples with GBMs, both pristine and functionalized, exhibited a clear mechanical strength enhancement compared to the *Standard* sample. This result is valid both after 7 and 28 days of curing.

In addition, Figure 43 shows that the use of functionalized GBMs provided the best results independently of the graphenic support and allowed to obtain better performances than pristine graphenic materials. After 28 days of curing, mortars containing functionalized few-layers graphene (*m-PP-f(-)*) reached flexural and compressive strengths equal to 7.8 MPa and 51.4 MPa respectively, and represent the products with the best performance measured for method A (an analogous trend was recorded for mechanical strength at 7 days). It seems that the functionalization process results more effective when take place on lower quality graphene. The mortar sample *m-PP-f(-)*, prepared with functionalized few layers graphene, exhibited + 8% in flexural and compressive strength if compared to sample *m-PP*, prepared with pristine product (e.g. the compressive strength at 28 days passes from 47.7 MPa for *m-PP* to 51.4 MPa for *m-PP-f(-)*). The compressive strength improvement between functionalized and pristine GBMs was +8%, +7%, +5%, and 1% for Procene, Xplore 0X, Xpolore 3X and Carlo Erba CE, respectively.

3.2 Method B: wet sonicated solution

The most used techniques for the homogeneous dispersion of GBMs in cementitious matrix can be categorized in two groups: mechanical and chemical methods.

Among mechanical methods, the sonication process represents the most used technique [25]. It works by mechanical vibrations and creating pressure waves that collapse producing microscopic bubbles (cavitation) useful for the dispersion of the graphenic materials. The sonication process can be performed using either a bath sonicator or a probe/tip.

The chemical methods include covalent functionalization and noncovalent interaction; the first involves the chemical modification of the graphenic material, while the latter is based on weak bonds (in particular with superplasticizers) that preserve the GBMs structure. In terms of noncovalent interaction, the use of superplasticizers represents an appropriate mixing technique for cementitious systems as these products are already widely used in construction.

Even though the mechanical and chemical methods are generally used individually, their combination can be beneficial for a better dispersion of GBMs in cementitious composites. In this section, we evaluated the simultaneous used of these techniques to maximize the strengths of cementitious materials. In particular, the mechanical performance of mortar samples, containing 0.05% of GBMs, was evaluated combining covalent functionalization, noncovalent interaction (addition of SP), and sonication process. For each preparation, the selected GBM was sonicated with water and superplasticizer and was used for the mortar preparations. Both, the sonication and the superplasticizer, should yield excellent dispersion conditions to prevent GBMs from agglomerating.

The water-to-cement ratio was kept at 0.42 and the quantity of sand at a proportion of 3 times the weight of cement; while the superplasticizer, necessary to set the right workability, was kept at 0.4% by weight of cement.

Twelve different batch mortars were prepared using a mortar mixer and were investigated at the ages of 7 and 28 days by compressive and flexural strength tests. In order to verify the reproducibility of the results, we prepared at least three samples for each evaluation. The control samples, *Standard* and *Reference-SP*, were realized without GBMs and following the mix proportions reported in Table 11. Due to the presence of the superplasticizer, the *Reference-SP* sample contains less water than the *Standard* (190 ml rather than 225 ml).

Table 11: mix proportion of mortar samples prepared following method B.

	Mortar code	GBMs	Functionalization	GBM [g]	Cement [g]	Sand [g]	Water [g]	SP [g]
Method B Wet sonicated mortars	**m-CE-SP**	Carlo Erba	-	0.225	449.8	1350	190	1.8
	m-CE-f(+)-SP	Carlo Erba	Positive	0.225	449.8	1350	190	1.8
	m-CE-f(N)-SP	Carlo Erba	Neutral	0.225	449.8	1350	190	1.8
	m-CE-f(-)-SP	Carlo Erba	Negative	0.225	449.8	1350	190	1.8
	m-PP-SP	Procene	-	0.225	449.8	1350	190	1.8
	m-PP-f(-)-SP	Procene	Negative	0.225	449.8	1350	190	1.8
	m-0X-SP	Xplore 0X	-	0.225	449.8	1350	190	1.8
	m-0X-f(-)-SP	Xplore 0X	Negative	0.225	449.8	1350	190	1.8
	m-3X-SP	Xplore 3X	-	0.225	449.8	1350	190	1.8
	m-3X-f(-)-SP	Xplore 3X	Negative	0.225	449.8	1350	190	1.8
	Reference-SP	-	-	-	500.0	1350	190	1.8
	Standard	-	-	-	500.0	1350	225	-

Results and discussion

Figure 44 plots the mechanical strengths of mortar samples prepared with method B, containing 0.05 % of CE single layer graphene functionalized with positive, neutral, and negative groups (sulfonate, polyethylene glycol chain, and quaternary ammonium). The light and the dark bars refer to the mechanical performance at the age of 7 and 28 days, respectively.

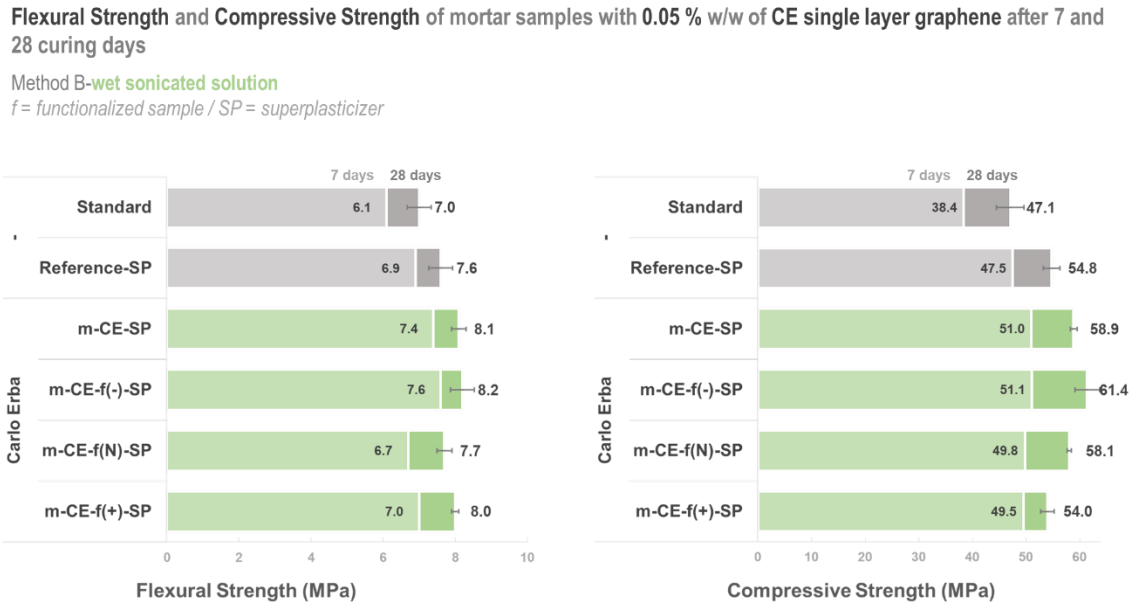

Figure 44: mechanical strengths of mortars with 0.05% of functionalized single layer graphene CE – method B.

The results demonstrated that mortars with 0.05 % of pristine single layer graphene, *m-CE-SP*, exhibit a slight increase of flexural and compressive strength up to 7% compared to the *Reference-SP* sample. As we already discussed for mortars prepared following method A, the use of functionalized GBMs does not guarantee the development of high mechanical strength.

For example, the GBMs functionalized with neutral (polyethylene glycol chain), and positive (quaternary ammonium) groups, *m-CE-f(+)-SP* and *m-CE-f(N)-SP*, allowed to reach strength values lower than the mortars realized with pristine single layer graphene, *m-CE-SP*. This trend remained valid both for 7 and 28 days of curing.

The GBMs used for the preparation of these mortar samples, *CE-f(+)* and *CE-f(N),* obtained positive results during dispersion tests, both in water and in alkaline environment (see paragraph 2.4). In addition, the combined use of the superplasticizer and the sonication process of method B should guarantee a better distribution of the graphenic materials in the cementitious matrix. Nevertheless, positive and neutral functionalized GBMs seem limit the hydration reaction of the cement, and consequently, the mechanical strength improvements of the mortars.

The compressive strengths rise considerably when the GBMs was functionalized with arylsulfonate groups (negative charge). In this case, a gradually increasing trend from 51.1 MPa at 7 days to 61.4 MPa at 28 days was observed for *m-CE-f(-)-SP*. If compared with the *Reference-SP* sample, prepared without graphene, we measured an increment of compressive strength by 12%. This value reached 30% when sample *m-CE-f(-)-SP* was compared to the *Standard* (from 47.1 MPa to 61.4 MPa). An analogous trend was recorded for flexural strength, that reached a maximum value of 8.2 MPa at 28 days, slightly higher than the 7.6 MPa measured for the control sample (*Reference-SP)*.

These favourable findings can be ascribed not only to the better distribution of the GBMs in the cementitious matrix (that was guaranteed for all the samples prepared with method B), but also to the specific functional groups used for the functionalization of *CE-f(-)*.

Figure 45 plots the flexural and the compressive strengths of mortars samples prepared with 0.05% of GBMs functionalized with negative groups. The graph refers to mortar samples prepared using different graphenic support: single layer graphene (Carlo Erba), few layers graphene (Procene), and graphene nanoplatelets (Xplore 0X, and 3X). In addition to the preparation of the control samples (*Reference-SP*, and *Standard*), we cast mortars with pristine GBMs.

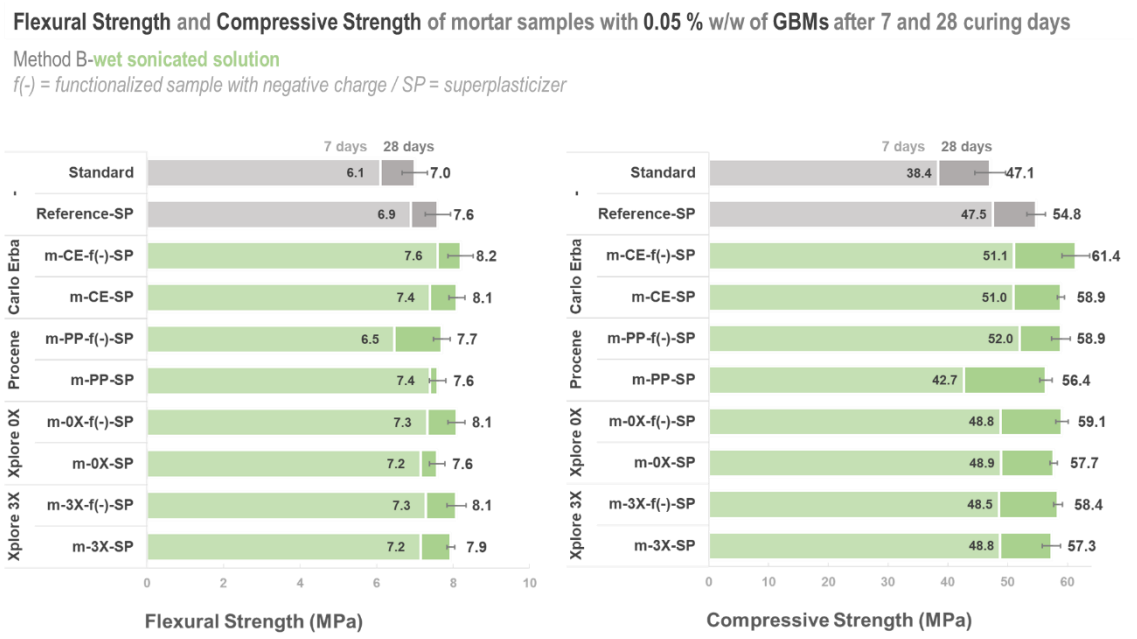

Figure 45: mechanical strengths of mortar samples with different GBMs – method B.

The bars in Figure 45 confirmed the positive effects related to the use of GBMs. All the mortars containing graphenic products exhibited higher mechanical strength than the *Reference-SP* sample.

Despite these positive results, the use of functionalized GBMs always allowed to reach higher mechanical strengths than pristine materials, independently of the graphenic support. Mortars containing functionalized single layer graphene *m-CE-f(-)-SP*, showed flexural and compressive strengths equal to 8.2 MPa and 61.4 MPa respectively, that represent the best performances measured for method B after 28 days of curing. This trend is valid both after 7 and 28 days of curing.

The functionalization process provided positive results also when performed on lower quality materials; for example, the mortar sample *m-0X-f(-)-SP*, prepared with functionalized graphene nanoplatelets, exhibited + 8% in flexural and compressive strength if compared to the control sample (e.g. the compressive strength at 28 days reached 59.1 MPa for sample *m-0X-f(-)-SP*).

This enhanced mechanical strength could result from the improved dispersion of graphenic materials, related to the combination of different dispersion techniques.

3.3 Cementitious mortars: GBMs' dosage

The main purpose of this section is to study the effects of GBMs dosage on the mechanical properties of cementitious mortars. Several studies declare that high GBMs percentage (greater than 0.05%) would result ineffective to improve the mechanical strength of cementitious products because of their difficulties to be well distributed in the cementitious matrix [22]. Nevertheless, all of them report only mechanical and noncovalent chemical methods to improve the GBMs' dispersion, and no specific covalent functionalization for cementitious application were evaluated in the case of elevated dosage.

The GBMs studied for this project are specifically functionalized to improve their dispersion in cementitious matrix and their efficiency had to be evaluated also for percentage greater than 0.05%. High dosages, as well as the covalent functionalization of GBMs, represent extra costs for the application in the construction field. Furthermore, high dosage of single layer graphene would not be considered due to its high cost (monolayer material can reach a price up to a billion dollars per kilogram [52]).

For these reasons we selected low grade products (nanoplatelets 0X and 3X) functionalized with negatively charged groups (that represent the easier and more economic reaction processed in this study). In this section, we evaluated the mechanical performance of mortar samples containing 0.05%, 0.1%, and 0.5% of graphene nanoplatelets (0X, and 3X), that were dispersed following method B (that guarantee a better GBMs' distribution and higher performances).

A total of fourteen different recipes were prepared using a mortar mixer and were investigated after 7 and 28 days by compressive and flexural strength tests. In order to verify the reproducibility of the results, we prepared at least three samples for each evaluation.

The water-to-cement ratio was kept at 0.42 and the quantity of sand at a proportion of 3 times the weight of cement. The superplasticizer was varied from 0.4% to 0.5% by weight of cement to achieve the same workability for all the mortars.

The control samples, *Standard* and *Reference-SP*, were realized without GBMs and following the mix proportions reported in Table 12. Due to the presence of the superplasticizer, the *Reference-SP* contains less water than the Standard (190 ml rather than 225 ml).

Table 12: mix proportion of mortar samples containing different GBMs percentage – method B.

	Mortar code	GBMs	[%]	Functionalization	GBM [g]	Cement [g]	Sand [g]	Water [g]	SP [g]
Method B Wet sonicated mortars	**m-0X-0.05%**	Xplore 0X	0.05	-	0.225	449.8	1350	190	1.8
	m-0X-f(-)-0.05%	Xplore 0X	0.05	Negative	0.225	449.8	1350	190	1.8
	m-0X-0.1%	Xplore 0X	0.10	-	0.450	449.6	1350	190	2.0
	m-0X-f(-)-0.1%	Xplore 0X	0.10	Negative	0.450	449.6	1350	190	2.0
	m-0X-0.5%	Xplore 0X	0.50	-	2.250	447.8	1350	190	2.2
	m-0X-f(-)-0.5%	Xplore 0X	0.50	Negative	2.250	447.8	1350	190	2.2
	m-3X-0.05%	Xplore 0X	0.05	-	0.225	449.8	1350	190	1.8
	m-3X-f(-)-0.05%	Xplore 0X	0.05	Negative	0.225	449.8	1350	190	1.8
	m-3X-0.1%	Xplore 0X	0.10	-	0.450	449.6	1350	190	2.0
	m-3X-f(-)-0.1%	Xplore 0X	0.10	Negative	0.450	449.6	1350	190	2.0
	m-3X-0.5%	Xplore 0X	0.50	-	2.250	447.8	1350	190	2.2
	m-3X-f(-)-0.5%	Xplore 0X	0.50	Negative	2.250	447.8	1350	190	2.2
	Reference-SP	-	-	-	-	500.0	1350	190	1.8
	Standard	-	-	-	-	500.0	1350	225	-

Results and discussion

Figure 46 reports the mechanical strengths of mortar samples at different GBMs dosage. The red bars refer to the mechanical performance of mortars containing *pristine GBMs*, while the green bars represent the performance of mortars containing *functionalized GBMs*. The control samples (*Standard* and *Reference-SP*) are represented with grey bars.

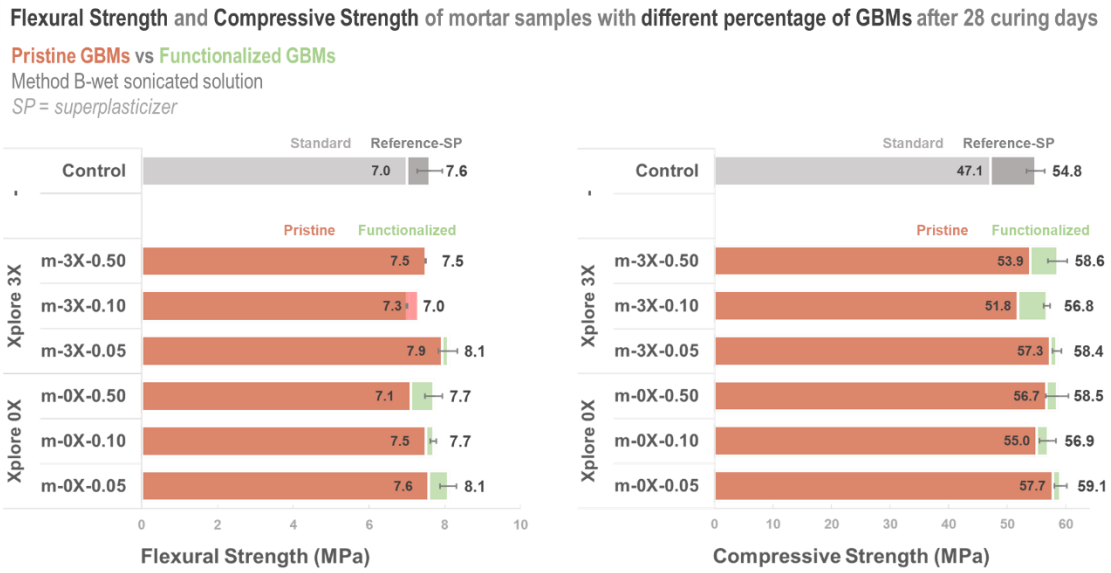

Figure 46: mechanical strengths of mortar samples containing different dosage of GBMs – method B.

The mechanical strengths of samples produced with pristine GBMs seem to be noticeably influenced by the dosage used. For example, the mortar samples containing 0.05%, 0.1%, and

0.5% of pristine 3X nanoplatelets, (*m-3X-0.05/0.1/0.5*) reached irregular compressive strengths, equal to 57.3, 51.8, and 53.9 MPa, respectively.

On the contrary, excluding the case of specimens prepared with 0.1% of 3X nanoplatelets (*m-3X-0.10*), all the mortars containing functionalized GBMs showed mechanical strengths higher than mortars containing pristine materials. In this case, the GBMs' percentage seems to be ineffective to improve the mechanical strengths; for example, samples prepared with 0.1, and 0.5% of functionalized 0X nanoplatelets provided flexural and compressive strengths slightly lower than samples prepared using 0.05% (*m-0X-0.5* = 58.5 MPa, *m-0X-0.05* = 59.1 MPa).

These results demonstrated that the functionalization process with arylsulfonate allowed to obtain a better distribution of the GBMs in the cementitious matrix when their percentage exceeds 0.05%.

Figure 47 shows some of the specimens used for the mechanical characterization of mortars containing 0,1%, and 0.5% of graphene nanoplatelets. We can observe a colour variation of the samples passing from control samples to mortars containing 0.1%, and 0.5% of graphenic materials, that led to obtain a homogeneous distribution of the GBMs at macroscopic scale.

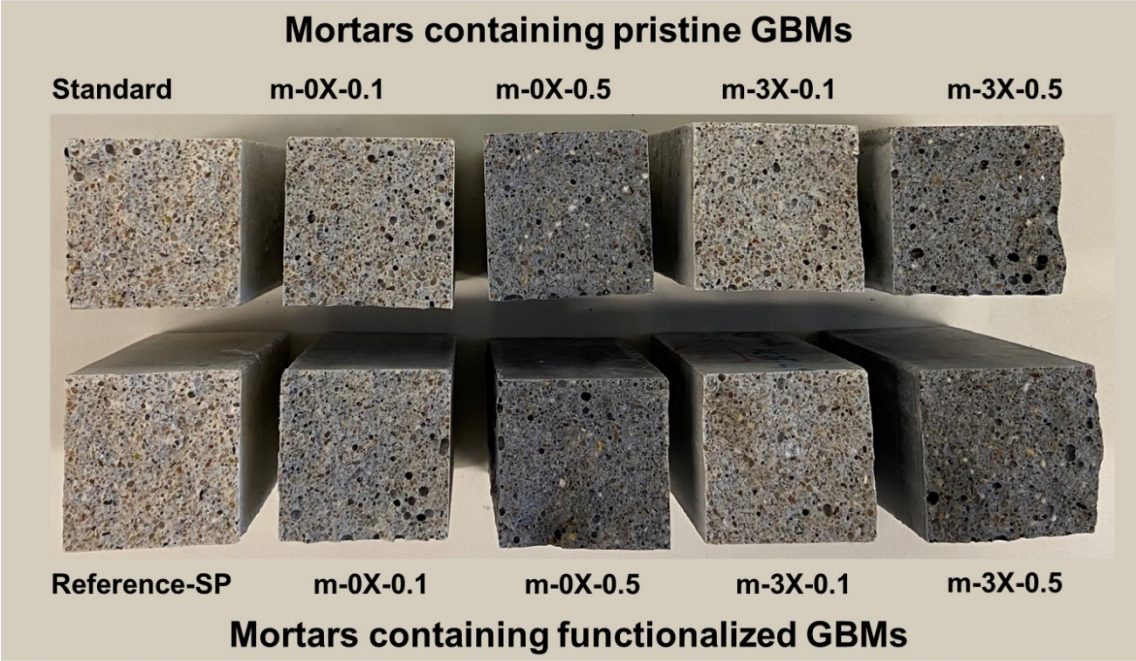

Figure 47: mortars containing 0.1%, and 0.5% of graphene nanoplatelets.

3.4 Final findings

In this section, we have investigated the role of functionalized GBMs to improve the mechanical performance of CCMs by preparing mortar samples with different percentage of graphenic products. In addition, we evaluated two different mixing procedures, method A, and method B, combining mechanical and chemical approaches. Method A involves a dry premixing process to obtain a versatile cementitious binder, while method B involves the combination of covalent functionalization, superplasticizers, and sonication process, to maximize the mechanical performance of CCMs.

The experimental results demonstrated that all the mortar samples containing pristine GBMs, exhibited a slight increase of flexural and compressive strength if compared to the control sample (*Standard* or *Reference-SP*). Despite single layer graphene (high quality) allowed to obtain the best mechanical performance, it seems that the quality (and cost) of GBMs is not fundamental to obtain positive results. Mortar samples containing high quality pristine graphene reached compressive strength comparable to those containing low quality pristine graphene (e.g. 50.9 MPa the first, 49.3 MPa the latter). This finding is valid both for method A and method B.

Independently to the GBMs used, the functionalization process resulted most effective when it was carried out with arylsulfonate groups (providing negative charges). Both for method A, and method B, the negative functionalization allowed to obtain the highest mechanical performance improvements, in particular, when it was applied on single layer graphene (mortar samples with negatively charged SLG and prepared following method B, reached compressive strength up to +12% compared to the *Reference-SP*, and +30% compared to *Standard*). These positive results prove the correlation between mechanical performances and the nature of the functional group attached to the graphene lattice.

Despite all the functionalized SLGs (positively, neutral, and negatively charged) provided similar results during the dispersion tests, we measured a flexural and compressive strength reduction only for mortars with neutral (polyethylene glycol chain), and positive (quaternary ammonium) GBMs. In these cases, the mortar samples reached mechanical strengths values lower than the control samples; probably the long polyethylene glycol chain, as well as quaternary ammonium groups, influenced the cement hydration, reducing its mechanical performances.

In general, the combined use of a SP and sonication allowed to maximize the GBMs' effects and the achievement of the best mechanical performances. Figure 48 shows the compressive strength of mortar samples containing GBMs functionalized with negative charge, prepared with method A, and method B. Grey bars represent the compressive strength of control samples for

each method: *Standard* for method A, and *Reference-SP* for method B (that contains superplasticizer and less water than the *Standard*).

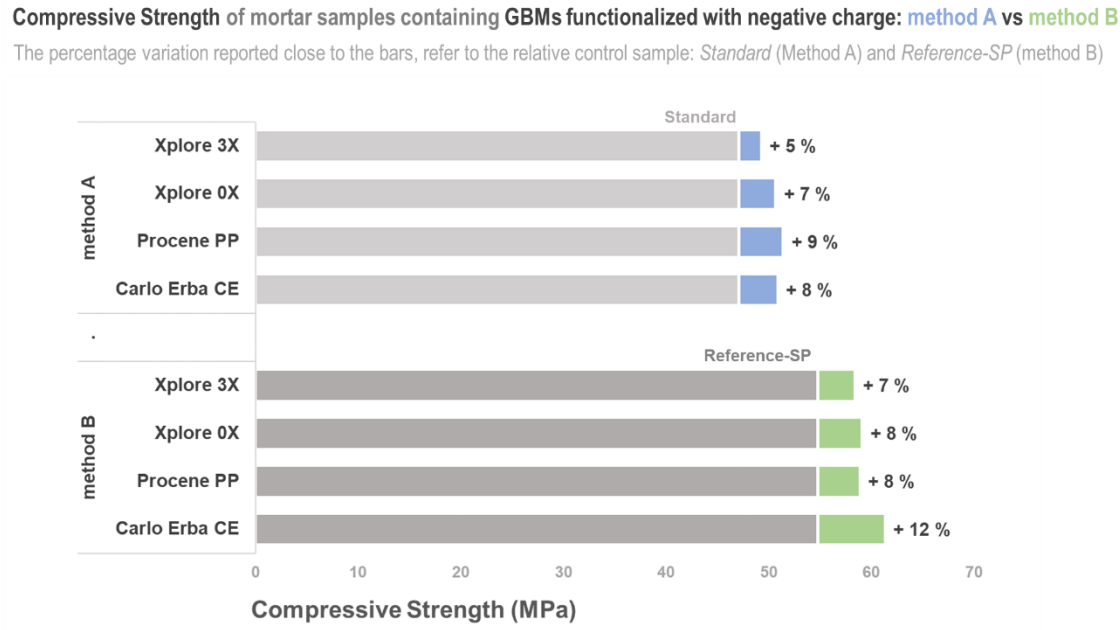

Figure 48: mortar samples containing GBMs functionalized with negative charge: strengths improvements compared to the control samples.

The percentage reported close to the bars, represent the compressive strengths improvement with respect to the relative control sample. For example, mortars containing functionalized single layer graphene (CE), showed strengths improvement up to 8% for method A, while, this value, reached 12% for method B.

Finally, it seems that high GBMs dosages (> 0.05%) are not essential to obtain mechanical performance improvements. Nevertheless, the functionalization process allows to better disperse the GBMs, providing similar mechanical performance, independently to the GBMs' percentage.

3.5 Experimental Section

Materials and Reagents

The cement used for this study was i.design ROCCA BIANCA, supplied by Italcementi S.p.A., that is a white Portland limestone cement type II featuring high normalized strength and high early strength. In compliance with UNI EN 197-1 standard specifications (see Table 13), i.design ROCCABIANCA 42,5 R contains 65-79% of white clinker by cement mass excluding calcium sulphate and mineral additions, while the remaining portion is limestone with a TOC value ≤ 0,20% by mass (LL), and other minor constituents, if any.

Table 13: standard specifications of i.design ROCCA BIANCA, according to UNI EN 197-1.

Chemical requirements	
Sulphates (as SO_3)	≤ 4,0%
Chlorides	≤ 0,10%
Physical requirements	
Initial setting time	≥ 60 min
Expansion	≤ 10 mm
Mechanical requirements	
compressive strength 2 days	≥ 20.0 MPa
compressive strength 28 days	≥ 42.5 MPa

The superplasticizer used for the mortars preparation was Creactive IV K, purchased from Sika Italia. It is a high-performance superplasticizer and water reducer, in liquid form, based on polycarboxylate (PCE) polymer technology, that works based on a combination of electrostatic forces and steric repulsion effects. The main characteristics are shown in Table 14.

Table 14: product information of Creactive IV K.

Composition	modified polycarboxylate polymers
Appearance	Yellowish to brownish liquid
Density	1.095 ± 0.02 kg/dm^3 at 20°C
pH-Value	~ 7.0

CEN Standard Sand, according to EN 196-1, was used for the preparation of the mortar samples. The characteristic of CEN Standard Sand is its specific grain size distribution. It ranges between 0.08 and 2.00 mm. The maximum moisture content is 0.2%. There is no natural sand available, which fulfills the grain size distributions demand of EN 196-1. It is an artificial product consisting of several different sand type fractions, produced by sieving, and blended in defined portions.

Preparation and Mechanical characterization of the mortar samples

The mechanical performance of the mortar samples was evaluated according to the standard method UNI EN 196-1:2016, measuring the flexural and the compressive strength after 7 and 28 days of curing time in water. The standard describes both the mortar sample preparation and the mechanical tests.

All the specimens were prepared mixing cementitious binder (450 g), standard sand (1350 g), water (225 or 195 g), and superplasticizer (1.8 or 2.2 g only for method B) with specific proportion by Hobart mixer (see Figure 49).

Figure 49: Hobart mixer.

Below the mixing procedure used:

a) pour the liquid (method A: water; method B: water + GBMs + SP) into the bowl and add the cementitious binder (method A: cement + GBMs; method B: cement);

b) immediately start the mixer at low speed and add the sand after 30 s, with constant flow over the next 30 s;

c) stop the mixer for 1 min and 30 s. In the first 15 s remove all the mortar that adheres to the bowl's wall and re-place it in the bowl itself;

d) continue mixing at the higher speed for 60 s.

The fresh cementitious mixes were cast into rectangle molds (40 mm x 40 mm x 160 mm) and maintained at 20 ± 1 °C and a relative humidity of 90 ± 15% for 24 hours; then they were demolded and submerged into a tank of water for the curing (7 or 28 days). Not more than 20

minutes before the mechanical investigations, the mortar samples were removed from the water and left to stand at room temperature.

Figure 50 shows the Compression-Flexure Cement Testing Frames used for the mechanical characterization (model Controls 65-L18Z10).

Figure 50: Compression-Flexure Cement Testing Frames.

4. Conclusion

The use of GBMs represents an invaluable opportunity to enhance CCMs performance and represents a new technology enabling more performing and/or sustainable concrete. The main potential benefits include the use of lower cement amount, while preserving mechanical/durability properties, and also adding to the matrix unconventional properties (i.e. electrical/thermal conductivity, etc.). Moreover, GBMs can contribute to accelerate strengths development over time and, therefore, reducing the construction cycle time. To optimize these positive results, the homogenous distribution of the GBMs in cementitious matrix plays a crucial role, to such an extent that the efficient dispersion of graphene derivatives in concrete and mortar is a widely debated topic in literature.

During this thesis work, we have faced these problems combining different well-known techniques (mechanical and chemical methods) and studying a specific covalent functionalization strategy. In particular, we have functionalized four commercial GBMs (from single layer to graphene nanoplatelets), using aryl fragment containing a hydrophilic group, with the aim to improve their dispersion in water and, therefore, to optimize their distribution in a cementitious matrix.

Since the possibility to use dry cementitious binders, added with strengthening nanomaterials, can guarantee several advantages for the industrial applications, we studied a premixing process to obtain a dry cementitious binder (method A). On the other hand, the necessity to maximize mechanical performance of CCMs led us to combine all the known dispersion techniques: adding the use of a superplasticizer and a sonication process (method B). The optimal GBMs content in the cementitious matrix was also evaluated.

Literature data assert that single layer graphene is an optimal substrate for the functional groups' attachment; for this reason, we started to study the functionalization of GBMs using single layer graphene (CE). We improved the hydrophilicity, and the water dispersion capability of single layer graphene (SLG), using arylsulfonate groups, polyethylene glycol chains, and quaternary ammonium groups. All the functional moieties reached consistent weight variation in TGA (between 10-30%), but we measured the higher functionalization degree using arylsulfonate moieties (FD = 1/65).

For an efficient graphene dispersion, essential criteria must be met: the graphene must disperse at a proper concentration, in a solvent appropriate to the application, and must remain dispersed over a reasonable period of time. Indeed, the stability of the dispersions of functionalized GBMs was evaluated in water, and in severe conditions (saturated $Ca(OH)_2$

solution and simulated cement pore solution), obtaining homogenously dispersed mixtures over several hours.

Since the functionalization with sulfonate moieties guaranteed the best results in the case of single layer graphene (high quality CE), we replicated this reaction using different quality of GBMs: few layers graphene (mid quality product PP), and graphene nanoplatelets (mid and low-quality products 0X, 3X), but TGA, and UV-vis analyses confirmed the necessity to use high quality graphene to obtain measurable functionalization yield and, consequently, good dispersion in water.

Due to their different chemical-physical characteristics and dispersibility in aqueous media, we believed that the functionalized GBMs should differently influence the final properties of cementitious materials.

The use of pristine GBMs provided always flexural and compressive strength improvements. Despite high quality GBM (SLG) guarantees the best mechanical performance, it seems that their quality is not fundamental to obtain strength improvements. The compressive and flexural performance resulted extremely influenced by the functional groups ad an enhancement was observed only with arylsulfonate functionalization. The negatively charged groups allowed to obtain the highest mechanical performance improvements; in particular, when it was applied on single layer graphene SLG (the compressive strength reached ~ 62 MPa, while the control sample fall behind 55 MPa).

These positive results can be correlated not only to the elevated specific surface of SLG, but also to the specific functional group which have enabled SLG to perform efficiently. When the GBMs was functionalized with neutral (polyethylene glycol chain), and positive (quaternary ammonium) groups, mortar samples reached mechanical strengths values lower than the relative control samples; probably the long polyethylene glycol chain, as well as quaternary ammonium groups, negatively influenced the hydration of the cement, reducing its performance. This finding demonstrated that the chemical characteristics of the functional groups can play a key role for the strength improvement.

The positive contribution of the GBMs was confirmed for both the mixing methods. In the case of method B, the combination of covalent functionalization, SP, and sonication process allowed to maximize the GBMs' positive effects and the achievement of best mechanical performance. Thanks to the simultaneous sonication of functionalized SLG and superplasticizer, it was possible to reach mechanical strengths improvement up to +12% compared to the control sample. In the case of method A, the maximum strength increase compared to the relative control sample was only +8%. It is worth noting this value was obtained using a dry premixed binder, for which no

sonication process and superplasticizers were necessary. These aspects are of primary importance in the case of real applications and for economic evaluations, as they avoid the above mentioned steps in the productive process.

Moreover, it seems that high GBMs dosages (more than 0.05%) are not essential to obtain mechanical performance enhancement. Nevertheless, the functionalization process allows to better disperse GBMs, providing comparable mechanical performance, independently on the quantity of GBMs.

If we focus on mechanical performance, the use of high dosage of GBMs can be ineffective (or negative), but this aspect can be relevant for the improvement of other characteristics, for example thermal and electrical properties. In those cases where the use of high dosage of GBM is necessary, but can excessively affect the mechanical performance, the possibility to use functionalized GBMs can represent a feasible solution.

This research confirmed that functionalized GBMs allow to produce more effective cementitious binders than the pristine GBMs. In addition, the mixing methods implemented (method A and method B) represent a reasonable matching point between mechanical performance and cost impact. Designing dry cementitious binders, based on functionalized GBMs (method A), becomes useful for versatile uses, allowing the preparation of mechanically improved concrete in a faster, cheaper and easier way, as the absence of sonication treatment and superplasticizers addition. On the other hand, preparing CCMs with functionalized GBMs, superplasticizer, and sonication process (method B) leads to stronger concrete at the expense of costs and use flexibility.

The mechanical improvements attained in this study could be considered unpretentious if compared to literature data, where, occasionally, prodigious compressive and flexural strengths improvement are reported. Nevertheless, a comparison between these different studies would become unreliable due to the different GBMs used and the well-known difficulty in their correct classification. The results obtained in this study, instead, put in evidence the possibility to enhance the application of GBMs in cementitious matrix, through their well-designed functionalization, regardless their chemical-physical characteristics and costs.

5. Extra chapter: Carbon nanotubes for cementitious mortars strengthening

The promising cement composite materials (CCMs) performance presented so far regards the benefits deriving from the enhanced dispersion of 2D GBM in cementitious environment, when chemically functionalized with sulfonate groups. These results led us to explore the possibility of extending the know-how about the functionalization of GBMs, not only for 2D materials, but also for 1D.

In this regards, CNTs functionalization with sulfonate groups was successfully studied by the research group of Prof. Menna/Università degli Studi di Padova, to improve their dispersion in aqueous environment [130]. Taking advantage from this result, functionalized 1D Multi-Walled Carbon Nanotubes (MWCNTS), chemically modified (similarly to 2D GBMs subject of the previous chapters), were experimentally tested in the most complex cementitious matrix, extending further the study of this thesis work. The objective was the evaluation of their potential better dispersion in high alkaline environment of cementitious environment to promote increased CCMs mechanical properties.

5.1 Introduction

The procedure used for CNTs has been widely studied as promoters for reinforcement in cement composite materials (CCMs) at nanoscale [131]. Within the nanocarbon family, CNTs are 1D carbon allotropes with a cylindrical nanostructure, that may be viewed as a rolled up from a single planar sheet of graphene. CNTs exhibit extraordinary elastic modulus, tensile strength, and surface area; in the context of reinforcing cementitious composites, these fundamental attributes can offer positive contribution improving the mechanical properties of brittle CCMs as well as promoting the reactivity of cement hydrates. In addition, CNTs, as one-dimensional tubes with high aspect ratio, have the distinctive crack-bridging effect to inhibit the crack propagation within cement composites [132].

When embedded in cementitious matrix, CNTs producing a more compact composite by filling the pores between hydration products of Portland cement and leading to a stronger matrix [133], [134].

Despite all these interesting characteristics, good dispersion of CNTs in CCMs is particularly difficult to attain due to their high surface energy, strong Van der Waals interactions, and hydrophobic behaviour. As a result, CNTs display high tendency to form irreversible

agglomerates, which limit their practical application in cement composites as nano-reinforcement.

As we already discussed in the previous sections, chemical functionalization can be used to improve the hydrophilic behaviour of CNTs, reducing their tendency to form agglomerates in cementitious matrix. Several attempts were already made to improve the hydrophilicity of CNTs, but most of them aimed to oxidize CNTs, bonding carboxylic acid (–COOH) or hydroxyl groups (–OH) [135]–[138]. Despite the use of these functional groups improves the dispersion of CNTs in aqueous media, their presence in alkaline environment causes the CNTs' agglomeration. As high concentration of alkaline ions (i.e. Ca^{2+}, Na^{+}, K^{+}) in the cementitious matrix, the repulsion between CNTs is weakened and they crosslink, causing severe aggregation that hampers the full utilization of CNTs to improve mechanical properties of cement-based materials [139].

In the previous section of these thesis work, we demonstrated that 2D-GBMs, functionalized with sulfonate groups, maintain their dispersion capability also in severe conditions, opening the possibility to successfully use this product as reinforcing agent in CCMs.

Hence, we studied mechanical performance of mortar samples, prepared with different percentage of CNTs functionalized with aryl sulfonate groups.

5.2 Functionalization of CNT with Sulfonate group

The procedure used for the functionalization of CNT presented is based on the Tour reaction between a commercial MWCNT (multi-walled Carbon Nanotube supplied by IoLiTec) and sodium sulfanilate. The reaction led to the attachment of SO_3^- groups on the nanotube surfaces, as indicated in Figure 51.

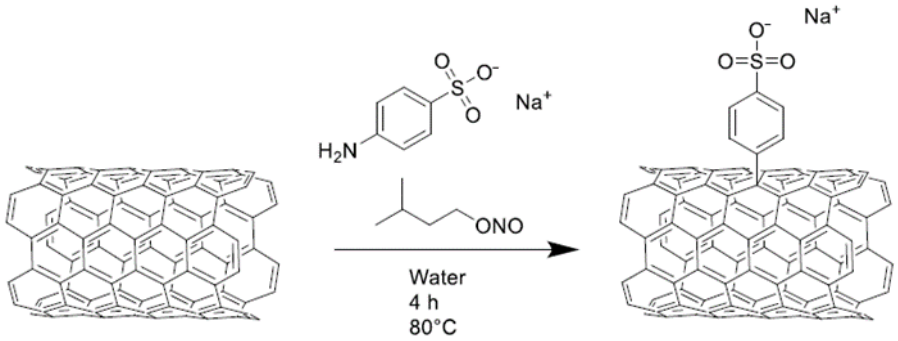

Figure 51: covalent functionalization of MWCNT by Tour reaction.

The MWCNTs main characteristics are reported in Table 15.

Table 15: MWCNTs characteristics.

Characteristic	Value
Diameter (nm)	10-20
Length (μm)	5-15
Weight loss in N_2 between 100 °C – 600 °C (%)	16.3
Functional degree	1/76
Dispersibility in water (mg/mL)	1.18
UV absorbance at 1000 nm	0.74

More detail about the synthesis and the characterization of functionalized CNTs used in this section are reported in the thesis work "Functionalized Carbon Nanotubes as Fillers in Nanocomposite Hydrogels for Biomedical Applications" [130].

Table 5 reports the main characteristics and the nomenclature used for the functionalized CNT.

Starting CNTs	Feature	Functionalization	Code
IoLiTec	MWCNT	*Negative charge*	***CNT-f(-)***

Table 16: functionalized single layer graphene with Sulfonate group.

5.3 Method B: wet sonicated solution

In this section, we evaluated the simultaneous used of covalent functionalization, noncovalent interaction (addition of SP), and sonication process to maximize the strengths of cementitious materials containing CNTs. In particular, we prepared mortar samples containing 0.05, 0.1, and 0.5% of MWCNTs functionalized with sulfonate groups.

For each preparation, the selected MWCNTs was firstly sonicated with water and superplasticizer and, subsequently, was used for the mortar preparations (according to method B). The water-to-cement ratio was kept at 0.42 and the quantity of sand at a proportion of 3 times the weight of cement. The superplasticizer (SP) was varied from 0.4% to 0.5% by weight of cement to achieve the same workability for all the mortars (more detail about the sample preparation is reported in experimental section 3.5).

Eight different mortar recipes were prepared using a mortar mixer and were investigated at the ages of 7 and 28 days by compressive and flexural strength tests. In order to verify the reproducibility of the results, we prepared at least three samples for each evaluation. The control samples, *Standard* and *Reference-SP*, were realized without CNTs and following the mix proportions reported in Table 117. Due to the presence of the superplasticizer, the *Reference-SP* sample contains less water than the *Standard* (190 ml rather than 225 ml).

Table 17: mix proportion of mortar samples prepared following method B.

	Mortar code	CNTs	Functionalization	GNT [g]	Cement [g]	Sand [g]	Water [g]	SP [g]
Method B Wet sonicated mortars	**m-CNT-0.05**	IoLiTec	-	0.225	449.8	1350	190	1.8
	m-CNT-f(-)-0.05	IoLiTec	Negative	0.225	449.8	1350	190	1.8
	m-CNT-0.10	IoLiTec	-	0.450	449.5	1350	190	2.0
	m-CNT-f(-)-0.10	IoLiTec	Negative	0.450	449.5	1350	190	2.0
	m-CNT-0.50	IoLiTec	-	2.250	447.7	1350	190	2.2
	m-CNT-f(-)-0.50	IoLiTec	Negative	2.250	447.7	1350	190	2.2
	Reference-SP	-	-	-	500.0	1350	190	1.8
	Standard	-	-	-	500.0	1350	225	-

Results and discussion

Figure 52 plots the mechanical strengths of mortar samples prepared with method B, containing 0.05 % of MWCNT functionalized with sulfonate group. The light and the dark bars refer to the mechanical performance at the age of 7 and 28 days, respectively.

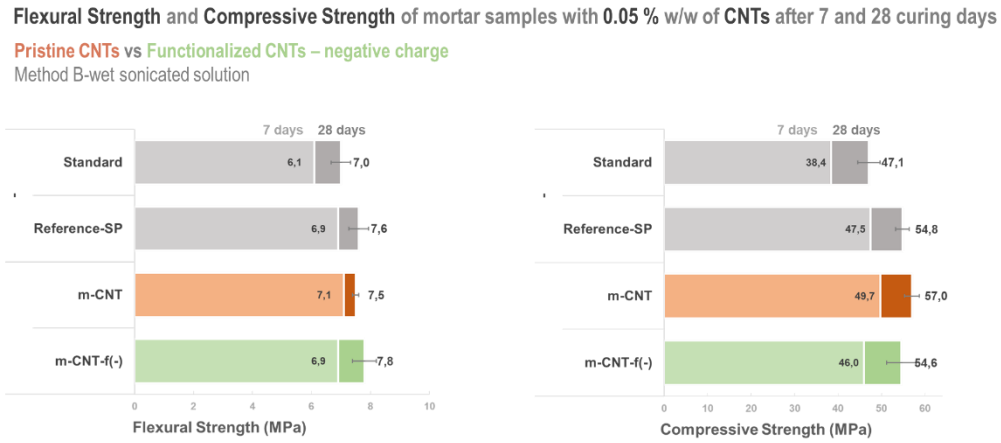

Figure 52: mechanical strengths of mortars with 0.05% of functionalized CNT with sulfonate group – method B.

At this percentage, the use of functionalized CNTs does not guarantee the development of high mechanical strength. Indeed, the compressive performance of sample *m-CNT-f(-),* reached strength values lower than the control *Reference-SP*. On the contrary, mortars with 0.05 % of pristine carbon nanotubes, *m-CNT*, exhibit a slight increase in compressive strength, reached improvement up to 4% compared to the *Reference-SP* sample. This trend remained valid both for 7 and 28 days of curing.

Figure 4553 shows the mechanical strengths of mortar samples containing 0.1 % of MWCNT functionalized with sulfonate group. The light and the dark bars refer to the mechanical performance at the age of 7 and 28 days, respectively.

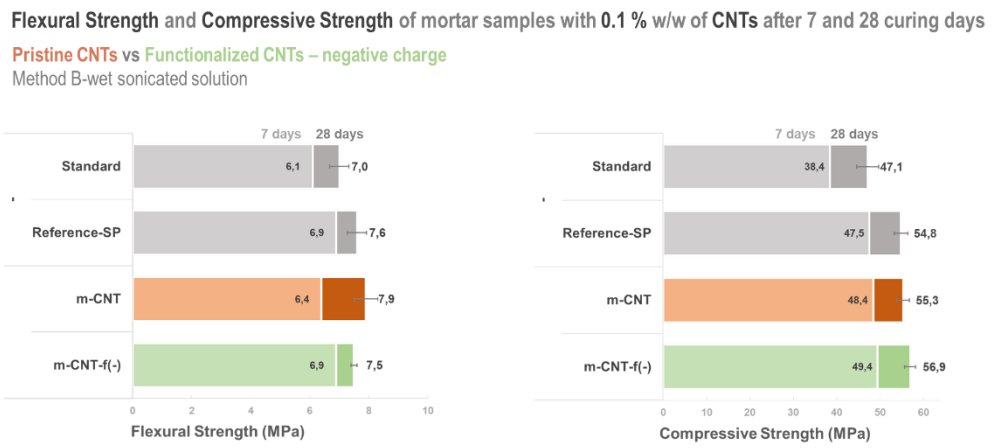

Figure 53: mechanical strengths of mortars with 0.1% of functionalized CNT with sulfonate group – method B.

Despite the CNTs' percentage was increased up to 0.1% by weight of cement, the mechanical performance remains similar to the control sample (*Reference-SP*). The use of functionalized MWCNT results ineffective to improve flexural strength, while allow to slightly improve the compressive performance (compressive strength of *m-CNT-f(-)* resulted +4% compared to the control sample).

Figure 54 shows the mechanical strengths of mortar samples containing 0.5 % of MWCNT functionalized with sulfonate group. The light and the dark bars refer to the mechanical performance at the age of 7 and 28 days, respectively.

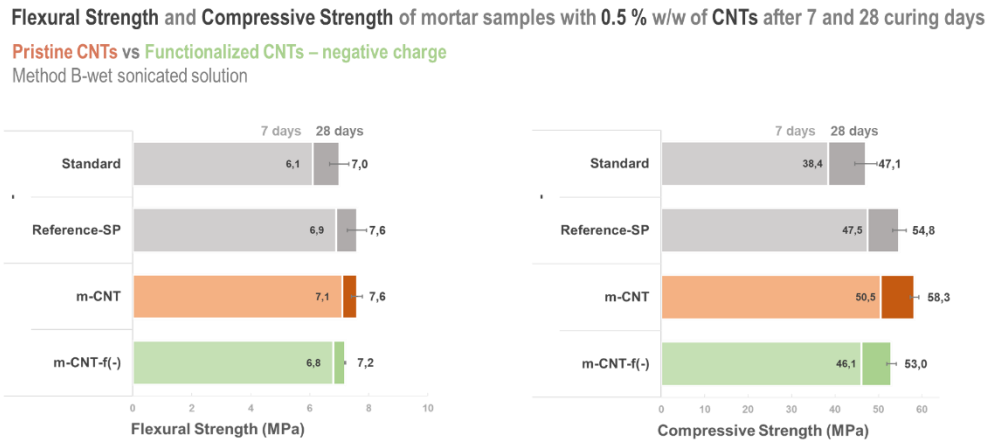

Figure 54: mechanical strengths of mortars with 0.5% of functionalized CNT with sulfonate group – method B.

The mechanical behaviour of the mortar samples remains the same also for 0.5% of CNTs. The use of functionalized products reduces the mortar strengths both for flexural and compressive test. The only positive result concern the mortar samples prepared with pristine product, *m-*

CNT, that reached the higher value measured in these trials (58.3 MPa, +6% compared to *Reference-SP*). This trend remained valid both for 7 and 28 days of curing.

The behaviour of compressive and flexural strength as a function of CNTs' percentage, after 28 days of curing, is highlighted in Figure 48. The red bars refer to the mechanical performance of mortars containing pristine MWCNT, while the green bars represent the performance of mortars containing functionalized MWCNT. The control samples (Standard and Reference-SP) are represented in grey.

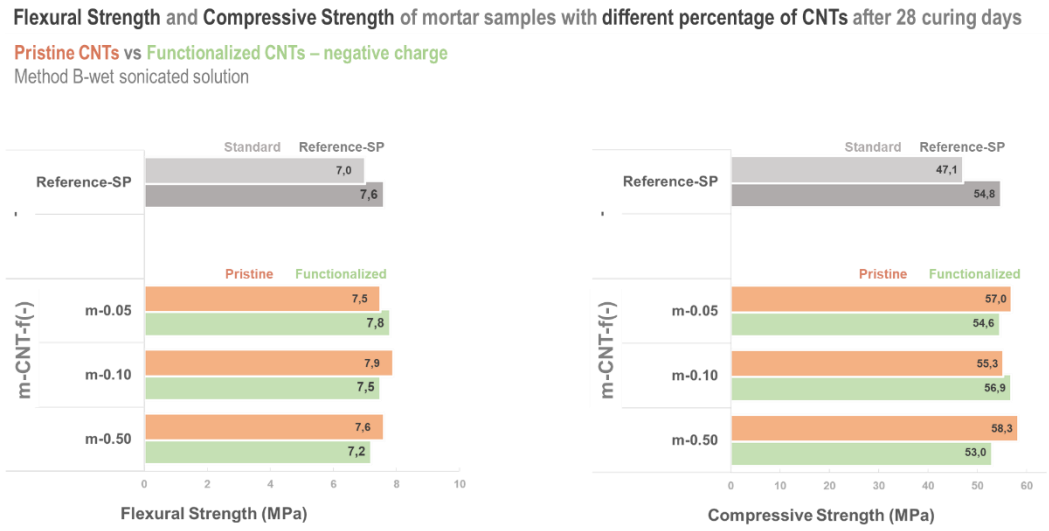

Figure 55: mortar samples containing GBMs functionalized with negative charge: strengths improvements compared to the control samples.

The experimental results demonstrated that all the mortar samples containing pristine CNTs, exhibited a slight increase of the flexural and compressive strength if compared to the control (*Reference-SP*). It seems that low percentages of pristine MWCNT (less than 0.1%) are favourable for strength improvements. On the contrary, no clear trends were identified in the case of functionalized products.

5.4 Final findings

In this section, we have investigated the role of functionalized MWCNTs to improve the mechanical performance of CCMs by preparing mortar samples with different percentage of carbon-based materials. The previous study highlighted the positive effect of method B to maximize the mechanical performance of CCMs, for this reason we directly evaluated the combined effects of covalent functionalization, superplasticizers, and sonication process.

Despite the functionalization of MWCNTs with sulfonate moieties obtained positive results in terms of functional degree and dispersibility in water, the use of these products resulted ineffective to improve mechanical performance of CCMs. Moreover, it seems that high MWCNTs dosages (more than 0.05%) are unfavourable to obtain mechanical performance enhancement.

A possible explanation of these negative results could be ascribed to the more flexibility of 2D functionalized graphene compared to the 1D products, that would facilitate their distribution in the cementitious matrix.

Since the favourable conditions evaluated in the previous study resulted ineffective in the case of CNTs functionalization, no other test and experimental trials were evaluated in this thesis work.

6. Bibliography

[1] S. Sahoo, P. K. Parhi, e B. Chandra Panda, «Durability properties of concrete with silica fume and rice husk ash», *Clean. Eng. Technol.*, vol. 2, p. 100067, giu. 2021, doi: 10.1016/j.clet.2021.100067.

[2] F. N. Costa e D. V. Ribeiro, «Reduction in CO2 emissions during production of cement, with partial replacement of traditional raw materials by civil construction waste (CCW)», *J. Clean. Prod.*, vol. 276, p. 123302, dic. 2020, doi: 10.1016/j.jclepro.2020.123302.

[3] P. J. M. Monteiro, S. A. Miller, e A. Horvath, «Towards sustainable concrete», *Nat. Mater.*, vol. 16, fasc. 7, Art. fasc. 7, lug. 2017, doi: 10.1038/nmat4930.

[4] J. W. Bullard *et al.*, «Mechanisms of cement hydration», *Cem. Concr. Res.*, vol. 41, fasc. 12, pp. 1208–1223, dic. 2011, doi: 10.1016/j.cemconres.2010.09.011.

[5] K. L. Scrivener, P. Juilland, e P. J. M. Monteiro, «Advances in understanding hydration of Portland cement», *Cem. Concr. Res.*, vol. 78, pp. 38–56, dic. 2015, doi: 10.1016/j.cemconres.2015.05.025.

[6] «Mechanisms and parameters controlling the tricalcium aluminate reactivity in the presence of gypsum. - Archive ouverte HAL». https://hal.archives-ouvertes.fr/hal-00418705 (consultato 20 settembre 2022).

[7] J. W. Bullard *et al.*, «Mechanisms of cement hydration», *Cem. Concr. Res.*, vol. 41, fasc. 12, pp. 1208–1223, dic. 2011, doi: 10.1016/j.cemconres.2010.09.011.

[8] «A.K. Geim, K.S. Novoselov, The rise of graphene, Nat. Mater. 6 (3) (2007) 183-191.pdf».

[9] C. Lam, J. T. James, R. McCluskey, S. Arepalli, e R. L. Hunter, «A Review of Carbon Nanotube Toxicity and Assessment of Potential Occupational and Environmental Health Risks», *Crit. Rev. Toxicol.*, vol. 36, fasc. 3, pp. 189–217, gen. 2006, doi: 10.1080/10408440600570233.

[10] E. E. Tkalya, M. Ghislandi, G. de With, e C. E. Koning, «The use of surfactants for dispersing carbon nanotubes and graphene to make conductive nanocomposites», *Curr. Opin. Colloid Interface Sci.*, vol. 17, fasc. 4, pp. 225–232, ago. 2012, doi: 10.1016/j.cocis.2012.03.001.

[11] S. Chuah, Z. Pan, J. G. Sanjayan, C. M. Wang, e W. H. Duan, «Nano reinforced cement and concrete composites and new perspective from graphene oxide», *Constr. Build. Mater.*, vol. 73, pp. 113–124, dic. 2014, doi: 10.1016/j.conbuildmat.2014.09.040.

[12] A. Bianco *et al.*, «All in the graphene family – A recommended nomenclature for two-dimensional carbon materials», *Carbon*, vol. 65, pp. 1–6, dic. 2013, doi: 10.1016/j.carbon.2013.08.038.

[13] P. Wick *et al.*, «Classification Framework for Graphene-Based Materials», *Angew. Chem. Int. Ed.*, vol. 53, fasc. 30, pp. 7714–7718, lug. 2014, doi: 10.1002/anie.201403335.

[14] X. Yu, H. Cheng, M. Zhang, Y. Zhao, L. Qu, e G. Shi, «Graphene-based smart materials», *Nat. Rev. Mater.*, vol. 2, 2017, doi: 10.1038/natrevmats.2017.46.

[15] Z. Li *et al.*, «Enhanced Mechanical Properties of Graphene (Reduced Graphene Oxide)/Aluminum Composites with a Bioinspired Nanolaminated Structure», *Nano Lett.*, vol. 15, fasc. 12, pp. 8077–8083, dic. 2015, doi: 10.1021/acs.nanolett.5b03492.

[16] «Electric Field Effect in Atomically Thin Carbon Films | Science». https://www.science.org/doi/full/10.1126/science.1102896 (consultato 26 settembre 2022).

[17] «Graphene: Status and Prospects». https://www.science.org/doi/10.1126/science.1158877 (consultato 26 settembre 2022).

[18] «Graphene-based composite materials | Nature». https://www.nature.com/articles/nature04969 (consultato 27 settembre 2022).

[19] J. Phiri, P. Gane, e T. C. Maloney, «General overview of graphene: Production, properties and application in polymer composites», *Mater. Sci. Eng. B*, vol. 215, pp. 9–28, gen. 2017, doi: 10.1016/j.mseb.2016.10.004.

[20] Y. Zhou, Q. Bao, L. A. L. Tang, Y. Zhong, e K. P. Loh, «Hydrothermal Dehydration for the “Green” Reduction of Exfoliated Graphene Oxide to Graphene and Demonstration of Tunable Optical Limiting Properties», *Chem. Mater.*, vol. 21, fasc. 13, pp. 2950–2956, lug. 2009, doi: 10.1021/cm9006603.
[21] H. Du e S. D. Pang, «Dispersion and stability of graphene nanoplatelet in water and its influence on cement composites», *Constr. Build. Mater.*, vol. 167, pp. 403–413, apr. 2018, doi: 10.1016/j.conbuildmat.2018.02.046.
[22] I. Papanikolaou, L. Ribeiro de Souza, C. Litina, e A. Al-Tabbaa, «Investigation of the dispersion of multi-layer graphene nanoplatelets in cement composites using different superplasticiser treatments», *Constr. Build. Mater.*, vol. 293, p. 123543, lug. 2021, doi: 10.1016/j.conbuildmat.2021.123543.
[23] X. Zhang, W. R. Browne, e B. L. Feringa, «Preparation of dispersible graphene through organic functionalization of graphene using a zwitterion intermediate cycloaddition approach», *RSC Adv.*, vol. 2, fasc. 32, p. 12173, 2012, doi: 10.1039/c2ra22440b.
[24] P. Livesey, A. Donnelly, e C. Tomlinson, «Measurement of the heat of hydration of cement», *Cem. Concr. Compos.*, vol. 13, fasc. 3, pp. 177–185, gen. 1991, doi: 10.1016/0958-9465(91)90018-D.
[25] H. Yang, H. Cui, W. Tang, Z. Li, N. Han, e F. Xing, «A critical review on research progress of graphene/cement based composites», *Compos. Part Appl. Sci. Manuf.*, vol. 102, pp. 273–296, nov. 2017, doi: 10.1016/j.compositesa.2017.07.019.
[26] M. H. Beigi, J. Berenjian, O. Lotfi Omran, A. Sadeghi Nik, e I. M. Nikbin, «An experimental survey on combined effects of fibers and nanosilica on the mechanical, rheological, and durability properties of self-compacting concrete», *Mater. Des.*, vol. 50, pp. 1019–1029, set. 2013, doi: 10.1016/j.matdes.2013.03.046.
[27] «Morphological Characteristics of Hardened Cement Pastes Incorporating Nano-palm Oil Fuel Ash - ScienceDirect». https://www.sciencedirect.com/science/article/pii/S235197891500089X (consultato 23 settembre 2022).
[28] A. Nazari, S. Riahi, S. Riahi, S. F. Shamekhi, e A. Khademno, «Mechanical properties of cement mortar with Al2O3 nanoparticles», p. 4.
[29] Z. Li, H. Wang, S. He, Y. Lu, e M. Wang, «Investigations on the preparation and mechanical properties of the nano-alumina reinforced cement composite», *Mater. Lett.*, vol. 60, fasc. 3, pp. 356–359, feb. 2006, doi: 10.1016/j.matlet.2005.08.061.
[30] A. R. Jayapalan, B. Y. Lee, e K. E. Kurtis, «Effect of Nano-sized Titanium Dioxide on Early Age Hydration of Portland Cement», in *Nanotechnology in Construction 3*, Berlin, Heidelberg, 2009, pp. 267–273. doi: 10.1007/978-3-642-00980-8_35.
[31] H. Li, M. Zhang, e J. Ou, «Flexural fatigue performance of concrete containing nano-particles for pavement», *Int. J. Fatigue*, vol. 29, fasc. 7, pp. 1292–1301, lug. 2007, doi: 10.1016/j.ijfatigue.2006.10.004.
[32] M. S. Morsy, S. H. Alsayed, e M. Aqel, «Hybrid effect of carbon nanotube and nano-clay on physico-mechanical properties of cement mortar», *Constr. Build. Mater.*, vol. 25, fasc. 1, pp. 145–149, gen. 2011, doi: 10.1016/j.conbuildmat.2010.06.046.
[33] P. Stynoski, P. Mondal, e C. Marsh, «Effects of silica additives on fracture properties of carbon nanotube and carbon fiber reinforced Portland cement mortar», *Cem. Concr. Compos.*, vol. 55, pp. 232–240, gen. 2015, doi: 10.1016/j.cemconcomp.2014.08.005.
[34] C. S. R. Indukuri, R. Nerella, e S. R. C. Madduru, «Effect of graphene oxide on microstructure and strengthened properties of fly ash and silica fume based cement composites», *Constr. Build. Mater.*, vol. 229, p. 116863, dic. 2019, doi: 10.1016/j.conbuildmat.2019.116863.
[35] R. A. e Silva, P. de Castro Guetti, M. S. da Luz, F. Rouxinol, e R. V. Gelamo, «Enhanced properties of cement mortars with multilayer graphene nanoparticles», *Constr. Build. Mater.*, vol. 149, pp. 378–385, set. 2017, doi: 10.1016/j.conbuildmat.2017.05.146.

[36] R. Palla, S. R. Karade, G. Mishra, U. Sharma, e L. P. Singh, «High strength sustainable concrete using silica nanoparticles», *Constr. Build. Mater.*, vol. 138, pp. 285–295, mag. 2017, doi: 10.1016/j.conbuildmat.2017.01.129.
[37] M.-H. Zhang e J. Islam, «Use of nano-silica to reduce setting time and increase early strength of concretes with high volumes of fly ash or slag», *Constr. Build. Mater.*, vol. 29, pp. 573–580, apr. 2012, doi: 10.1016/j.conbuildmat.2011.11.013.
[38] T. Phoo-ngernkham, P. Chindaprasirt, V. Sata, S. Hanjitsuwan, e S. Hatanaka, «The effect of adding nano-SiO2 and nano-Al2O3 on properties of high calcium fly ash geopolymer cured at ambient temperature», *Mater. Des.*, vol. 55, pp. 58–65, mar. 2014, doi: 10.1016/j.matdes.2013.09.049.
[39] Y. Lin e H. Du, «Graphene reinforced cement composites: A review», *Constr. Build. Mater.*, vol. 265, p. 120312, dic. 2020, doi: 10.1016/j.conbuildmat.2020.120312.
[40] D. Wanasinghe, F. Aslani, G. Ma, e D. Habibi, «Advancements in electromagnetic interference shielding cementitious composites», *Constr. Build. Mater.*, vol. 231, p. 117116, gen. 2020, doi: 10.1016/j.conbuildmat.2019.117116.
[41] M. K. Hassanzadeh-Aghdam, R. Ansari, M. J. Mahmoodi, A. Darvizeh, e A. Hajati-Modaraei, «A comprehensive study on thermal conductivities of wavy carbon nanotube-reinforced cementitious nanocomposites», *Cem. Concr. Compos.*, vol. 90, pp. 108–118, lug. 2018, doi: 10.1016/j.cemconcomp.2017.09.021.
[42] Q. Liu, Q. Xu, Q. Yu, R. Gao, e T. Tong, «Experimental investigation on mechanical and piezoresistive properties of cementitious materials containing graphene and graphene oxide nanoplatelets», *Constr. Build. Mater.*, vol. 127, pp. 565–576, nov. 2016, doi: 10.1016/j.conbuildmat.2016.10.024.
[43] W. Li, F. Qu, W. Dong, G. Mishra, e S. P. Shah, «A comprehensive review on self-sensing graphene/cementitious composites: A pathway toward next-generation smart concrete», *Constr. Build. Mater.*, vol. 331, p. 127284, mag. 2022, doi: 10.1016/j.conbuildmat.2022.127284.
[44] N. Asim *et al.*, «Application of graphene-based materials in developing sustainable infrastructure: An overview», *Compos. Part B Eng.*, vol. 245, p. 110188, ott. 2022, doi: 10.1016/j.compositesb.2022.110188.
[45] W. Li, X. Li, S. J. Chen, Y. M. Liu, W. H. Duan, e S. P. Shah, «Effects of graphene oxide on early-age hydration and electrical resistivity of Portland cement paste», *Constr. Build. Mater.*, vol. 136, pp. 506–514, apr. 2017, doi: 10.1016/j.conbuildmat.2017.01.066.
[46] C. Lin, W. Wei, e Y. H. Hu, «Catalytic behavior of graphene oxide for cement hydration process», *J. Phys. Chem. Solids*, vol. 89, pp. 128–133, feb. 2016, doi: 10.1016/j.jpcs.2015.11.002.
[47] X. Li *et al.*, «Effects of graphene oxide agglomerates on workability, hydration, microstructure and compressive strength of cement paste», *Constr. Build. Mater.*, vol. 145, pp. 402–410, ago. 2017, doi: 10.1016/j.conbuildmat.2017.04.058.
[48] X. Li *et al.*, «Effects of graphene oxide agglomerates on workability, hydration, microstructure and compressive strength of cement paste», *Constr. Build. Mater.*, vol. 145, pp. 402–410, ago. 2017, doi: 10.1016/j.conbuildmat.2017.04.058.
[49] Z. Lu, B. Chen, ChristopherK. Y. Leung, Z. Li, e G. Sun, «Aggregation size effect of graphene oxide on its reinforcing efficiency to cement-based materials», *Cem. Concr. Compos.*, vol. 100, pp. 85–91, lug. 2019, doi: 10.1016/j.cemconcomp.2019.04.005.
[50] J. Lin, E. Shamsaei, F. Basquiroto de Souza, K. Sagoe-Crentsil, e W. H. Duan, «Dispersion of graphene oxide–silica nanohybrids in alkaline environment for improving ordinary Portland cement composites», *Cem. Concr. Compos.*, vol. 106, p. 103488, feb. 2020, doi: 10.1016/j.cemconcomp.2019.103488.

[51] S. Ghazizadeh, P. Duffour, N. T. Skipper, M. Billing, e Y. Bai, «An investigation into the colloidal stability of graphene oxide nano-layers in alite paste», *Cem. Concr. Res.*, vol. 99, pp. 116–128, set. 2017, doi: 10.1016/j.cemconres.2017.05.011.
[52] «2020_Carbon Nanomaterials Global Market March modif.pdf».
[53] V. D. Ho *et al.*, «Electrochemically produced graphene with ultra large particles enhances mechanical properties of Portland cement mortar», *Constr. Build. Mater.*, vol. 234, p. 117403, feb. 2020, doi: 10.1016/j.conbuildmat.2019.117403.
[54] B. Wang e D. Shuang, «Effect of graphene nanoplatelets on the properties, pore structure and microstructure of cement composites», *Mater. Express*, vol. 8, fasc. 5, pp. 407–416, ott. 2018, doi: 10.1166/mex.2018.1447.
[55] H. Du, H. J. Gao, e S. D. Pang, «Improvement in concrete resistance against water and chloride ingress by adding graphene nanoplatelet», *Cem. Concr. Res.*, vol. 83, pp. 114–123, mag. 2016, doi: 10.1016/j.cemconres.2016.02.005.
[56] A. M. Onaizi, G. F. Huseien, N. H. A. S. Lim, M. Amran, e M. Samadi, «Effect of nanomaterials inclusion on sustainability of cement-based concretes: A comprehensive review», *Constr. Build. Mater.*, vol. 306, p. 124850, nov. 2021, doi: 10.1016/j.conbuildmat.2021.124850.
[57] R. Zhang, X. Cheng, P. Hou, e Z. Ye, «Influences of nano-TiO2 on the properties of cement-based materials: Hydration and drying shrinkage», *Constr. Build. Mater.*, vol. 81, pp. 35–41, apr. 2015, doi: 10.1016/j.conbuildmat.2015.02.003.
[58] P. Mudasir e J. A. Naqash, «Impact of carbon Nano tubes on fresh and hardned properties of conventional concrete», *Mater. Today Proc.*, giu. 2021, doi: 10.1016/j.matpr.2021.05.645.
[59] M. Oltulu e R. Şahin, «Effect of nano-SiO2, nano-Al2O3 and nano-Fe2O3 powders on compressive strengths and capillary water absorption of cement mortar containing fly ash: A comparative study», *Energy Build.*, vol. 58, pp. 292–301, mar. 2013, doi: 10.1016/j.enbuild.2012.12.014.
[60] Y. Qing, Z. Zenan, K. Deyu, e C. Rongshen, «Influence of nano-SiO2 addition on properties of hardened cement paste as compared with silica fume», *Constr. Build. Mater.*, vol. 21, fasc. 3, pp. 539–545, mar. 2007, doi: 10.1016/j.conbuildmat.2005.09.001.
[61] S. Lv, Y. Ma, C. Qiu, T. Sun, J. Liu, e Q. Zhou, «Effect of graphene oxide nanosheets of microstructure and mechanical properties of cement composites», *Constr. Build. Mater.*, vol. 49, pp. 121–127, dic. 2013, doi: 10.1016/j.conbuildmat.2013.08.022.
[62] W. Li, X. Li, S. J. Chen, Y. M. Liu, W. H. Duan, e S. P. Shah, «Effects of graphene oxide on early-age hydration and electrical resistivity of Portland cement paste», *Constr. Build. Mater.*, vol. 136, pp. 506–514, apr. 2017, doi: 10.1016/j.conbuildmat.2017.01.066.
[63] Z. Pan *et al.*, «Mechanical properties and microstructure of a graphene oxide–cement composite», *Cem. Concr. Compos.*, vol. 58, pp. 140–147, apr. 2015, doi: 10.1016/j.cemconcomp.2015.02.001.
[64] L. Lavagna, D. Massella, E. Priola, e M. Pavese, «Relationship between oxygen content of graphene and mechanical properties of cement-based composites», *Cem. Concr. Compos.*, vol. 115, p. 103851, gen. 2021, doi: 10.1016/j.cemconcomp.2020.103851.
[65] X. Yan, D. Zheng, H. Yang, H. Cui, M. Monasterio, e Y. Lo, «Study of optimizing graphene oxide dispersion and properties of the resulting cement mortars», *Constr. Build. Mater.*, vol. 257, p. 119477, ott. 2020, doi: 10.1016/j.conbuildmat.2020.119477.
[66] Z. Pan *et al.*, «Mechanical properties and microstructure of a graphene oxide–cement composite», *Cem. Concr. Compos.*, vol. 58, pp. 140–147, apr. 2015, doi: 10.1016/j.cemconcomp.2015.02.001.
[67] D. Lu, X. Shi, H. S. Wong, Z. Jiang, e J. Zhong, «Graphene coated sand for smart cement composites», *Constr. Build. Mater.*, vol. 346, p. 128313, set. 2022, doi: 10.1016/j.conbuildmat.2022.128313.

[68] W. Meng e K. H. Khayat, «Mechanical properties of ultra-high-performance concrete enhanced with graphite nanoplatelets and carbon nanofibers», *Compos. Part B Eng.*, vol. 107, pp. 113–122, dic. 2016, doi: 10.1016/j.compositesb.2016.09.069.
[69] W. Baomin e D. Shuang, «Effect and mechanism of graphene nanoplatelets on hydration reaction, mechanical properties and microstructure of cement composites», *Constr. Build. Mater.*, vol. 228, p. 116720, dic. 2019, doi: 10.1016/j.conbuildmat.2019.116720.
[70] H. Sixuan e B. Eng, «MULTIFUNCTIONAL GRAPHITE NANOPLATELETS (GNP) REINFORCED CEMENTITIOUS COMPOSITES», p. 167.
[71] «Effect of graphene nanoplatelets on the properties, pore structur...: Ingenta Connect». https://www.ingentaconnect.com/content/asp/me/2018/00000008/00000005/art00002;jsessionid=2n2rk4h694rf0.x-ic-live-03 (consultato 26 settembre 2022).
[72] B. Wang e B. Pang, «Mechanical property and toughening mechanism of water reducing agents modified graphene nanoplatelets reinforced cement composites», *Constr. Build. Mater.*, vol. 226, pp. 699–711, nov. 2019, doi: 10.1016/j.conbuildmat.2019.07.229.
[73] H. Du e S. Pang, «Dispersion and stability of graphene nanoplatelet in water and its influence on cement composites», *Constr. Build. Mater.*, vol. 167, pp. 403–413, apr. 2018, doi: 10.1016/j.conbuildmat.2018.02.046.
[74] A. H. Korayem, N. Tourani, M. Zakertabrizi, A. M. Sabziparvar, e W. H. Duan, «A review of dispersion of nanoparticles in cementitious matrices: Nanoparticle geometry perspective», *Constr. Build. Mater.*, vol. 153, pp. 346–357, ott. 2017, doi: 10.1016/j.conbuildmat.2017.06.164.
[75] B. Han, S. Ding, e X. Yu, «Intrinsic self-sensing concrete and structures: A review», *Measurement*, vol. 59, pp. 110–128, gen. 2015, doi: 10.1016/j.measurement.2014.09.048.
[76] M. S. Konsta-Gdoutos, Z. S. Metaxa, e S. P. Shah, «Highly dispersed carbon nanotube reinforced cement based materials», *Cem. Concr. Res.*, vol. 40, fasc. 7, pp. 1052–1059, lug. 2010, doi: 10.1016/j.cemconres.2010.02.015.
[77] H. Du e S. D. Pang, «Dispersion and stability of graphene nanoplatelet in water and its influence on cement composites», *Constr. Build. Mater.*, vol. 167, pp. 403–413, apr. 2018, doi: 10.1016/j.conbuildmat.2018.02.046.
[78] J. An, M. McInnis, W. Chung, e B. H. Nam, «Feasibility of Using Graphene Oxide Nanoflake (GONF) as Additive of Cement Composite», *Appl. Sci.*, vol. 8, fasc. 3, Art. fasc. 3, mar. 2018, doi: 10.3390/app8030419.
[79] «Aggregation and Stability of Reduced Graphene Oxide: Complex Roles of Divalent Cations, pH, and Natural Organic Matter | Environmental Science & Technology». https://pubs.acs.org/doi/10.1021/acs.est.5b01866 (consultato 20 settembre 2022).
[80] «A novel branched claw-shape lignin-based polycarboxylate superplasticizer_ Preparation, performance and mechanism | Elsevier Enhanced Reader». https://reader.elsevier.com/reader/sd/pii/S0008884618310068?token=4B36A2509D5C4DDA7E35FD41742D0A4FF736ADC74C8BB00EA1D3491A694FB19472C332754AEB8E981CF7D4ABD1B6084B&originRegion=eu-west-1&originCreation=20220927122358 (consultato 27 settembre 2022).
[81] L. Zhao *et al.*, «Investigation of dispersion behavior of GO modified by different water reducing agents in cement pore solution», *Carbon*, vol. 127, pp. 255–269, feb. 2018, doi: 10.1016/j.carbon.2017.11.016.
[82] L. Zhao *et al.*, «Mechanical behavior and toughening mechanism of polycarboxylate superplasticizer modified graphene oxide reinforced cement composites», *Compos. Part B Eng.*, vol. 113, pp. 308–316, mar. 2017, doi: 10.1016/j.compositesb.2017.01.056.
[83] H. Yang, M. Monasterio, H. Cui, e N. Han, «Experimental study of the effects of graphene oxide on microstructure and properties of cement paste composite», *Compos. Part Appl. Sci. Manuf.*, vol. 102, pp. 263–272, nov. 2017, doi: 10.1016/j.compositesa.2017.07.022.

[84] L. Zhao *et al.*, «Hydration kinetics, pore structure, 3D network calcium silicate hydrate, and mechanical behavior of graphene oxide reinforced cement composites», *Constr. Build. Mater.*, vol. 190, pp. 150–163, nov. 2018, doi: 10.1016/j.conbuildmat.2018.09.105.
[85] S. Ghazizadeh, P. Duffour, N. T. Skipper, e Y. Bai, «Understanding the behaviour of graphene oxide in Portland cement paste», *Cem. Concr. Res.*, vol. 111, pp. 169–182, set. 2018, doi: 10.1016/j.cemconres.2018.05.016.
[86] «Effects of the charge characteristics of polycarboxylate superplasticizers on the adsorption and the retardation in cement pastes - ScienceDirect». https://www.sciencedirect.com/science/article/abs/pii/S0008884614001987 (consultato 21 settembre 2022).
[87] E. E. Tkalya, M. Ghislandi, G. de With, e C. E. Koning, «The use of surfactants for dispersing carbon nanotubes and graphene to make conductive nanocomposites», *Curr. Opin. Colloid Interface Sci.*, vol. 17, fasc. 4, pp. 225–232, ago. 2012, doi: 10.1016/j.cocis.2012.03.001.
[88] S. Chuah, Z. Pan, J. G. Sanjayan, C. M. Wang, e W. H. Duan, «Nano reinforced cement and concrete composites and new perspective from graphene oxide», *Constr. Build. Mater.*, vol. 73, pp. 113–124, dic. 2014, doi: 10.1016/j.conbuildmat.2014.09.040.
[89] C. E. Hamilton, J. R. Lomeda, Z. Sun, J. M. Tour, e A. R. Barron, «High-Yield Organic Dispersions of Unfunctionalized Graphene», *Nano Lett.*, vol. 9, fasc. 10, pp. 3460–3462, ott. 2009, doi: 10.1021/nl9016623.
[90] Z. Jin *et al.*, «Click chemistry on solution-dispersed graphene and monolayer CVD graphene», *Chem. Mater.*, vol. 23, fasc. 14, pp. 3362–3370, lug. 2011, doi: 10.1021/cm201131v.
[91] «Functionalization of Graphene via 1,3-Dipolar Cycloaddition | ACS Nano». https://pubs.acs.org/doi/10.1021/nn100883p (consultato 25 settembre 2022).
[92] L.-H. Liu, M. M. Lerner, e M. Yan, «Derivitization of Pristine Graphene with Well-Defined Chemical Functionalities», *Nano Lett.*, vol. 10, fasc. 9, pp. 3754–3756, set. 2010, doi: 10.1021/nl1024744.
[93] C. Kiang Chua, A. Ambrosi, e M. Pumera, «Introducing dichlorocarbene in graphene», *Chem. Commun.*, vol. 48, fasc. 43, pp. 5376–5378, 2012, doi: 10.1039/C2CC31936E.
[94] S. Sarkar, E. Bekyarova, S. Niyogi, e R. C. Haddon, «Diels−Alder Chemistry of Graphite and Graphene: Graphene as Diene and Dienophile», *J. Am. Chem. Soc.*, vol. 133, fasc. 10, pp. 3324–3327, mar. 2011, doi: 10.1021/ja200118b.
[95] G. Bottari *et al.*, «Chemical functionalization and characterization of graphene-based materials», *Chem. Soc. Rev.*, vol. 46, fasc. 15, pp. 4464–4500, 2017, doi: 10.1039/C7CS00229G.
[96] G. Schmidt, S. Gallon, S. Esnouf, J.-P. Bourgoin, e P. Chenevier, «Mechanism of the Coupling of Diazonium to Single-Walled Carbon Nanotubes and Its Consequences», *Chem. - Eur. J.*, vol. 15, fasc. 9, pp. 2101–2110, feb. 2009, doi: 10.1002/chem.200801801.
[97] J. L. Bahr, J. Yang, D. V. Kosynkin, M. J. Bronikowski, R. E. Smalley, e J. M. Tour, «Functionalization of Carbon Nanotubes by Electrochemical Reduction of Aryl Diazonium Salts: A Bucky Paper Electrode», *J. Am. Chem. Soc.*, vol. 123, fasc. 27, pp. 6536–6542, lug. 2001, doi: 10.1021/ja010462s.
[98] J. L. Bahr, J. Yang, D. V. Kosynkin, M. J. Bronikowski, R. E. Smalley, e J. M. Tour, «Functionalization of Carbon Nanotubes by Electrochemical Reduction of Aryl Diazonium Salts: A Bucky Paper Electrode», *J. Am. Chem. Soc.*, vol. 123, fasc. 27, pp. 6536–6542, lug. 2001, doi: 10.1021/ja010462s.
[99] C. A. Dyke e J. M. Tour, «Unbundled and highly functionalized carbon nanotubes from aqueous reactions», *Nano Lett.*, vol. 3, fasc. 9, pp. 1215–1218, 2003, doi: 10.1021/nl034537x.
[100] J. R. Lomeda, C. D. Doyle, D. V. Kosynkin, W.-F. Hwang, e J. M. Tour, «Diazonium Functionalization of Surfactant-Wrapped Chemically Converted Graphene Sheets», *J. Am. Chem. Soc.*, vol. 130, fasc. 48, pp. 16201–16206, dic. 2008, doi: 10.1021/ja806499w.

[101] R. Sharma, J. H. Baik, C. J. Perera, e M. S. Strano, «Anomalously Large Reactivity of Single Graphene Layers and Edges toward Electron Transfer Chemistries», *Nano Lett.*, vol. 10, fasc. 2, pp. 398–405, feb. 2010, doi: 10.1021/nl902741x.
[102] G. Biagiotti *et al.*, «Nanostructured carbon materials decorated with organophosphorus moieties: synthesis and application», p. 9, 2017.
[103] Z. Qiu, J. Yu, P. Yan, Z. Wang, Q. Wan, e N. Yang, «Electrochemical Grafting of Graphene Nano Platelets with Aryl Diazonium Salts», *ACS Appl. Mater. Interfaces*, vol. 8, fasc. 42, pp. 28291–28298, ott. 2016, doi: 10.1021/acsami.5b11593.
[104] L. Rodríguez-PØrez e R. García, «Modified SWCNTs with Amphoteric Redox and Solubilizing Properties», *Chem Eur J*, p. 9, 2014.
[105] E. Bailón-García, «The use of functionalized carbon xerogels in cells growth», *Mater. Sci.*, p. 10, 2019.
[106] Y. Si e E. T. Samulski, «Synthesis of Water Soluble Graphene», *Nano Lett.*, vol. 8, fasc. 6, pp. 1679–1682, giu. 2008, doi: 10.1021/nl080604h.
[107] B. K. Price e J. M. Tour, «Functionalization of Single-Walled Carbon Nanotubes "On Water"», *J. Am. Chem. Soc.*, vol. 128, fasc. 39, pp. 12899–12904, ott. 2006, doi: 10.1021/ja063609u.
[108] M. C. Pirrung, «Acceleration of Organic Reactions through Aqueous Solvent Effects», *Chem. – Eur. J.*, vol. 12, fasc. 5, pp. 1312–1317, 2006, doi: 10.1002/chem.200500959.
[109] S. Narayan, J. Muldoon, M. G. Finn, V. V. Fokin, H. C. Kolb, e K. B. Sharpless, «"On Water": Unique Reactivity of Organic Compounds in Aqueous Suspension», *Angew. Chem. Int. Ed.*, vol. 44, fasc. 21, pp. 3275–3279, 2005, doi: 10.1002/anie.200462883.
[110] Z. Tavakkoli, H. Goljani, H. Sepehrmansourie, D. Nematollahi, e M. A. Zolfigol, «New insight into the electrochemical reduction of different aryldiazonium salts in aqueous solutions», *RSC Adv.*, vol. 11, fasc. 42, pp. 25811–25815, 2021, doi: 10.1039/D1RA04482F.
[111] S. Park, K.-S. Lee, G. Bozoklu, W. Cai, S. T. Nguyen, e R. S. Ruoff, «Graphene Oxide Papers Modified by Divalent Ions—Enhancing Mechanical Properties *via* Chemical Cross-Linking», *ACS Nano*, vol. 2, fasc. 3, pp. 572–578, mar. 2008, doi: 10.1021/nn700349a.
[112] C. Hadad *et al.*, «Positive graphene by chemical design: tuning supramolecular strategies for functional surfaces», *Chem Commun*, vol. 50, fasc. 7, pp. 885–887, 2014, doi: 10.1039/C3CC47056C.
[113] S. Silvestrini *et al.*, «Controlled Functionalization of Reduced Graphene Oxide Enabled by Microfluidic Reactors», *Chem. Mater.*, vol. 30, fasc. 9, pp. 2905–2914, mag. 2018, doi: 10.1021/acs.chemmater.7b04740.
[114] S. Bai, L. Jiang, N. Xu, M. Jin, e S. Jiang, «Enhancement of mechanical and electrical properties of graphene/cement composite due to improved dispersion of graphene by addition of silica fume», *Constr. Build. Mater.*, vol. 164, pp. 433–441, mar. 2018, doi: 10.1016/j.conbuildmat.2017.12.176.
[115] J. M. Harris *et al.*, «Synthesis and characterization of poly(ethylene glycol) derivatives», *J. Polym. Sci. Polym. Chem. Ed.*, vol. 22, fasc. 2, pp. 341–352, feb. 1984, doi: 10.1002/pol.1984.170220207.
[116] S. Deng e V. Berry, «Wrinkled, rippled and crumpled graphene: an overview of formation mechanism, electronic properties, and applications», *Mater. Today*, vol. 19, fasc. 4, pp. 197–212, mag. 2016, doi: 10.1016/j.mattod.2015.10.002.
[117] F. Farivar, P. Lay Yap, R. U. Karunagaran, e D. Losic, «Thermogravimetric Analysis (TGA) of Graphene Materials: Effect of Particle Size of Graphene, Graphene Oxide and Graphite on Thermal Parameters», *C*, vol. 7, fasc. 2, p. 41, apr. 2021, doi: 10.3390/c7020041.
[118] M. Krystek *et al.*, «High-Performance Graphene-Based Cementitious Composites», *Adv. Sci.*, vol. 6, fasc. 9, p. 1801195, mag. 2019, doi: 10.1002/advs.201801195.

[119] S. Eigler e A. Hirsch, «Chemistry with Graphene and Graphene Oxide-Challenges for Synthetic Chemists», *Angew. Chem. Int. Ed.*, vol. 53, fasc. 30, pp. 7720–7738, lug. 2014, doi: 10.1002/anie.201402780.
[120] S. C. Paul, A. S. van Rooyen, G. P. A. G. van Zijl, e L. F. Petrik, «Properties of cement-based composites using nanoparticles: A comprehensive review», *Constr. Build. Mater.*, vol. 189, pp. 1019–1034, nov. 2018, doi: 10.1016/j.conbuildmat.2018.09.062.
[121] S. Fritzsche *et al.*, «Derivatization of Methylglyoxal for LC-ESI-MS Analysis—Stability and Relative Sensitivity of Different Derivatives», *Molecules*, vol. 23, fasc. 11, Art. fasc. 11, nov. 2018, doi: 10.3390/molecules23112994.
[122] «The intermediate body of polyethylene glycol derivatives and manufacturing method - Current Patent Assignee SENKA PHARMACY - JP5651291, 2015 - B2.pdf».
[123] J. M. Harris, N. H. Hundley, T. G. Shannon, e E. C. Struck, «Polyethylene glycols as soluble, recoverable, phase-transfer catalysts», *J. Org. Chem.*, vol. 47, fasc. 24, pp. 4789–4791, nov. 1982, doi: 10.1021/jo00145a041.
[124] P. Ghods, O. B. Isgor, G. McRae, e T. Miller, «The effect of concrete pore solution composition on the quality of passive oxide films on black steel reinforcement», *Cem. Concr. Compos.*, vol. 31, fasc. 1, pp. 2–11, gen. 2009, doi: 10.1016/j.cemconcomp.2008.10.003.
[125] L. Zhao, X. Guo, L. Song, Y. Song, G. Dai, e J. Liu, «An intensive review on the role of graphene oxide in cement-based materials», *Constr. Build. Mater.*, vol. 241, p. 117939, apr. 2020, doi: 10.1016/j.conbuildmat.2019.117939.
[126] M. Han, Y. Muhammad, Y. Wei, Z. Zhu, J. Huang, e J. Li, «A review on the development and application of graphene based materials for the fabrication of modified asphalt and cement», *Constr. Build. Mater.*, vol. 285, p. 122885, mag. 2021, doi: 10.1016/j.conbuildmat.2021.122885.
[127] H. Yang, H. Cui, W. Tang, Z. Li, N. Han, e F. Xing, «A critical review on research progress of graphene/cement based composites», *Compos. Part Appl. Sci. Manuf.*, vol. 102, pp. 273–296, nov. 2017, doi: 10.1016/j.compositesa.2017.07.019.
[128] E. Shamsaei, F. B. de Souza, X. Yao, E. Benhelal, A. Akbari, e W. Duan, «Graphene-based nanosheets for stronger and more durable concrete: A review», *Constr. Build. Mater.*, vol. 183, pp. 642–660, set. 2018, doi: 10.1016/j.conbuildmat.2018.06.201.
[129] D. W. Johnson, B. P. Dobson, e K. S. Coleman, «A manufacturing perspective on graphene dispersions», *Curr. Opin. Colloid Interface Sci.*, vol. 20, fasc. 5–6, pp. 367–382, ott. 2015, doi: 10.1016/j.cocis.2015.11.004.
[130] «Ludovica Ceroni, Enzo Menna, Functionalized Carbon Nanotubes as Fillers in Nanocomposite Hydrogels for Biomedical Applications.pdf».
[131] «Carbon nanotube–cement composites: A retrospect: The IES Journal Part A: Civil & Structural Engineering: Vol 4, No 4». https://www.tandfonline.com/doi/abs/10.1080/19373260.2011.615474 (consultato 28 settembre 2022).
[132] S. Parveen, S. Rana, R. Fangueiro, e M. C. Paiva, «Microstructure and mechanical properties of carbon nanotube reinforced cementitious composites developed using a novel dispersion technique», *Cem. Concr. Res.*, vol. 73, pp. 215–227, lug. 2015, doi: 10.1016/j.cemconres.2015.03.006.
[133] B. Wang, Y. Han, e S. Liu, «Effect of highly dispersed carbon nanotubes on the flexural toughness of cement-based composites», *Constr. Build. Mater.*, vol. 46, pp. 8–12, set. 2013, doi: 10.1016/j.conbuildmat.2013.04.014.
[134] T. Nochaiya e A. Chaipanich, «Behavior of multi-walled carbon nanotubes on the porosity and microstructure of cement-based materials», *Appl. Surf. Sci.*, vol. 257, fasc. 6, pp. 1941–1945, gen. 2011, doi: 10.1016/j.apsusc.2010.09.030.
[135] G. Y. Li, P. M. Wang, e X. Zhao, «Mechanical behavior and microstructure of cement composites incorporating surface-treated multi-walled carbon nanotubes», *Carbon*, vol. 43, fasc. 6, pp. 1239–1245, mag. 2005, doi: 10.1016/j.carbon.2004.12.017.

[136] G. Y. Li, P. M. Wang, e X. Zhao, «Pressure-sensitive properties and microstructure of carbon nanotube reinforced cement composites», *Cem. Concr. Compos.*, vol. 29, fasc. 5, pp. 377–382, mag. 2007, doi: 10.1016/j.cemconcomp.2006.12.011.
[137] «Effect of Carbon Nanotube Aqueous Dispersion Quality on Mechanical Properties of Cement Composite». https://www.hindawi.com/journals/jnm/2012/169262/ (consultato 28 settembre 2022).
[138] V. S. Melo, J. M. F. Calixto, L. O. Ladeira, e A. R. Silva, «Macro- and micro-characterization of mortars produced with carbon nanotubes», *ACI Mater. J.*, vol. 108, fasc. 3, pp. 327–332, 2011.
[139] O. Mendoza, G. Sierra, e J. I. Tobón, «Influence of super plasticizer and Ca(OH)2 on the stability of functionalized multi-walled carbon nanotubes dispersions for cement composites applications», *Constr. Build. Mater.*, vol. 47, pp. 771–778, ott. 2013, doi: 10.1016/j.conbuildmat.2013.05.100.

Appendix

Below the NMR spectra of the molecules synthesized for this thesis work.

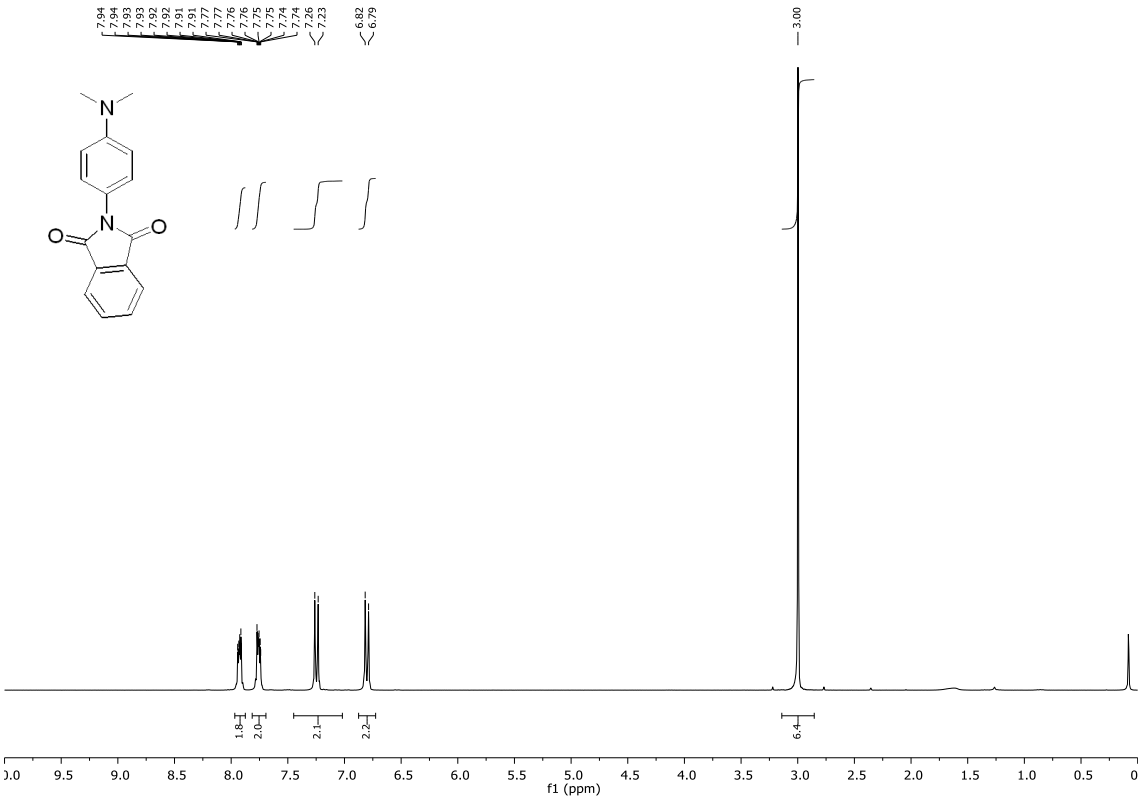

Figure 56: NMR spectra of Compound 1b.

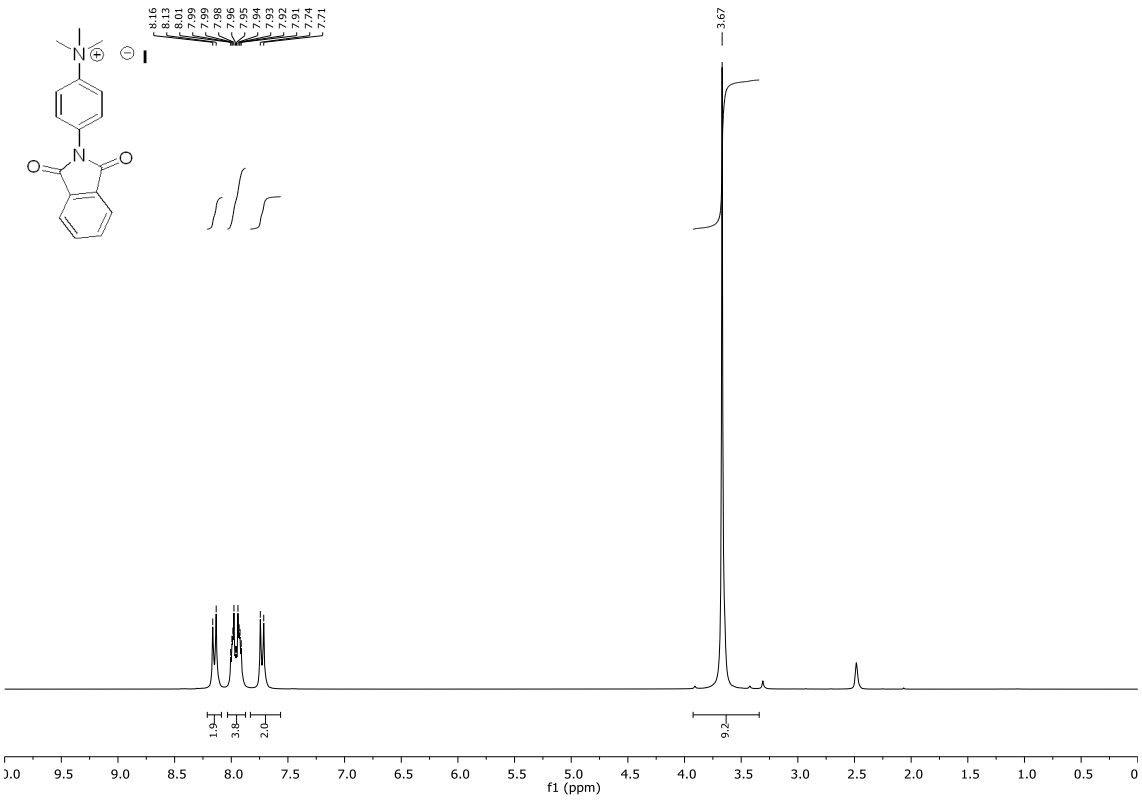

Figure 57: NMR spectra of Compound 1c.

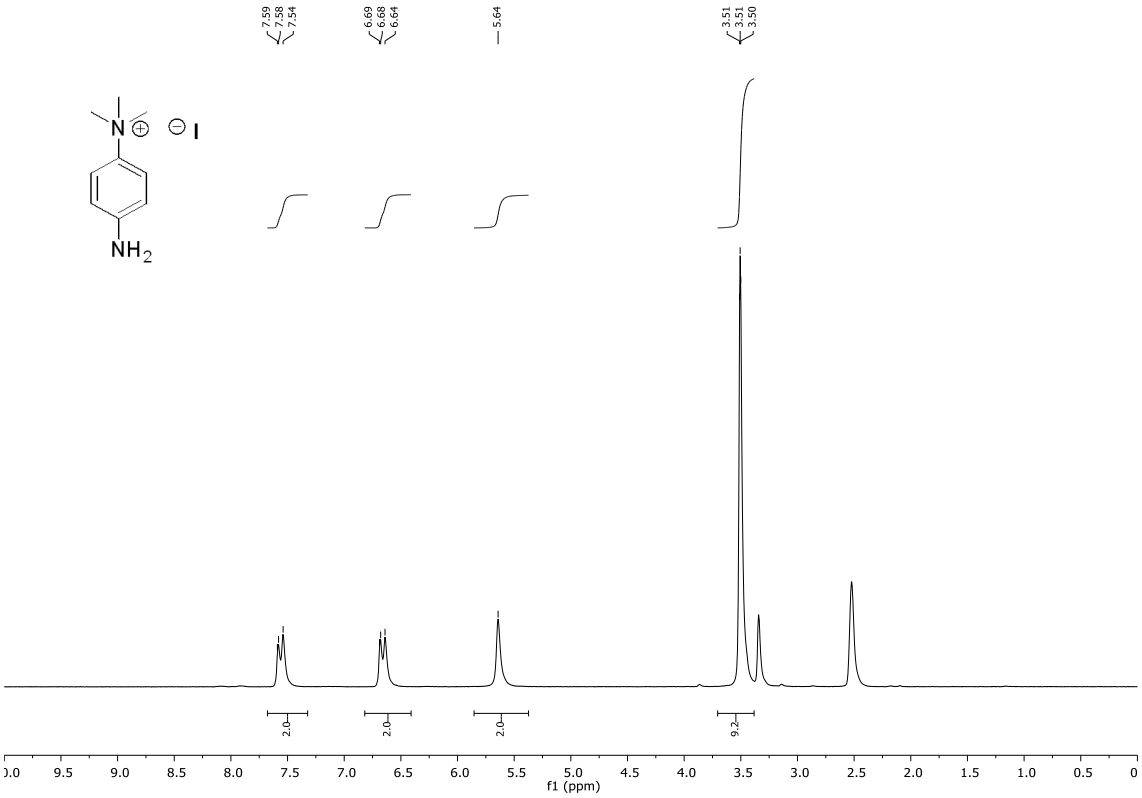

Figure 58: NMR spectra of Compound 1d.

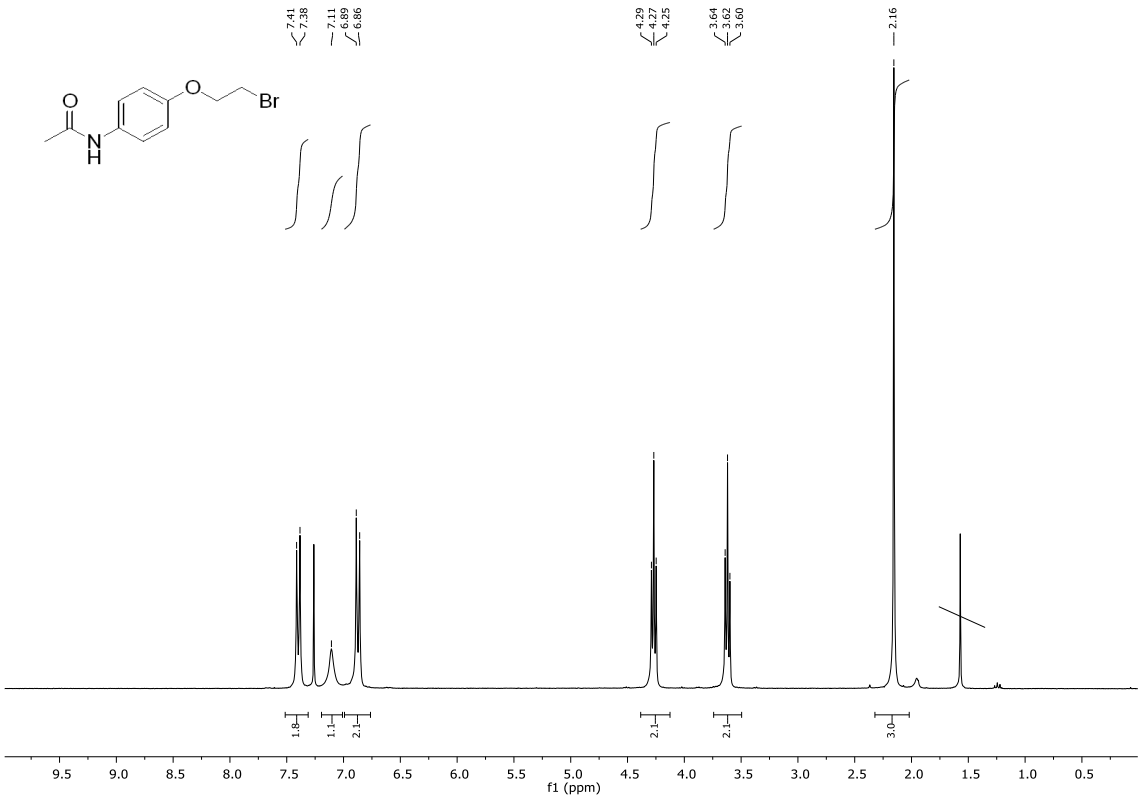

Figure 59: NMR spectra of Compound 2b.

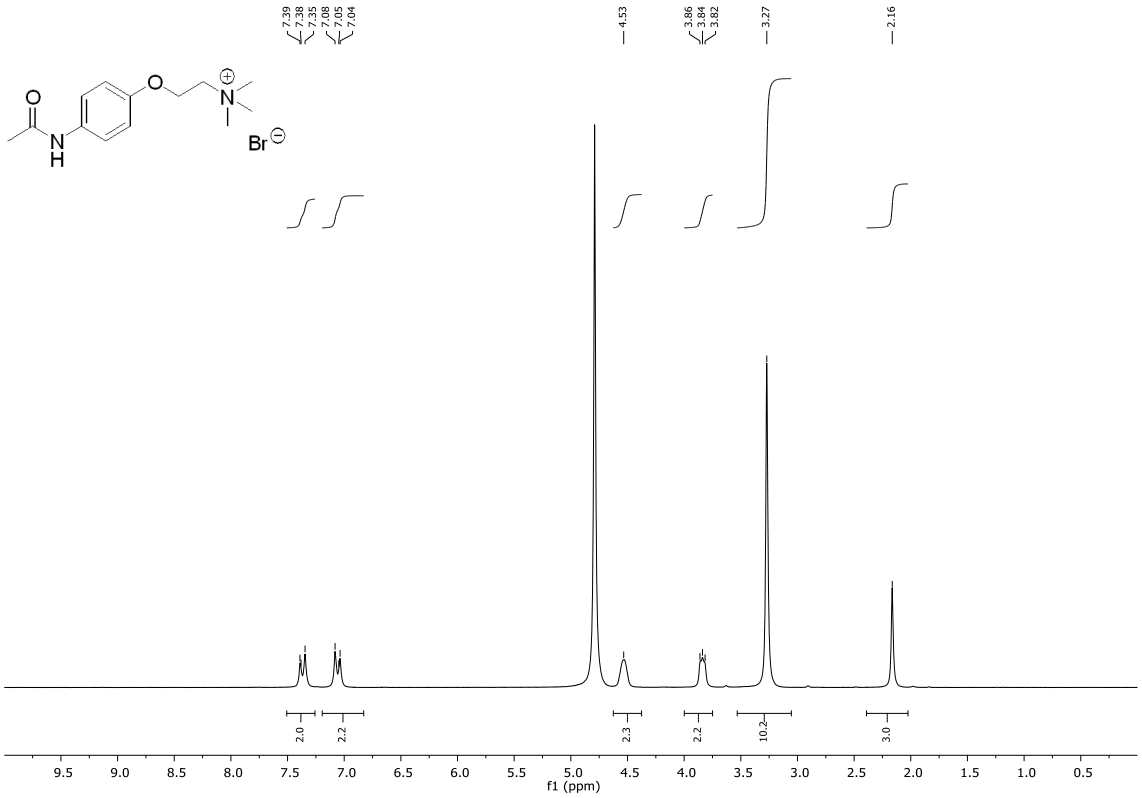

Figure 60: NMR spectra of Compound 2c.

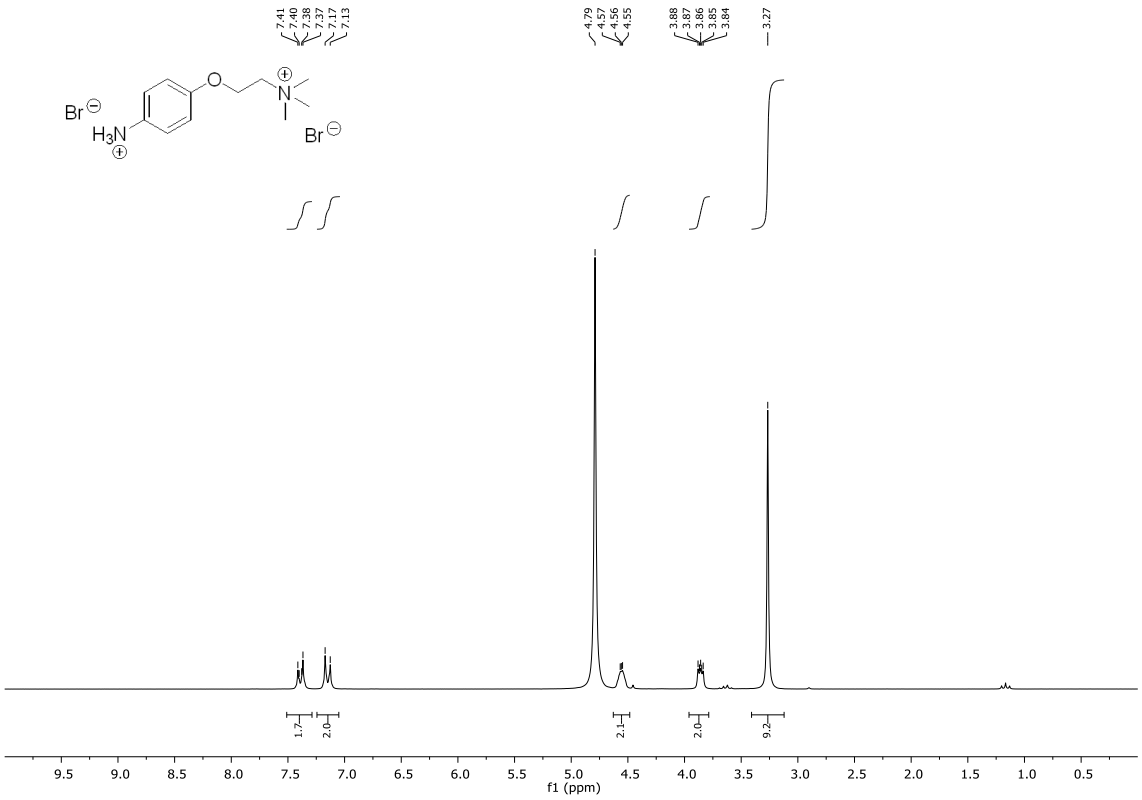

Figure 61: NMR spectra of Compound 2d.

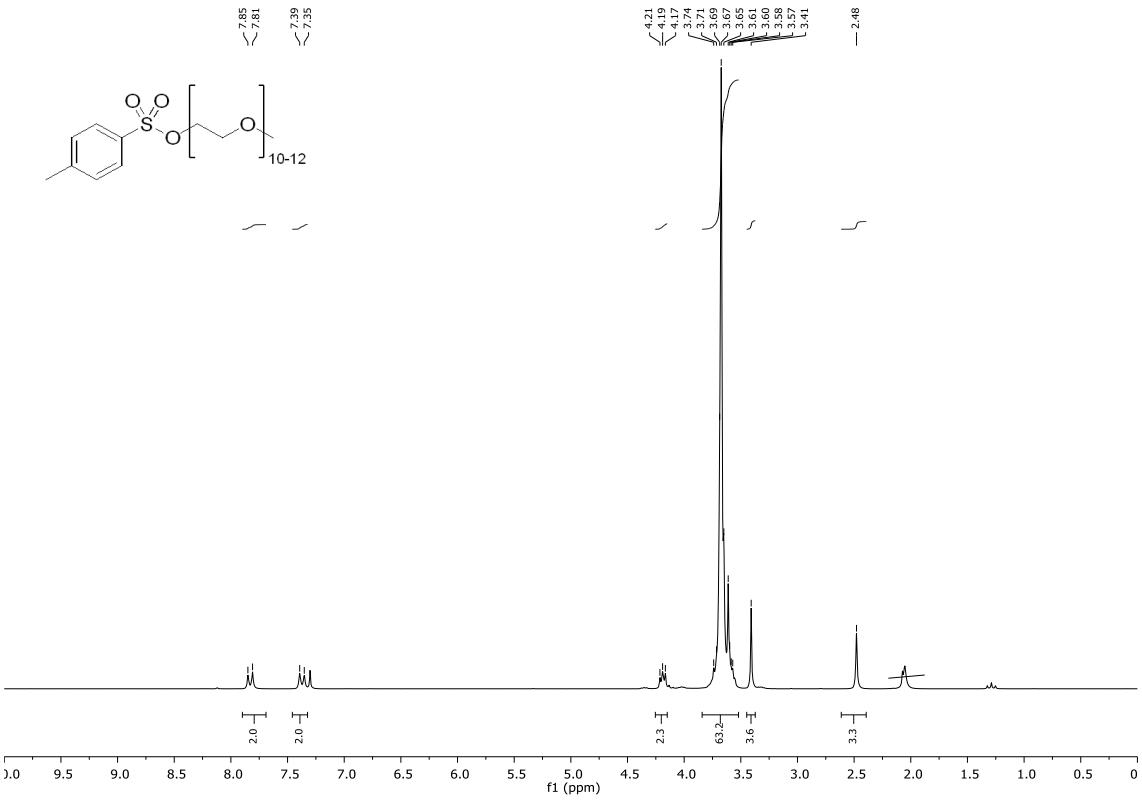

Figure 62: NMR spectra of Compound 3b.

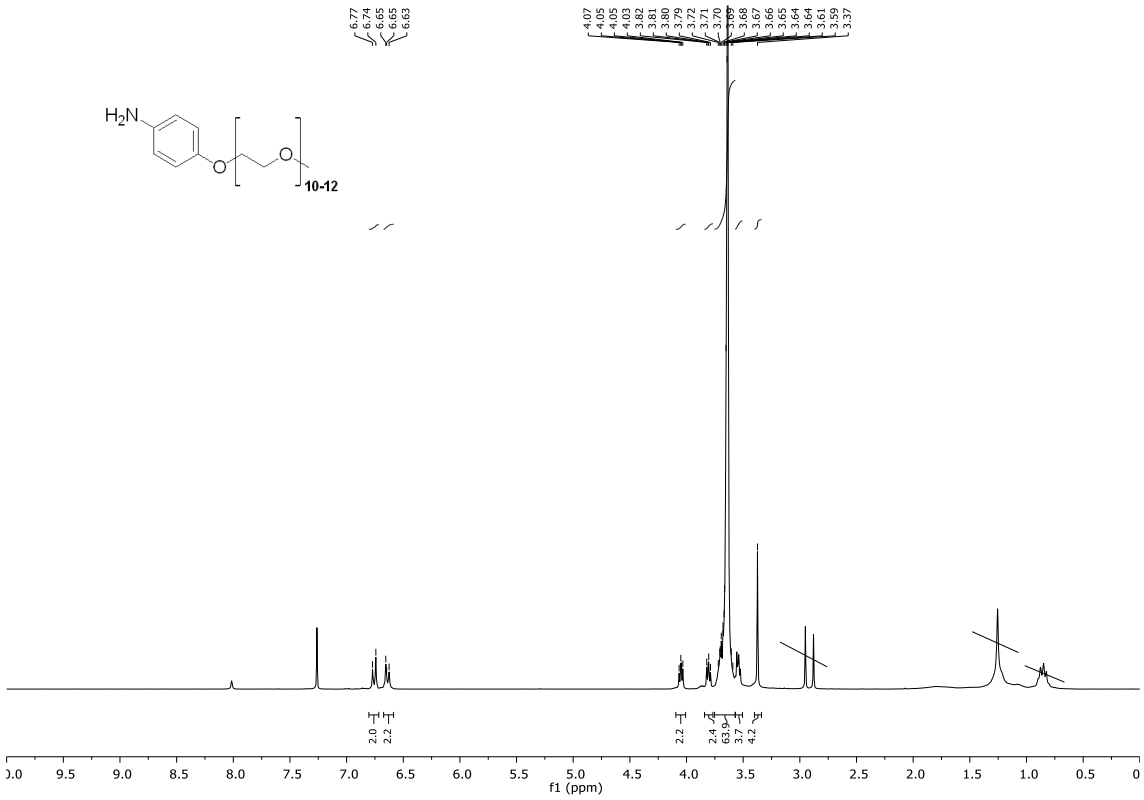

Figure 63: NMR spectra of Compound 3c.

Ringraziamenti

Vorrei dedicare questo spazio a chi, con dedizione, ha contribuito alla realizzazione di questo elaborato.

Ringrazio il Prof. Michele Maggini, la sua guida e le sue competenze hanno reso ancora più stimolante questo percorso formativo.

Ringrazio il Dr. Paolo Zardi, per la sua disponibilità, per il continuo supporto e per i preziosi consigli. Immagino che sarebbe stato tutto estremamente più complicato senza di lui.

Ringrazio l'Ing. Claudia Capone, per la premura e la dedizione con cui mi ha seguito negli ultimi tre lunghissimi anni.

Ringrazio Maurizio Marchi, senza i suoi consigli probabilmente non avrei mai iniziato questo percorso.

Infine, vorrei dedicare questo piccolo traguardo alla mia compagna Maria Elena, grazie per avermi sopportato, in particolare nelle ultime settimane.